



11.03.87  
La Silla  
La Serena  
Santiago

## EL MENSAJERO

ESO

No. 47 – March 1987

-54

### New Meteorite Finds At Imilac

H. PEDERSEN, ESO, and F. GARCIA, c/o ESO

#### Introduction

Stones falling from the sky have been collected since prehistoric times. They were, until recently, the only source of extraterrestrial material available for laboratory studies and they remain, even in our space age, a valuable source for investigation of the solar system's early history.

It is estimated that, on the average, each square kilometre of the Earth's surface is hit once every million years by a meteorite heavier than 500 grammes. Most are lost in the oceans, or fall in sparsely populated regions. As a result, museums around the world receive as few as about 6 meteorites annually from witnessed falls. Others are due to accidental finds. These have most often fallen in prehistoric times.

Each of the two groups, 'falls' and 'finds', consists of material from about one thousand catalogued, individual meteorites. The total number of fragments is considerably higher, since many break up when hitting the atmosphere. Mineralogically, they can be divided into three classes: stones, irons and stony-irons. Falls are largely stony, while finds have a high percentage of irons. This is due to the stony meteorites' faster erosion and lesser visibility. The geographical pattern of falls is strongly correlated with population density: most are reported from Europe and North America. Finds, on the other

hand, depend more on the preserving conditions of the terrain, and the extent to which it allows meteorites to be spotted. Most meteorites are found by chance. Active searching is, in general, too time consuming to be of interest. However, the blue-ice fields of Antarctica have proven to be a happy hunting ground. During the last two decades

some 7,500 meteorites were recovered by Japanese and American expeditions. They come from a smaller, but yet unknown number of independent falls. The meteorites appear where glaciers are pressed up towards a mountain range, allowing the ice to evaporate. Some have been lying in the ice for as much as 700,000 years.



Figure 1: The 19-kg fragment in its 80-cm diameter crater. The meteorite protrudes about 5 cm above the crater floor and reaches approximately 18 cm below. It is remarkable that such a small structure has resisted erosion during 166 years, possibly much longer.

Supernova 1987A in LMC:  
see pp. 26–35

## Imilac Meteorites

Other areas where many meteorites are found are some of the world's desert regions, e.g. Western Australia, the North American prairies, and the Atacama desert in Chile. At the latter, the annual precipitation is lower than anywhere else on the earth, less than 5 mm, which obviously eases the meteorites' preservation. As a result, one of the Atacamenean meteorites, found at Tamarugal, has a terrestrial age of 2,700,000 years, the oldest known. During the last century, many mineral prospectors travelled through Atacama, in search for precious ores. Occasionally, they came upon iron meteorites which they brought home, often unaware of the material's true character. They gave much less attention to stony meteorites, though these undoubtedly also have been preserved in large numbers.

The Atacama desert is noted for its deposits of nitrates. These were exploited, on a huge scale, during the first decades of this century. In the process, several meteorites were found.

Many Chilean meteorites are of the rare Pallasite type (see box), for which reason they most likely stem from a single fall. They carry names which correspond to geographical locations scattered over a 100 by 100 km area. In most cases, however, the find site was reported without precision and, until recently, it was believed that the meteorites had been picked up inside a 100 by 500 metre area near the small salt-pan Salar de Imilac, about 170 km from Antofagasta. At this place, there is a crater-like excavation, 8 metres in diameter. This may have been made by Indians in search for the fancied iron vein. Several minor excavations on the neighbouring hills indicate places where, in the past, meteorites have been collected. Still, the top-soil contains many small iron fragments, weighing typically 1 gramme.

There is no reliable account of the meteorite's fall. The first fragments were found around 1820. Buchwald (1975) estimates that the fall occurred several hundred years earlier. From geological considerations, Martinez (private communication) deduces an age of about 500 years before present. Nearby, ancient Indian populations could conceivably have forged tools or ornaments from meteoritic iron. This might put a minimum age to the fall. However, no such artifacts have yet been identified. Another dating method relates to the decay of radioactive isotopes, activated by cosmic ray irradiation prior to the fall. To our knowledge, no such measurements have been published.

Imilac meteorites have made their



Figure 2: The 35-kg fragment before excavation. The diameter of the crater is 125 cm. The meteorite reached about 6 cm above and 14 cm below the crater floor.

way to many museums and private collections, all over the world. The largest specimen known, 198 kg, is in the British Museum. Another fragment, originally 95 kg, is in Copiapo. The total amount of recovered material, plausibly originating at Imilac, is calculated at 500 kg (Buchwald, 1975).

### The New Finds

Following the visit of several expeditions, it was believed that all large meteorites had been collected. We can, however, report the recent discovery of three more meteorites, totalling 59 kg. The find was made by one of the authors (F.G.) who is a geologist\*. During water prospection for a mining enterprise he learned about the meteorite fall at Imilac. A local resident told him that some meteorites had been found several kilometres south-west of the 'crater'. During his own search he managed to locate a further three. They have masses of 5, 19 and 35 kg, respectively.

The new meteorites were spotted at 3,250 metres altitude, on some promontories which stretch towards east and north-east from a 3,870 m high mountain, Morro de La Mina. The find locations form an approximately equilateral triangle, with side lengths of 900 metres. The centre of that triangle is 7 km southwest of the 'crater'. The two largest meteorites were lying, only partially ex-

posed, in circular impact craters (Figure 1 and 2) of diameter 80 and 125 cm. In both cases, the crater floors were about 15 cm below level and covered with smaller pebbles than the surrounding desert. The edges were white, bringing into view a soft underground material, rich in gypsum. The crater of the 35-kg meteorite did not have an elevated rim, except possibly towards east. This can be concluded from the inspection of a stereo-photo taken prior to the excavation. Its depth is estimated at 5 to 10 cm. The 5-kg iron was lying, nearly fully exposed, on top of the desert surface, and apparently not '*in situ*'. Therefore, we cannot exclude the possibility that it is a transported mass, originally found somewhere else.

The 5-kg meteorite measures 16 by 13.5 by 10 cm. It is an elongated lump without any sharp corners. The 19-kg meteorite is roughly cubic, 23.5 by 18.5 by 18 cm. One of its edges is quite sharp, clearly indicating the meteorite as a fragment. The 35-kg meteorite is slightly banana-shaped and measures 50 by 24 by 15 cm. All three meteorites have specific gravities near 4.6 g/cm<sup>3</sup>, which is typical for Pallasites.

The submerged parts of the two large specimens are covered by a thin crust of corrosion products, due to the presence of nitrates in the soil.

Universidad del Norte in Antofagasta has inspected two of the meteorites and classified them as Pallasites. For reasons of similar surface texture and specific gravity, we believe that also the third meteorite belongs to that group.

\* Editor's note: F.G. is the husband of ESO's secretary in Santiago, Mariam G., through whom scientists at La Silla were informed about the find.

Since, from the whole Earth, only 33 Pallasite-finds (and 2 falls) have been described, this is a strong indication that the new specimens are part of the well-known Imilac fall.

The site of the old crater-like excavation was also visited. In the 'splinters area' about 1 kg of minor fragments (0.1 to approximately 250 grammes were collected. A few particles were found up to 1,000 m north-east of the 'crater'. Otherwise, we can confirm Buchwald's statements as to the shape and extent of the area. We estimate that it still holds of the order of 1,000 kg of meteoritic iron.

### The Imilac Strewn-Field

The existence of the splinters area indicates that a large chunk of the meteorite suffered a violent break-up. This must have happened at a late point of the trajectory through the atmosphere. Its mass exceeded, by far, those which fell further to the south-west. Therefore, it seems likely that the parent body arrived from south-west, rather than opposite. The splinters area is approximately aligned with the new find locations, giving a further argument for their association. Measured from north over east, the azimuth of the combined strewn-field is  $47^\circ \pm 3^\circ$ .

The new finds show that the strewn-field is at least 8 km long and about 1 km wide. It cannot be excluded that some of the meteorites collected a long time ago were found in the 'new' area. We did, in fact, notice a small number of minor holes from where it is conceivable that specimens (in the 10-kg class) have been picked up. Indications are that the strewn-field is even longer than mentioned. This topic, and other aspects of the Imilac fall, are discussed in a forthcoming thesis work by E. Martínez, Universidad del Norte. The total weight of recovered material is now about 560 kg. To this adds the estimated 1,000 kg of small meteorite particles still left in the top-soil. Although impressive, at least one other Pallasite find is larger. That at Brenham, USA, had a mass of 4.5 tons (Nininger, 1957, Peck, 1979). It too suffered violent fragmentation.

### Asteroidal Origin for Pallasites

Pallasite meteorites form a rather homogeneous group, clearly distinct from the other type of stony-irons, the mesosiderites. They may hold clues to the origin of solar-system bodies. Their creation is therefore a much debated issue between 'cosmogonists'. One theory says that they formed in asteroids, at the interface between a molten core and a partially molten mantle,

rich in olivine silicates (Greenberg and Chapman, 1984). Following the asteroid's colling, the top layer of silicates may have been stripped off, exposing the now contracted and cracked Pallasitic layer to erosion.

The asteroidal origin could, in principle be ascertained by orbital calculation of meteorite falls. This has been done on three occasions (the falls at Příbram, Lost City, Innisfree) but none of the meteorites in question were Pallasites. Ground-based observations may nevertheless help solving the question. By infrared spectroscopy three candidate parent-asteroids have been found: 246 Asporina, 289 Nenetta, 446 Aeternitas (Cruikshank and Hartmann, 1984, Scott, 1984). Their spectra show an absorption band at  $1.06\text{ }\mu\text{m}$ , as does olivine in its meteoritic form. Also the general trend of the spectra is consistent with the presence of a metallic phase.

It is rare that asteroids can be associated with one particular type of mineral. Detailed studies of asteroids and comets will, in general, require spacecraft to do "sample-return" missions. Such are, in fact, being considered. But perhaps it is superfluous to include Asporina, Nenetta or Aeternitas in the itinerary: the stuff may already be in our hands . . .

### Tentative Time-table of Council Sessions and Committee Meetings for First Half of 1987

May 18	Users Committee
May 19	Scientific Technical Committee
May 20–21	Finance Committee
May 26–27	Observing Programmes Committee, Venice
June 3	Committee of Council, Bruges
June 4	Council, Bruges

All meetings will take place at ESO in Garching unless stated otherwise.

### References

- Buchwald, V.F., 1975, *Handbook of Iron Meteorites*, University of California press, Berkeley, vol. 1–3.  
Cruikshank, D.P., and Hartmann, W.K., 1984, *Science* **223**, 281.  
Greenberg, R., and Chapman, C.R., 1984, *Icarus*, **57**, 267.  
Nininger, H.H., 1952, *Out of the Sky*, Dover, New York.  
Peck, E., 1979, *Sky and Telescope*, **58**, p. 126.  
Scott, E.R.D., *Nature*, **311**, 708.

### Pallasite Meteorites

Meteorites can be divided into three classes: Stones, Irons, and Stony Irons. A subgroup of the latter is quite peculiar: an iron/nickel mixture forms a sponge-like structure. Olivine crystals, of cross-section 1 to 10 mm fill out the holes, so that the volume ratio metal/olivine is about 1 : 1. The first such meteorite was found in 1771/72 by the German explorer Peter Simon Pallas, during his travels through East Russia. Pallasite meteorites are quite rare: less than 1 per cent of all falls and 3.5 per cent of all finds belong to this group.

### Meteorite Craters

Upon hitting the ground, a large meteorite may form a crater. If the terminal velocity is sufficiently high, the conversion of kinetic energy will lead to the meteorite's instantaneous evaporation. An explosion crater is thereby formed. Smaller masses may form impact craters. 13 genuine meteor craters (or crater fields) are known and some 100 others are considered probable. The largest is the meteorite crater in Arizona, USA, which has a diameter of 1,200 metres. Third on the list is the more than 100,000-year old, 370-m diameter crater at Monturaqui. This is only 60 km from the location mentioned in the article, but unrelated. European probable meteorite craters include the 15-million-year-old, 27-km-diameter Nördlinger Ries structure in West Germany and

the nearby 3.5-km diameter Steinheim Basin. There is geological evidence that both are meteoritic, but the proof (meteoritic material) is not yet found. It may long since have weathered away.

### Strewn-fields

The hyper-sonic velocity, 15 to 72 km/sec, with which meteorites enter the Earth's atmosphere, creates a shock, which often forces the meteorite to break up. Masses less than a few tons will reach the ground with sub-sonic speed, 100–300 metres per second. Small particles tend to fall along steeper trajectories than heavier ones. This creates a characteristic elliptical distribution pattern, with particle size increasing along the major axis, in the direction of flight. This simple picture holds, if just one event of fragmentation took place. Strewn-fields can reach considerable sizes. The Gibeon-fall at South-West Africa covered approximately 100 by 400 km.

### Meteorite Collections

Collections of meteorites exist at many museums. Prominent between these are the museums of natural history in London, Paris, Vienna, and the Academy of Sciences, Moscow. The heaviest meteorite on display in Europe is 'Agpalilik', a 14-ton iron from Greenland, now at the Geological Museum, Copenhagen.

# Giant HII Regions and the Quest for the Hubble Constant

J. MELNICK, ESO

The search for yardsticks with which to measure cosmic distances is one of the fundamental endeavours of observational astronomy but this is a difficult task and it was not until the beginning of this century, when astronomy was already hundreds of years old, that the size of our own Galaxy could be determined. The yardstick which made this possible was the discovery, by Miss Henrietta Swan Leavitt, of a relation between the period of pulsation of Delta Cephei stars and their luminosities. The Cepheid period-luminosity relation was subsequently calibrated by Harlow Shapley who then used it together with the absolute magnitudes of RR Lyrae stars to measure the Milky Way.

Soon after the galactic distance scale was determined by Shapley, a great controversy arose as to whether the spiral nebulae, which were very well known at the time from the work of William and John Herschel and others, were galactic or extragalactic objects. The controversy was not settled until after the 100-inch Hooker telescope was brought into operation at Mount Wilson, and Hubble discovered cepheid variables in the Great Andromeda Nebula (M31) in 1924 and later in other spiral nebulae. The "island universe" hypothesis of Kant was thus proved and for the first time it was observationally established that the Universe extends far beyond the limits of the Milky Way.

Soon after the work of Hubble, several astronomers began to measure radial velocities of galaxies and discovered that these velocities increased linearly with distance. Thus, if  $R$  is the distance of a galaxy and  $V$  its radial velocity, the two are related as,

$$V = H_0 \times R$$

where  $H_0$  is a universal constant. In 1931, Hubble and Humason calibrated this relationship in galaxies where they had previously found Cepheid variables and obtained a value of  $H_0 = 558 \text{ km/sec/Mpc}$  for this constant which is now known as the Hubble constant. Almost ten years before the work of Hubble and Humason, the Russian mathematician Alexander Friedmann had found a solution of Einstein's General Relativity equations which predicted that the Universe should be either expanding or contracting according to a linear relation between velocity and distance. Thus, immediately after Hubble's results were published, the idea that our Universe is expanding gained universal acceptance.

The Friedmann solutions have a singularity where the radius of the Universe is zero and mass density infinite. In fact the Hubble relation ( $V = H_0 R$ ) implies that some time in the past all galaxies were on top of each other. For obvious onomatopoeic reasons the singularity is called the "Big-Bang"; thus the singularity is interpreted as a magnificent cosmic firework which marked the beginning of time. Friedmann cosmologies can be parametrized in terms of the expansion rate  $H_0$ , the mass density  $\Omega_0$ , and an elusive parameter called the cosmological constant,  $\Lambda$ , which has bedeviled cosmology since it was first introduced by Einstein himself.

Einstein's theory allows for the existence of this additive constant which represents either an additional attractive or repulsive "gravitational" force but there is no compelling reason in the general theory of relativity for this force to exist in nature. It is merely allowed by the mathematical structure of the equations. Einstein found that in order to construct a statical model for the Universe, he had to introduce a repulsion term to balance gravity. Of course, in 1917 everybody, including Einstein, thought that the Universe was static!

With no cosmological constant ( $\Lambda = 0$ ), Friedmann's models give simple relationships between the age of the Universe ( $T_0$ , the time elapsed since the Big-Bang) and the Hubble constant and  $\Omega_0$ . In general  $T_0$  is always smaller than  $H_0^{-1}$  and it is equal to  $H_0^{-1}$  if the mass density is zero ( $\Omega_0 = 0$ ).

Thus, the calibration of the Hubble relation provides not only the most powerful cosmic yardstick but also a means of determining the age of the Universe. It is not yet known how important the deceleration and the gravitational repulsion terms in Friedmann models are but, at least in principle, they can be determined observationally and this is one of the major tasks of modern observational cosmology. An important constraint on the Hubble constant is that, for  $\Lambda = 0$ ,  $H_0^{-1}$  must be larger than the age of the Galaxy. At the time of Hubble's work, this limit was the age of the earth, about 4,000 million years. Today, from the theory of stellar evolution and from observations of globular clusters the age of our galaxy is estimated to be more than 16,000 million years.

## The Determination of $H_0$

Periods and luminosities of Cepheids can be reliably determined from the

ground out to distances of about 5 Mpc. One of the major tasks of the Hubble Space Telescope will be to extend these observations to larger distances. Our Milky Way is a member of a group of galaxies (the Local Group) of roughly 1 Mpc in diameter of which the Andromeda nebula is also a member. The Local Group is itself member of a larger agglomeration of galaxies known as the Local Supercluster which is dominated by the Virgo cluster, distant 15–20 Mpc from the Local Group. Thus, the expansion of the Universe is perturbed at small distances by these mass concentrations and it is necessary to measure velocities and distances to galaxies beyond the Virgo cluster in order to derive a meaningful value for the Hubble constant. Hubble's own determination was too large because of a number of errors, including a large error in Shapley's calibration of the cepheid period-luminosity relation. But even today, almost 60 years after the pioneering work of Hubble and Humason, astronomers have not yet agreed on the exact value of  $H_0$  although most agree that it lies between 50 and 100 km/sec/Mpc. In fact, the opinions are divided in two groups; the  $H_0 = 50$  camp championed by Sandage and Tammann, and the  $H_0 = 100$  camp whose strongest advocates are Aaronson and co-workers and G. de Vaucouleurs. Both camps defend their cause with excellent observations but the controversy is still far from being resolved. The discrepancy is also philosophical; at  $H_0 = 50$ , the Big-Bang age of the Universe is consistent with the age of the oldest stars in our Galaxy while for  $H_0 = 100$  that age is too short and, in order to maintain consistency with the Friedmann models, the cosmological constant must be revived.

In this article I would like to present a new method (in fact a new version of an old method), developed in collaboration with Roberto Terlevich from the RGO and Mariano Moles from the IAA in Granada, which uses the properties of giant HII regions as distance indicators.

## Giant HII Regions as Distance Indicators

In the early 1960s Sersic discovered that the diameters of the largest HII regions in spiral galaxies increase with galaxy luminosity. This correlation was further developed by Sandage and it has since been used by many workers as a cosmic yardstick. The correlation, however, is not useful much beyond

## HII Galaxies

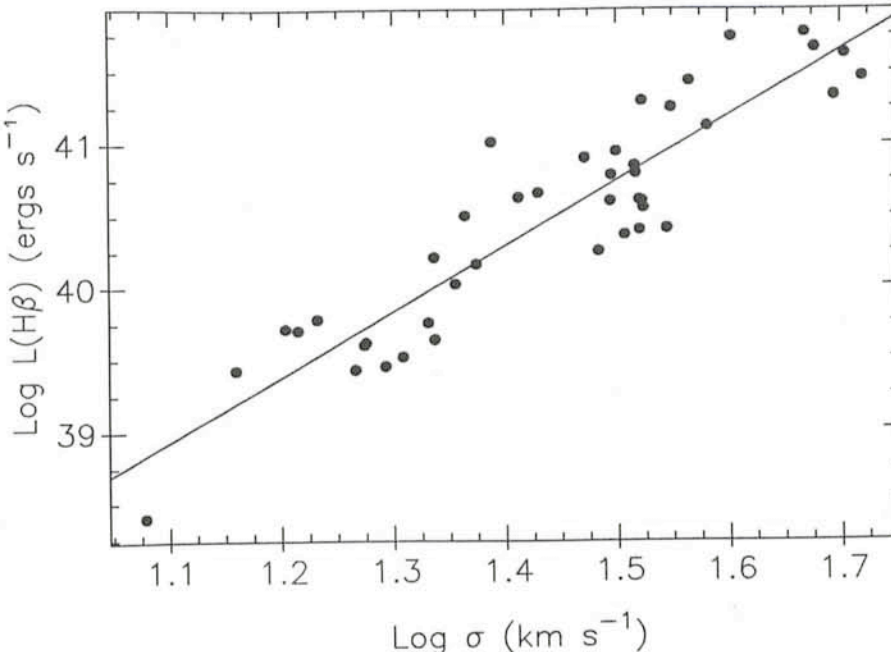


Figure 1: Logarithmic plot of the integrated  $H_{\beta}$  luminosities of HII galaxies as a function of their line-profile widths in velocity units.  $H_0 = 100 \text{ km/sec/Mpc}$  is assumed.

20 Mpc where the angular diameters of even the largest giant HII regions become comparable with the seeing disks. However, the linear diameters of giant HII regions correlate very well with the widths of the nebular emission lines, which in these bright HII regions are extremely easy to measure.

Thus, replacing HII region diameters by line-widths in the Sersic-Sandage correlations, a new powerful distance indicator is obtained. However, the emission line profile widths also correlate extremely well with the luminosities of giant HII regions and this correlation has the advantages (over the previous ones) that it does not require inclination corrections for the magnitudes of the parent galaxies and that the reddening corrections to the giant HII region luminosities can be done in a self-consistent way using the Balmer decrements. Thus, the method I am going to discuss here relies on the correlation between  $H_{\beta}$  luminosity ( $L(H_{\beta})$ ), the emission line-profile widths ( $\sigma$ ) and the Oxygen abundances ( $O/H$ ) of giant HII regions.

Since, to obtain a meaningful value of  $H_0$ , we must observe galaxies beyond the Virgo cluster we have applied the method not to giant HII regions in distant spiral galaxies (which would be too faint) but to the so-called "intergalactic HII regions" or "HII Galaxies" which may be defined as being dwarf galaxies with the spectrum of giant HII regions. In fact, while some HII galaxies are clearly dwarf irregular galaxies with one

obtained with the 3.6-m and 2.2-m telescopes at La Silla and the line-widths with the Echelle spectrograph at the 4-m telescope of Cerro Tololo.

The slope of the correlation is  $4.5 \pm 0.3$  and rms scatter is  $\delta \log L(H_{\beta}) = 0.32$  but the dispersion is correlated with the chemical composition of the nebular gas. A Principal Component Analysis of the data leads to the following relation.

$$\log L(H_{\beta}) = 5 \log \sigma - \log(O/H) + \text{constant}$$

Figure 2 presents a plot of  $L(H_{\beta})$  versus the distance independent parameter  $M_z = \sigma^5/(O/H)$  for 29 HII galaxies with accurate metallicities.

The linear fit to the data has a slope of  $1.03 \pm 0.05$  and an rms scatter of  $\delta \log(L(H_{\beta})) = 0.21$ , which is comparable to the scatter of the Tully-Fisher relation. Since HII galaxies can be easily observed out to very large distances, the correlation between  $L(H_{\beta})$  and  $M_z$  can indeed be a very useful cosmic yardstick provided its zero point can be accurately determined.

As I discussed above, the extragalactic distance scale is tied to the galactic scale via cepheid variables. Thus, in order to calibrate the zero point of the  $(L(H_{\beta}), M_z)$  relation for HII galaxies we must use giant HII regions in nearby spiral galaxies. The properties of many such HII regions have been extensively studied mainly by Sandage and Tamman who used the Sersic-Sandage correlation to calibrate distances.

## Giant HII regions

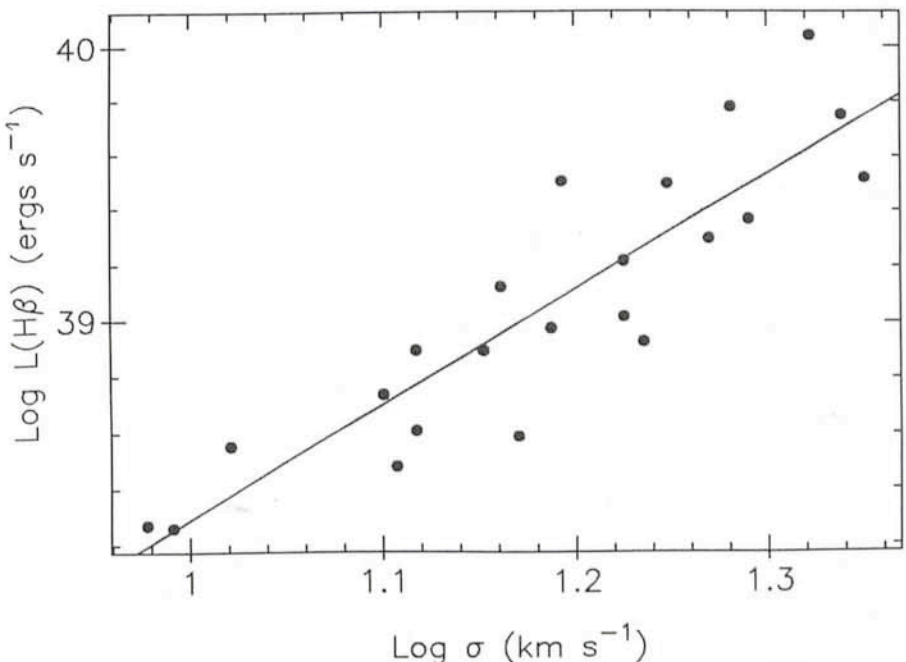


Figure 2: Logarithmic plot of the integrated  $H_{\beta}$  luminosities of giant HII regions in nearby galaxies as a function of line-profile width.

TABLE 1: The local distance scale

Galaxy	Number of HII regions	Distance adopted	(Kpc) ST	Notes
LMC	1	50.1	52.2	Local Group
SMC	1	60.0	71.4	Local Group
NGC 6822	2	457	616	Local Group
M 33	4	682	817	Local Group
NGC 2366	3	3160	3250	M81 group
NGC 2403	3	3160	3250	M81 group
Holmb II	1	3160	3250	M81 group
IC 2574	2	3160	3250	M81 group
NGC 4236	2	3160	3250	M81 group
M101	3	6920	6920	

We have studied the correlations between internal parameters for 22 giant HII regions in galaxies whose distances have been determined from studies of Cepheid variables. Table 1 summarizes the relevant parameters of these galaxies together with the distances we have adopted. Also listed in the Table are the distances adopted by Sandage and Tammann (ST) in their calibration of the Hubble constant.

In a few cases there are differences between the scale adopted here, which is essentially the scale adopted by Aaronson and co-workers in their calibration of the Tully-Fisher relation, and the Sandage-Tammann scale. These discrepancies have to do with the way in which the Cepheid luminosities are corrected for extinction in their parent galaxies and, although the local distance scale is still the subject of considerable controversy, its discussion is far beyond the scope of this article.

Figure 3 shows a logarithmic plot of  $L(H_{\beta})$  versus  $\sigma$  for giant HII regions. The slope of this relation is  $4.2 \pm 0.5$  and the rms scatter is  $\delta \log(L(H_{\beta})) = 0.23$ .

A Principal Component Analysis (PCA) for HII regions shows again the presence of 3 parameters of the form,

$$\log L(H_{\beta}) = \log RC \sigma^2 - \log(O/H) + \text{constant}$$

where  $Rc$  is a measure of the radius of giant HII regions introduced by Sandage and Tammann which they called the core radius. This relation cannot be directly compared with HII galaxies because we lack core radii for these distant objects. However, in giant HII regions, the core radii correlate with velocity dispersion approximately as  $Rc \sim \sigma^3$ . Thus, the parameter  $Rc \sigma^2$  is equivalent to the parameter  $\sigma^5$  which we found for HII galaxies. Indeed, the PCA analysis of HII galaxies in the  $(L(H_{\beta}), \sigma^5, O/H)$  domain and of giant HII regions in the  $(L(H_{\beta}), R_c \sigma^2, O/H)$  domain give essentially identical eigenvalues and eigenvectors.

This leads us to conclude that, independently of the mass of the parent

galaxies, the global luminosities of giant HII regions are a function only of their velocity dispersion, radii and chemical composition. Moreover, the  $RC\sigma^2$  dependence is strongly reminiscent of the Virial theory and Terlevich and I have proposed that giant HII regions are gravitationally bound objects, in which case the correlations would have a very simple physical interpretation. But, as almost everything in astronomy, this interpretation is controversial and its discussion will take us far from our present goal of getting to  $H_0$ .

From the  $(L(H_{\beta}), Mz)$  relation for giant HII regions we obtain a zero point of  $41.32 \pm 0.08$  and therefore the cosmic yardstick for HII galaxies is the equation,

$$\log L(H_{\beta}) = \log \frac{\sigma^5}{(O/H)} + 41.32$$

The distances for HII galaxies can then be obtained by comparing the

luminosities predicted by this equation to the observed fluxes corrected for extinction. Before discussing the results, however, I must say a few words about radial velocities and about Malmquist bias.

### Corrections . . .

#### (a) The Radial Velocities

If one knows velocities and distances,  $H_0$  is simply obtained as  $H_0 = V/R$ . The radial velocity of almost any galaxy can be easily obtained with present-day instrumentation from the Doppler shift of their spectral features. In the case of HII galaxies, for example, even at large distances the Doppler shifts of the emission lines can be obtained with exposures of only a few seconds. However, the Earth, the Sun and the Galaxy are moving and therefore we must subtract from the observed velocities the motion of our frame of reference. Thus, we must remove the motions of the Sun around the centre of our Galaxy, of the Galaxy in the Local Group, of the Local Group towards the Virgo Cluster and of the Virgo Cluster relative to the Cosmic Microwave Background. In addition, the galaxies themselves may be falling into Virgo or drifting relative to the Cosmic Microwave Background and these peculiar velocities must also be removed to extract the purely expansional velocities. Our radial velocities incorporate all these corrections with the exception of streaming motions relative to the Microwave Background which at

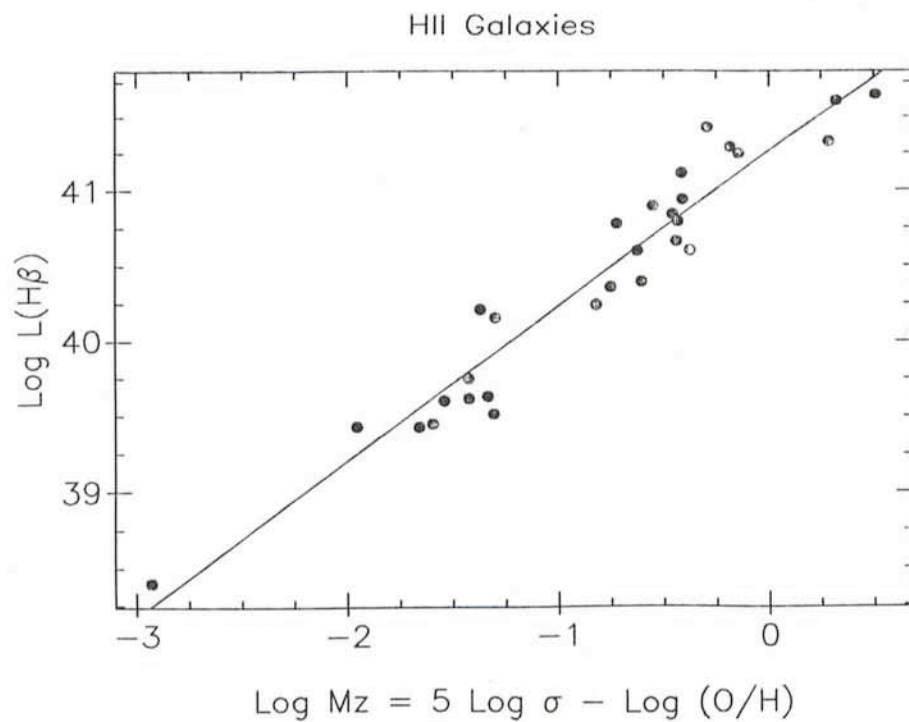


Figure 3: Logarithmic plot of integrated  $H_{\beta}$  luminosity as a function of the distance indicator  $Mz$ .  $O/H$  is the oxygen abundance of the nebular component.

present are very poorly understood. The most recent results tend to show that as far as they can be observed, all galaxies move relative to the CMWB with a velocity of several hundred kilometres per second in the direction of Centaurus. Thus, it is not clear at what distance one should start correcting the velocities for this effect or if one should correct them at all!

### (b) Malmquist Bias

This is an unpleasant effect which has caused and continues to cause endless troubles to those who engage in the quest for the Hubble constant. Malmquist bias occurs because all correlations used to determine distances have considerable cosmic scatter. So if one selects galaxies which are brighter than a certain limiting value, close to this value one tends to observe galaxies which are systematically brighter than the luminosities one would predict from the distance indicator in the absence of bias. This causes the distances to be biased towards lower values.

I am very fortunate to have Edmond Giraud ("Mr. Malmquist Bias") next doors who showed me how to correct magnitude limited samples for this effect. Because at any distance HII galaxies span a very large range of luminosities, and because there are luminous HII galaxies at small distances, the Malmquist effect on the distance indicator is, as we shall see, very small.

### The Hubble Constant from Giant HII Regions

The resulting values for  $H_0$  are given in Table 2 for different redshift cuts of the data.

The errors quoted are  $1\sigma$  deviations from the mean of all galaxies and do not include the zero point error. When this is included, our best estimate is  $H_0 = 85 \pm 10$  km/sec/Mpc. this value compares very well with the value of  $H_0 = 92 \pm 1$  found by Aaronson and co-workers using the Tully-Fisher relation (the error they quote does not include zero point uncertainties). Our value disagrees with the value of  $H_0 = 50 \pm 7$  km/sec/Mpc obtained by Sandage and Tamman. If we use the Sandage-Tamman local distance scale (Table 1) we obtain a value of  $78 \pm 10$  which still disagrees at the  $3\sigma$  level with  $H_0 = 50$ .

### Caveats

Recently, a well-known cosmologist told me: "Your results are very nice, so... what's wrong with them?" What he meant, of course, was that I had

TABLE 2: *The Hubble constant*

Redshift range	$\langle H_0 \rangle$ km/sec/Mpc	Malmquist correction	Number of galaxies
Full sample	$94 \pm 5$	-11	29
Excluding Virgo	$97 \pm 5$	-12	24
Redshift > 2000	$99 \pm 5$	-14	21
Redshift > 4000	$102 \pm 6$	-16	16

obtained the wrong value for  $H_0$ . This illustrates the philosophical prejudices involved in cosmology; this is only natural because Cosmology reaches the boundary between science and religion. Personally, I find the story of Adam and Eve more elegant and easier to believe than the Big-Bang!

Nevertheless, observers must forsake philosophical and theoretical prejudices in the analysis of the weak points of our own data. In the case of giant HII regions, the caveat is that the  $H_\beta$  luminosities of some HII galaxies may come from more than one giant HII region superimposed along the line of sight. This would not only bias the luminosities towards larger values but also introduce the gravitational potential of the parent galaxies as an additional parameter. As far as we can tell from deep CCD pictures and spatially resolved spectroscopy, the effect of multiplicity in our sample is small. The fact that the scatter of the HII galaxy correlations is similar to that exhibited by the giant HII region sample lends strong support to this conclusion.

It is clear, however, that if the emission-line component of all HII galaxies consisted of four identical giant HII regions of exactly the same redshift superimposed along the line of sight we would not distinguish them from single objects but our value of  $H_0$  would be overestimated by a factor of 2!

### Epilogue

A large value of  $H_0$  is only one of a number of new observations which are beginning to erode the old edifice of Big-Bang cosmology. Inflation, dark matter, superstrings and other scaffoldings are being used to save the "standard" Big-Bang but in the end it will surely fall. This should not worry us, for we know that new buildings are always more solid than old structures. Unfortunately, however, there are very few modern buildings that are nicer than the old ones they replace.

### References

For the sake of brevity I have not included formal references to the work I quoted. I have based the discussion on

the following works where complete lists of references can be found:

- (1) R. Kippenhahn: *Light from the Depths of Time* (Springer) for the history of the Hubble constant.
- (2) A. Sandage: "The Dynamical parameters of the Universe", in First ESO/CERN Symposium, *Large Scale Structure of the Universe, Cosmology and Fundamental Physics*, p. 127, for a modern account of the quest for the Hubble constant and the defence of  $H_0 = 50$ .
- (3) M. Aaronson and co-workers in *Astrophysical Journal* Vol. 302, p. 536 (1986) for a detailed discussion of the Tully-Fisher method, the various radial velocity corrections and a defence of the  $H_0 = 100$  view.
- (4) J. Melnick and co-workers in ESO preprint number 440 (1986) for a discussion of the use of giant HII regions as distance indicators.

## Visiting Astronomers

(April 1–October 1, 1987)

Observing time has now been allocated for Period 39 (April 1–October 1, 1987). The demand for telescope time was again much greater than the time actually available.

The following list gives the names of the visiting astronomers, by telescope and in chronological order. The complete list, with dates, equipment and programme titles, is available from ESO-Garching.

### 3.6-m Telescope

**April:** Martinet/Jarvis/Pfenniger/Bacon, Franz/Illingworth, Illovaisky/Chevalier/v.d. Klis/v. Paradis/Pedersen, Mathys/Stenflo, Francois/Spite M/Spite F, Jeffery/Hunger/Heber/Schönberner, Hunger/Heber/Werner/Rauch, Miley/Macchetto/Heckman, Kollatschny/Fricke, Maccagni/Vettolani.

**May:** Maccagni/Vettolani, Keel, Ortolani/Rosino, Cacciari/Clementini/Prévôt/Lindgren, Barbuy/Ortolani/Bica, Gratton/Ortolani, Lub/de Geus/ Blaauw/de Zeeuw/Mathieu, Cacciari/Clementini/Prévôt/Lindgren, Moorwood/Oliva, Danziger/Oliva/Moorwood, Tapia/Persi/Ferrari-Toniolo/Roth, Lacombe/Léna/Rouan/Slezak.

**June:** Lacombe/Léna/Rouan/Slezak, Chelli/Reipurth/Cruz-G., Richichi/Salinari/Lisi, Zinnecker/Perrier, Perrier/Mariotti, Habing/van der Veen, Sicardy/Brahic/Lecacheux/

Roques/Le Borgne/Barucci, Azzopardi/Rich, Azzopardi/Lequeux/Rebeiro/Rich, Baessgen M/Baessgen G/Grewing/Bianchi.

**July:** Baessgen M/Baessgen G/Grewing/Bianchi, Seitter, Angebault/Pakull/Beuermann/Motch, Barwig/Häfner/Mantel/Schoembs, Bertola/Guzzo, Schulz/Schmidt-Kaler, Metz/Häfner/Barwig, Schoembs/Roth, Houziaux/Kameswara Rao.

**August:** Houziaux/Kameswara Rao, D'Odorico/Pettini, Pizzichini/Pedersen, De Lapparent/Mazure, Sparks/Macchietto.

**September:** Ardeberg/Lindgren/Lundström, Webb/Vidal-Madjar/Carswell/Ferlet, Wolf/Baschek/Scholz/Krautter/Reitermann, Fosbury/Robinson/Danziger, Guzzo/Focardi, Rocca-Volmerange/Azzopardi/Guideroni/Roland, Danziger/Gilmozzi/Griffiths/Ward, Shaver/Clowes/Iovino/Cristiani, Christiani/Barbieri/Iovino/Nota, Wampler.

## 2.2-m Telescope

**April:** Le Bertre/Chelli/Perrier, Martinet/Jarvis/Pfenniger/Bacon, Jarvis/Martinet, Arpigny/Dossin/Manfroid/Häfner, Vreux/Manfroid/Magain, Trefzger/Grenon, Reinsch/Pakull/Festou, Gouffes/Cristiani, Loose/Thuan/Kollatschny, Röser/Hiltner/Meisenheimer, Magain/Courvoisier/Kühr/Surdej/Swings/Djorgovski, Schmutz/Hamann/Nussbaumer/Smith/Vogel.

**May:** Schmutz/Hamann/Nussbaumer/Smith/Vogel, Le Bertre/Chelli/Perrier, Galletta, Reipurth/Zinnecker, Seggewiss/Moffat, Gouffes/Cristiani, Reinsch/Pakull/Festou, Capaccioli, Paresce/Burrows/Vidal-Madjar, Christensen/Sommer-Larsen, de Jong/v.d. Broek/Lub.

**June:** de Jong/v.d. Broek/Lub, Courvoisier/Melnick/Mathys/Binette/Maeder.

**July:** de Vries/Verter/Habing, Gouffes/Cristiani, Binette/Fosbury/Courvoisier, Magain/Courvoisier/Kühr/Surdej/Swings/Djorgovski, Fusi, Pecci/Buonanno/Corsi/Ferraro, Ulrich, Metz/Häfner/Barwig/Schoembs/Roth.

**August:** Metz/Häfner/Barwig/Schoembs/Roth, Schwarz/Aspin/Magalhaes/Schulte-Ladbeck, Chini/Krügel, Gouffes/Cristiani, Skillman/Melnick/Terlevich, Prugniel/Davoust/Nieto, Pizzichini/Pedersen, Ortolani/Piotto/Rosino, v. Paradis/Pedersen.

**September:** v. Paradis/Pedersen, Schwope/Beuermann, Coyne/Magalhaes, Danziger/Dalgarno, Stanga/Rodriguez-E./Binette, Leitherer/Appenzeller, Westerlund/Azzopardi/Breysacher/Rebeiro, Véron, Getty-Véron, Lortet/Testor.

## 1.5-m Spectrographic Telescope

**April:** Rafanelli/Marziani, Trefzger/Grenon, Mathys/Maeder, Courvoisier/Bouchet, Rosa/Richter, Kollatschny/Hellwig.

**May:** Kollatschny/Hellwig, Schmutz/Hamann/Hunger/Wessolowski, Arpigny/Dossin/Manfroid/Häfner, de Jager/Nieuwenhuijzen, Pottasch/Pecker/Karaji/Sahu, Bues/Rupprecht/Pragal, Quintana/de Souza.

**June:** Quintana/de Souza, Schulte-Ladbeck/Krautter, van Genderen/Thé, Tozzi/Donati-Falchi/Falcianni/Smaldone, Alloin/Pelat/Phillips M/Phillips D, Hunt/Trinchieri,

Alloin/Pelat/Phillips M/Phillips D, Pauls/Kohoutek.

**July:** Pauls/Kohoutek, Acker/Stenholm/Lundström, Reichen/Lanz/Golay, Courvoisier/Bouchet, Metz/Häfner/Barwig/Schoembs/Roth, Kameswara Rao/Nandy, Alloin/Pelat/Phillips M/Phillips D.

**August:** Alloin/Pelat/Phillips M/Phillips D, Kameswara Rao/Nandy, Mantegazza, Magain, Alloin/Pelat/Phillips M/Phillips D, Tanzi/Bouchet/Falomo/Treves.

**September:** Alloin/Pelat/Phillips M/Phillips D, Balkowski/Proust/Talavera, Alloin/Pelat/Phillips M/Phillips D, Lortet/Testor.

## 1.4-m CAT

**April:** Vreux/Manfroid/Magain, Arpigny/Dossin/Manfroid/Häfner, Baade, Lucy/Baade, Malaney, Gustafsson/Edvardsson/Magain/Nissen.

**May:** Gustafsson/Edvardsson/Magain/Nissen, Arpigny/Dossin/Manfroid/Häfner, de Jager/Nieuwenhuijzen, Pottasch/Sahu, Pottasch/Srinivasan/Sahu/Desai, Ferlet/Vidal-Madjar/Gry/Lallement, Andreani/Ferlet/Vidal-Madjar, Lagrange/Ferlet/Vidal-Madjar, Reipurth/Lago.

**June:** Reipurth/Lago, Baade/Stahl, Mandolesi/Palazzi/Crane/Hegyi, Crane/Blades/Palazzi, Crane/Blades/Mandolesi/Palazzi, Crane/Palazzi/Lambert, de Vries/van Dishoeck/Habing.

**July:** de Vries/van Dishoeck/Habing, Thé/Tjin A Djie/Monderen, Waelkens, Foing/Beckman/Castelli/Crivellari/Vladilo.

**August:** Crivellari/Beckman/Arribas/Castelli/Vladilo/Foing, Foing/Beckman/Castelli/Crivellari/Vladilo, Chmielewski/Lambert, Magain, Lenhart/Grewing/Beck.

**September:** Lenhart/Grewing/Beck, da Silva/Spite F/Vieira Costa, Burkhardt/Coupry/van't Veer.

## 1-m Photometric Telescope

**April:** Le Bertre/Chelli/Perrier, Schultz, Persi/Preite-Martinez/Ferrari-Toniolo, Reinsch/Pakull/Festou, Mermilliod/Claria, Jockers/Geyer.

**May:** Jockers/Geyer, Reinsch/Pakull/Festou, Silvestro/Busso/Roberto/Scaltriti, de Jager/Nieuwenhuijzen, Cacciari/Clementini/Prévôt/Lindgren, Reinsch/Pakull/Festou, Fischerström/Lindroos/Liseau, Bues/Rupprecht/Pragal.

**June:** Tapia/Persi/Ferrari-Toniolo/Roth, Richichi/Salinari/Lisi, Reipurth/Zinnecker, Perrier/Mariotti, van Genderen/Thé, Habing/van der Veen/Geballe, Courvoisier/Bouchet, Bouchet/Cetty-Véron/Véron, Antonello/Conconi/Mantegazza/Poretti.

**July:** Antonello/Conconi/Mantegazza/Poretti, Kroll/Catalano F, Courvoisier/Bouchet, Spinoglio/Persi/Ferrari-Toniolo/Coe, Barwig/Häfner/Ritter/Schoembs/Mantel, Magain.

**August:** Magain, Braz/Epcstein, Wargau/Chini, Steiner/Jablonski/Cieslinski, Barucci/Fulchignoni/Harris/Zappalà/Di Martino/Binzel/Lagerkvist.

**September:** Barucci/Fulchignoni/Harris/Zappalà/Di Martino/Binzel/Lagerkvist, Clementini/Cacciari/Prévôt/Lindgren, Bergvall/Johansson/Olofsson, Liller/Alcaino.

## 50-cm ESO Photometric Telescope

**April:** Manfroid/Vreux/Magain, Mekkaden/Geyer, Kohoutek.

**May:** Kohoutek, Fischerström/Lindroos/Liseau, Manfroid/Arpigny/Häfner/Sterken.

**June:** van Genderen/Thé, Thé/Westerlund, Busso/Scaltriti/Corcione/Silvestre.

**July:** Busso/Scaltriti/Corcione/Silvestre, Group for Long Term Photometry of Variables.

**August:** Metz/Häfner/Barwig/Schoembs/Roth, Group for Long Term Photometry of Variables.

**September:** Group for Long Term Photometry of Variables.

## GPO 40-cm Astrograph

**April:** Scardia.

**May:** Scardia, Böhnhardt/Drechsel/Kohoutek.

**July:** Seitter/Duerbeck/Horstmann, Dommanget.

**August:** Dommanget, Elst/Ivanova/Shkodrov/Geffert.

**September:** Elst/Ivanova/Shkodrov/Geffert, Debehogne/Machado/Caldeira/Vieira/Netto/Mourao/Zappalà/De Sanctis/Lagerkvist/Protitch-Benishek/Javanshir.

## 1.5-m Danish Telescope

**April:** Leibundgut/Tammann, Rasmussen/Möller, Reipurth.

**May:** Reipurth, Sinachopolus, Arsenault/Roy, Ortolani/Gratton, Reimers/Koester/Schröder, Giraud.

**June:** Giraud, de Jong/v.d. Broek/Lub, Christensen, Reiz/Pirola.

**July:** Reiz/Pirola, Veillet/Dourneau/Oberti/Mignard/Martins/Lazzaro, Griffin RF/Griffin REM/Mayor/Clube, Mayor/Duquennoy/Andersen/Nordström, Collins/Stobie/MacGillivray/Heydon-Dumbleton/Shanks, Schulz/Schmidt-Kaler, Castellani/Calo, v. Paradis/v.d. Klis.

**August:** Rasmussen/Möller.

**September:** Ardeberg/Lindgren/Lundström, Clementini/Cacciari/Prévôt/Lindgren, Trefzger/Mayor/Pel, Grenon/Mayor.

## 50-cm Danish Telescope

**April:** Franco.

**May:** Olsen/Gray, Grenon/Hög/Petersen.

**June:** Waelkens/Cuypers.

**July:** Waelkens/Cuypers, Verschueren/Sterken/Hensberge.

**August:** Ardeberg/Lindgren/Lundström.

**September:** Ardeberg/Lindgren/Lundström.

## 90-cm Dutch Telescope

**April:** van Genderen/van der Hucht/Röttgering.

**May:** de Jager/Nieuwenhuijzen, Trefzger/Pel/Blaauw, de Zeeuw/Lub/de Geus/Blaauw.

**June:** de Zeeuw/Lub/de Geus/Blaauw.

**July:** Grenon/Lub, Waelkens/Heynderickx.

**August:** Waelkens/Heynderickx.

## 61-cm Bochum Telescope

- June: Pauls/Kohoutek, Barwig/Häfner/Ritter/Schoembs/Mantel.  
July: Barwig/Häfner/Ritter/Schoembs/Mantel.  
September: Debehogne/Di Martino/Zappalà/Di Sanctis.

## Italian Delegation Visits ESO

An Italian delegation, headed by the Italian Ambassador to the Federal Republic of Germany, His Excellency Prof. Luigi Vittorio Ferraris, and the Acting Italian Consul General in Munich, Dr. Lelio Crivellaro, visited the ESO Headquarters in the afternoon of January 14, 1987. After a show of the ESO film, the delegation had the opportunity to familiarize itself with a variety of sci-



entific and technical activities at ESO. This photo was taken in the Optical Laboratory (from left to right: Prof. Wolfgang Alles, Scientific Attaché at the Italian Embassy in Bonn; the Consul General; Prof. Giancarlo Setti, ESO; the Ambassador; Ms. Ursula Geiger, Italian General Consulate in Munich; Prof. Romano Toschi, Director of the NET Project, MPI, Garching).

## List of ESO Preprints

December 1986–February 1987

476. T.J.-L. Courvoisier et al.: The Radio to X-ray Continuum emission of the Quasar 3C 273 and its Temporal Variations. *Astronomy and Astrophysics*. December 1987.
477. T. Le Bertre: The Opacity of the Dust Around Carbon Star IRC+10216. *Astronomy and Astrophysics*. December 1986.
478. S. Cristiani and B. Koehler: Redshifts of Quasar Candidates. *Astronomy and Astrophysics*. December 1986.
479. T. Le Bertre and N. Epcstein: Optical and Infrared Observations of Two Oxygen Rich Unidentified IRAS Sources. *Astronomy and Astrophysics*. December 1986.
480. D. Baade and L.B. Lucy: A Search for Coronal Line Emission from Early-type Stars. I. Zeta Puppis. *Astronomy and Astrophysics*. January 1987.
481. E.J. Wampler: Observational Study of the Hubble Diagram. *Astronomy and Astrophysics*. January 1987.
482. C.N. Tadhunter et al.: Detached Nuclear-like Activity in the Radio Galaxy PKS 2152-69. *Nature*. January 1987.
483. J.-L. Nieto, A. Llebaria and S. di Serego Alighieri: Photon-counting Detectors in Time-resolved Imaging Mode: Image Recentering and Selection Algorithms. *Astronomy and Astrophysics*. January 1987.
484. R.N. Wilson, F. Franz and L. Noethen: Active Optics I: A System for Optimizing the Optical Quality and Reducing the Costs of Large Telescopes. *Optica Acta*. January 1987.
485. E. Brocato and V. Castellani: Evolutionary Constraints for Young Stellar Clusters: I. The Luminosity Function of H-Burning Stars. *Astronomy and Astrophysics*. February 1987.
486. M. Azzopardi: Small Magellanic Cloud: Hy Equivalent Widths and Luminosity Classes of the Brightest Blue Star Members. *Astronomy and Astrophysics Supplement Series*. February 1987.
487. A. Tornambè and F. Matteucci: Subluminous Type I SNe: Their Theoretical Rate in Our Galaxy and in Ellipticals. *Astrophysical Journal*. February 1987.
488. O. Stahl, B. Wolf and F.-J. Zickgraf: Photometry and Spectroscopy of the Eclipsing P Cygni Star R 81 of the Large Magellanic Cloud. *Astronomy and Astrophysics*. February 1987.
489. G.A. Tammann: The Cosmic Distance Scale. February 1987.
490. A. Robinson et al.: Emission Line Activity in Radio Galaxies. *Monthly Notices of the Royal Astronomical Society*. February 1987.

### First Announcement

A conference organized by NOAO (National Optical Astronomical Observatories) and ESO on

### High-Resolution Imaging by Interferometry

will be held from 15 to 18 March 1988 at ESO in Garching, FRG.

The scope of this conference is ground-based interferometry at visible and infrared wavelengths.

The programme will include the following topics:

- Scientific Goals
- Interferometric Imaging with Single-Dish Telescopes
- Ground-Based Long-Baseline Interferometer Projects
- Methods for Reconstructing Images and Spectral Information from Optical Long-Baseline Interferograms

For more information please write to F. Merkle, European Southern Observatory, Karl-Schwarzschild-Str. 2, D-8046 Garching bei München, Federal Republic of Germany.

# Long-term Photometric Campaign at ESO and the New Eclipsing P Cygni Star R 81 in the LMC

B. WOLF<sup>1</sup>, C. STERKEN<sup>2</sup>, O. STAHL<sup>3</sup> and J. MANFROID<sup>4</sup>

<sup>1</sup>Landessternwarte Heidelberg, <sup>2</sup>Vrije Universiteit Brussels, <sup>3</sup>ESO, <sup>4</sup>Université de Liège

## 1. A Programme for Long-term Photometry of Variable Stars

At the ESO workshop *The Most Massive Stars* in November 1981 (Eds. D'Odorico, Baade and Kjær), C. Sterken presented results of his observations of HD 160529 during a time span of more than 8 years. HD 160529 is an A2 hypergiant which was found to be variable by Wolf et al. (1974) in an irregular way with an amplitude of several hundredths of a magnitude. Sterken continued the monitoring of this star at every possible occasion in the period 1973–1981 and found evidence for the presence of periodic light variation of about 100 days. From the phase diagram he concluded that in spite of the intensive observations by one person, there still remain long gaps in the phase diagram. If sampling of observations happens in such an irregular way (gaps caused by irregularly allocated short observing runs), long-term orbital effects may be hidden by or ascribed to the supergiant's irregular intrinsic fluctuations. It was therefore suggested that the observations of e.g. variable supergiants be done by a larger team of observers at a dedicated small instrument. Such an approach would also be very useful for all differential photometry on a basis of one measurement per night or less: supergiants, Be stars, Ap stars . . .

During the discussions following the talk, several colleagues expressed their interest in the idea, and by the end of the Workshop, the project *Long-term Photometry of Variables* was born. In February 1982 a meeting was held at the University of Brussels, and the project finally started with an application for observing time submitted in April 1982. The participants (originally about 15) merged the objects for which photometry on a long-time basis was needed into one object list of about 70 entries, and then the file was split in seven sections according to the nature of the variable stars (see Sterken, 1983). Later on, an eighth section (Peculiar Late Type Stars) was added. For each section a principal investigator and a co-investigator were appointed. These scientists decide about which objects need monitoring, and they carry out and/or supervise the analysis of the data of the stars belonging to their sections. We agreed that the observers would be volunteering par-

ticipants who work in a tight team with the principal investigators. From the beginning we aimed at obtaining several months of observing time each observing season, and this for a time span of at least one decade.

A project of that size, including the interpretation of measurements obtained at different telescopes and by different observers cannot work without a strict agreement on observing procedures and reduction techniques. Especially for what concerns the data reduction, high requirements are needed so that the final data may be of the highest obtainable accuracy. It was decided that all reductions would be done centrally (and not by the individual observers) at the University of Liège by J. Manfroid. The reduction algorithm is a generalized method developed by Manfroid and Heck (1983) and is characterized by the use of practically every measurement of any non-variable star. In doing so, all measurements are transformed into a standard system and the observations obtained during different seasons and with different instruments can be re-evaluated regularly so that the homogeneity of the data is assured.

Because of the availability of the suitable photometers on the ESO 50 cm and the Danish 50 cm telescopes, and for the usefulness for astrophysical interpretation of the data, we decided to carry out all measurements in the Strömgren uvby system. Since we deal with variable stars, preference was given to differential measurements with two comparison stars (although we have also carried out absolute measurements).

In practice the participants may expect to receive their data not later than three to six weeks after termination of the observing run. Since 1982 the number of participants has doubled, and this is also so for the number of stars. At least 30 stars, for which enough data were obtained, have been omitted from the object list. 26 observing runs with a duration of about one month length each have already been allotted by ESO and a huge amount of data are already available. The results have already led to more than 20 published scientific papers.

The nature of some discoveries (like e.g. the binary nature of R 81 which is described below) clearly proofs that this

approach is a very efficient and useful one. Besides the direct yield of data, the project also offers to young scientists (e.g. Ph.D. students) the possibility to get into contact with the fields of research of the other participants, which substantially contributes to their observational experience.

## 2. R 81, the Counterpart of P Cyg in the LMC

P Cygni is one of the most outstanding stars of the Galaxy. It had a remarkable outburst in 1600 and is particularly distinguished by its unusual spectrum. The so-called P Cygni profiles in the visual range (which have been discovered already in the 19th century) are named after this prototype and indicate that this star is losing mass at an excessive rate. P Cygni belongs to the luminous ( $M_{bol} \approx -9$  to  $-11$ ) blue variables (LBV's) which have been recognized during the past few years as key-objects for the understanding of the evolution of the very massive (initial masses  $\geq 50 M_{\odot}$ ) stars. According to current evolutionary models (cf. e.g. Humphreys 1986, Chiosi and Maeder 1986) these very massive stars do not become red supergiants; instead a critical luminosity boundary exists (called Humphreys Davidson limit) beyond which the most luminous stars do not evolve. The LBV's are located close to this boundary and are supposed to be the immediate progenitors of the Wolf-Rayet stars.

The physical properties of P Cygni have been scrutinized during the past few years at a wide wavelength range from the UV with IUE to the IR with IRAS! A drawback of P Cygni is that both its interstellar reddening and its distance are difficult to determine (see e.g. Lamers, de Groot and Cassatella 1983). For this reason we searched the zoo of the luminous blue supergiants of the Large Magellanic Cloud (LMC). As outlined e.g. in our recent atlas of high dispersion spectra of luminous LMC stars (Stahl et al. 1985) the P Cygni type stars form in fact a populous group among the peculiar emission line stars.

Already in 1981 Wolf et al. presented a detailed spectroscopic and photometric study of R 81 of the LMC. R 81 turned out to be a particularly close counterpart of the galactic star P Cygni.

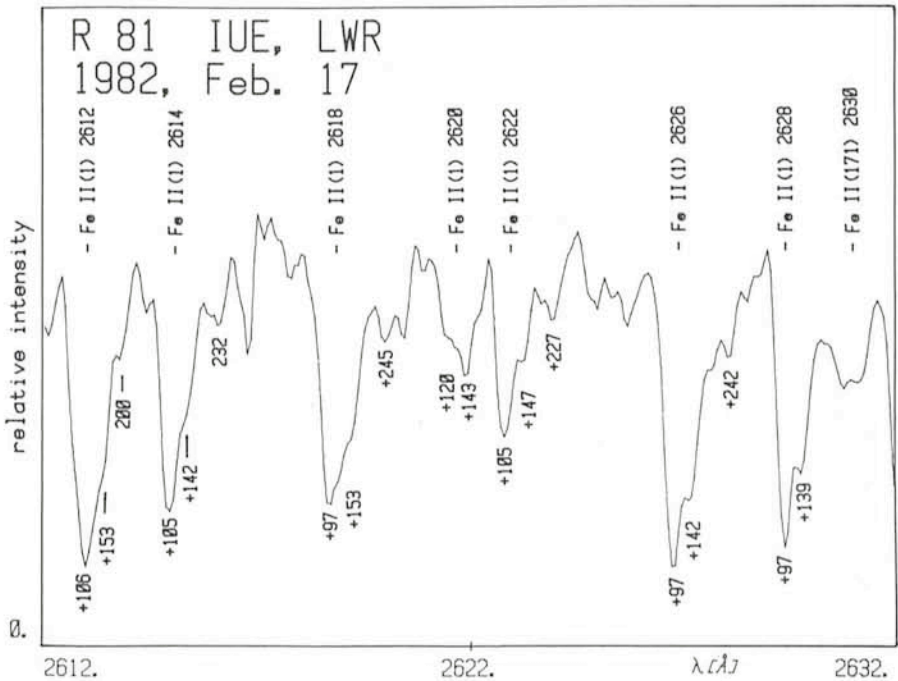


Figure 1: A section of the IUE high-dispersion spectrogram around 2600 Å. This wavelength range is dominated by Fe II absorption lines. Like in P Cyg, different components are present. The velocities of these components are indicated for different lines.

Both stars are (of course) characterized by strong P Cygni profiles of the Balmer lines and by very similar stellar parameters:  $T_{\text{eff}} \approx 20,000$  K,  $M_{\text{bol}} \approx -10$ , and  $R \approx 70 R_{\odot}$  for R 81 and  $T_{\text{eff}} \approx 19,300$  K,  $M_{\text{bol}} \approx -9.9$ , and  $R \approx 76 R_{\odot}$  for P Cygni (for the data for P Cyg see Lamers et al. 1983). They are located in the same part

of the Hertzsprung-Russell Diagram (HRD) close to the Humphreys-Davidson limit. The winds of both stars are slow ( $v_{\text{max}} \approx 250$  to  $300$  km s $^{-1}$ ) and very massive ( $\dot{M} \approx 3 \cdot 10^{-5} M_{\odot}$  yr $^{-1}$  for R 81 and  $\dot{M} \approx 1.5 \cdot 10^{-5} M_{\odot}$  yr $^{-1}$  for P Cyg). Like P Cyg (Waters and Wesselius 1986) R 81 is surrounded by a cool loosely

bound dust envelope since Stahl et al. (1987) identified R 81 as an IRAS point source. The dust formation could be a consequence of their slow and dense winds.

One of the most paradoxical results derived from the IUE spectrum of P Cygni (Cassatella et al. 1979) is that this hot star with its unusual P Cygni profiles in the visual range is right the other way distinguished by a lack of P Cygni profiles in the ultraviolet (which are otherwise so typical for hot stars in this range). Just this behaviour is found in the case of R 81 as well. Still more intriguing is the fact that e.g. the Fe II lines of both stars agree even in details. The complex profiles show a multiple component structure (for R 81 see Fig. 1) ascribed to the ejection of discrete shells (cf. Lamers et al. 1985 and Stahl et al. 1987).

In addition to the major historical outbursts of P Cygni in the 17th century, irregular photometric variations of 0.1 to 0.2 magnitude have been reported during this century by many authors. No strict periodicity has yet been found (van Gent and Lamers 1986). Likewise in the case of R 81, which until 1980 was repeatedly observed during various randomly distributed photometric observing runs, variations of about this amplitude are quoted. Wolf et al. (1981) regarded these variations as to be "of irregular nature rather than of a periodic one". Shortly after this the programme

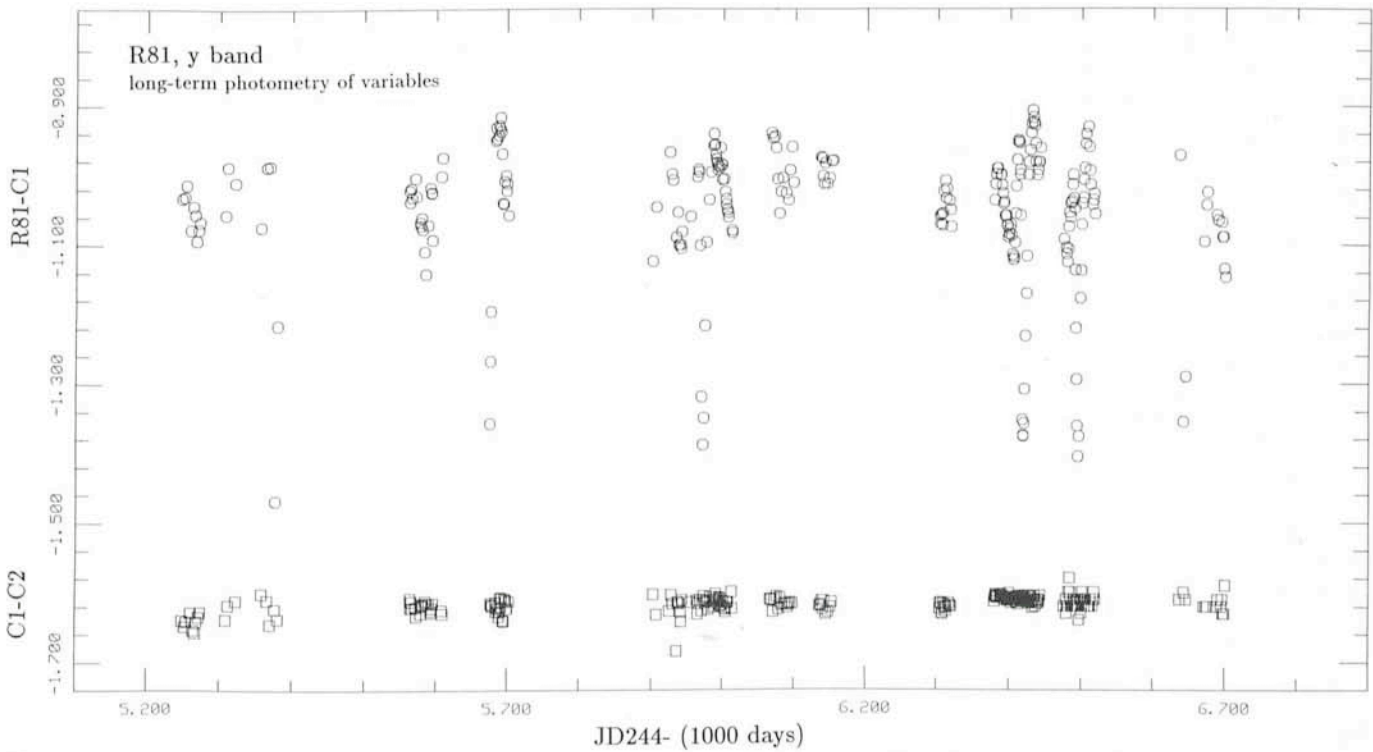


Figure 2: The differential light curve in the y band for the observations of R 81 obtained within the programme of long-term photometry of variables. The upper part shows the observations in the sense C1-R 81 and the lower part shows the same scale (but shifted) the differences of the two comparison stars. The y magnitudes of the comparison stars C1 (= HD 34144) and C2 (= HD 34651) are 9.32 and 8.37, respectively. The scatter in the differences y (C1-C2) of the two comparison stars is 0.007 which documents the quality of the photometry.

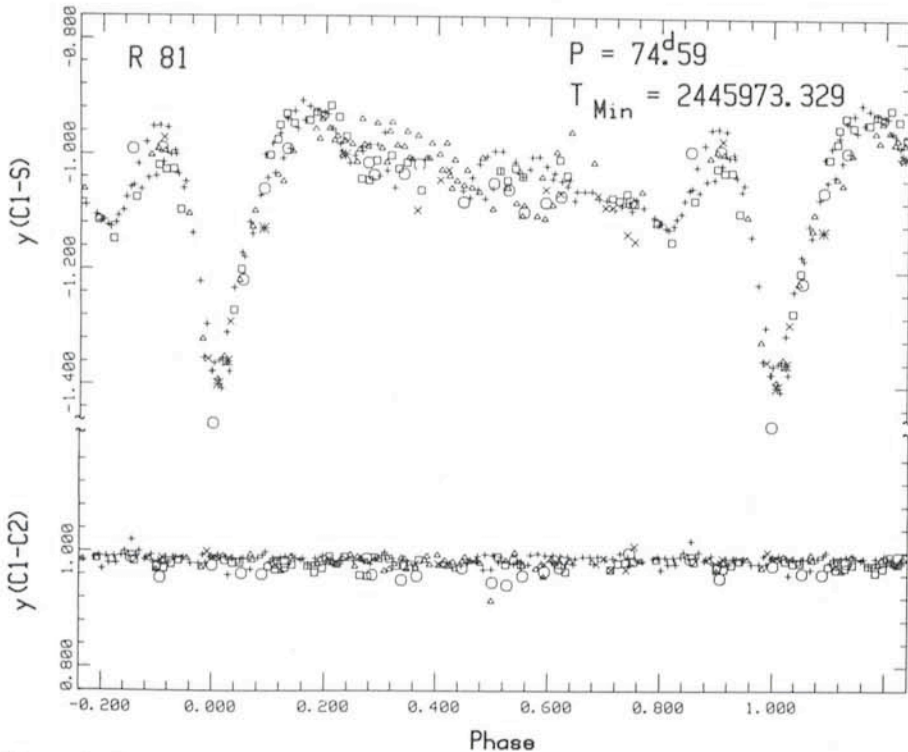


Figure 3: The phase diagram of the data shown in Figure 2. In addition the V data of Appenzeller (1972) have been included. The different symbols denote observations performed during different observing seasons ( $\circ$  for 1982/1983,  $\square$  for 1983/1984  $\triangle$  for 1985/1986,  $+$  for 1986/1987. Appenzeller's earlier observations (JD2441274 – 1292) are denoted by  $*$ . The period of the eclipses is particularly well defined due to the earlier observations of Appenzeller. The eclipse with a depth of 0.4 mag can clearly be seen. The shape of the light curve is particularly distinguished by the absence of a pronounced secondary minimum and by a pre-eclipse dip of 0.15 mag at phase 0.80.

of long-term photometry of variables described above was initiated. Undoubtedly, a detailed knowledge of the time dependence of brightness variations is important for the derivation of a physical model for P Cyg stars. Since "P Cyg of the Galaxy" has obviously never been monitored during several years by high-precision photometry at sites with comparable excellent weather conditions as at La Silla, we included "P Cyg of the LMC" (i.e. R 81) in the long-term photometry programme at ESO.

### 3. The Eclipsing Binary R 81

R 81 was already found by Appenzeller (1972) to exhibit variations with the rather large amplitude of 0.4 mag within two weeks. We subsequently observed R 81 in several years in observing runs of about two weeks each, but we were unable to find a similar event. Only variations of about 0.15 mag, which seemed to be irregular, were found. So R 81 was regarded as an irregularly variable P Cyg star, although the time coverage was too incomplete to do a meaningful period analysis.

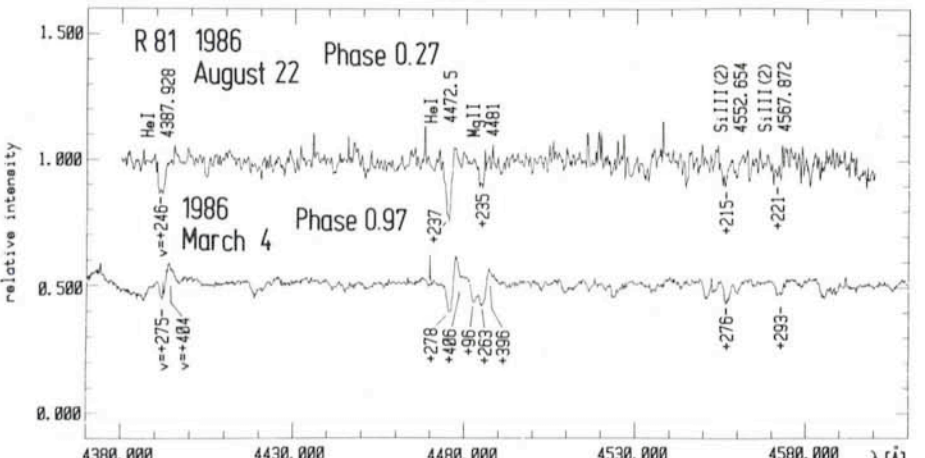
In the first three observing seasons of the long-term programme we had observed each year once that R 81 had faded far below its normal brightness. In

addition, we found that the minima repeated every 300 days. At that point we realized that the variations of R 81 might be at least partly periodic and we decided to give this star a high priority in the further observations since never before had strictly periodic variations been found in a classical P Cyg star. Until now we have collected observations in 240 different nights distributed over a period of more than four years. The observa-

tions are shown in Figure 2. This data set was analysed with a period searching algorithm and we finally found that the period of the variations was about 74.6 days. With the period already known with some precision, the observations of Appenzeller (1972) could also be tied in. They then define the period particularly well since they extend the time base by more than ten additional years (which is about 50 cycles). Taking all data together, we obtain a period of  $74.59 \pm 0.01$  days. The phase diagram of the y-band data which was constructed by using this period is shown in Figure 3. This phase diagram clearly implies that R 81 is an eclipsing binary. The light curve is very distorted which suggests that both components are in close contact.

Obviously, the detection of a binary P Cyg star is very important since we might hope to derive the parameters of the system, specifically the mass. This is a very important undertaking, since there are no direct mass determinations of a P Cyg star available. So far, we obtained two CASPEC spectra and one CES spectrum of R 81. A portion of the CASPEC spectra is shown in Figure 4. It is clear from this figure that most of the lines have a P Cyg profile or are blue-shifted absorption lines originating in the stellar wind of R 81. They are thus not very useful to determine the orbital velocity of the star. From the very few photospheric lines in the spectra we could so far not obtain a reliable radial velocity curve. In addition, no secondary spectrum has been found so far.

Luckily, some information can be obtained from the photometry: The absence of a pronounced secondary eclipse probably means that most of the visual brightness is supplied by one component. The depth of the eclipses suggests that the eclipsing body has a



radius which is comparable to the radius of the visible star, which is known from the brightness, temperature and distance of R 81. The width of the eclipses of the star with respect to the period then allows us to estimate the distance of both stars from each other and thus from Kepler's third law (with the period) the total mass of the system. We find a mass of about  $35 M_{\odot}$  for R 81. This result is in good agreement with the expectations for a luminous P Cyg star, but note that it is the first direct mass estimate for such a star. We note that this mass estimate is very uncertain so far and clearly more spectroscopy is needed in order to confirm this result.

Interestingly, the scatter around the mean curve of Figure 3 is only of the order of 0.05 mag. This means that also most of the smaller variability which we observed between the eclipses is due to the changing aspects of the observations and not intrinsic to the star. This result leads to the suspicion that also other variations of R 81, e.g. the spectroscopic variations of certain stellar

wind lines, are not irregular but phase-dependent. An important point to clarify is also the nature of the secondary. No obvious secondary minimum is present, so the star must be visually faint. New spectroscopic observations of high quality and good phase coverage are badly needed.

The more general question is, of course, whether many P Cyg stars are binaries. Our finding certainly does not prove this. However, the small scatter around the mean light curve shows that R 81 intrinsically is at most slightly variable. If other P Cyg stars (which are observed to be variable with relatively large amplitude) are similar to R 81 in this respect, then the variability observed in these stars requires an explanation.

### References

- Appenzeller, I.: 1972, *Publ. Astron. Soc. Japan* **24**, 483.  
 Cassatella, A., Beeckmans, F., Benvenuti, P., Clavel, J., Heck, A., Lamers, H.J.G.L.M., Macchietto, F., Penston, M., Selvelli, P.L., Stickland, D.: 1979, *Astron. Astrophys.* **79**, 223.  
 Chiosi, C., Maeder, A.: 1986, in *Ann. Rev. Astron. Astrophys.*, **24**, 329.  
 Humphreys, R.M.: 1986, in *Luminous stars and associations in galaxies*, IAU Symp. No. 116, eds. de Loore, Willis, Laskarides, p. 45.

- Lamers, H.J.G.L.M., de Groot, M.J.H., Cassatella, A.: 1983, *Astron. Astrophys.* **128**, 299.  
 Lamers, H.J.G.L.M., Korevaar, P., Cassatella, A.: 1985, *Astron. Astrophys.* **149**, 29.  
 Manfroid, J., Heck, A.: 1983, *Astron. Astrophys.* **120**, 302.  
 Stahl, O., Wolf, B., de Groot, M.J.H., Leitherer, C.: 1985, *Astron. Astrophys. Suppl.* **61**, 237.  
 Stahl, O., Wolf, B., Zickgraf, F.-J.: 1987, *Astron. Astrophys.*, submitted.  
 Sterken, C.: 1983, *The Messenger* **33**, 10.  
 van Gent, R.H., Lamers, H.J.G.L.M.: 1986, *Astron. Astrophys.* **158**, 335.  
 Waters, L.B.F.M., Wesselius, P.P.: 1986, *Astron. Astrophys.* **155**, 104.  
 Wolf, B., Campusano, L., Sterken, C.: 1974, *Astron. Astrophys.* **36**, 87.  
 Wolf, B., Stahl, O., de Groot, M.J.H., Sterken, C.: 1981, *Astron. Astrophys.* **99**, 351.

## Blue Horizontal Branch Field Stars in the Outer Galactic Halo

J. SOMMER-LARSEN and P.R. CHRISTENSEN, *The Niels Bohr Institute, University of Copenhagen*

### 1. Introduction

It is a well-known hypothesis that galaxies are surrounded by extended massive envelopes of "dark" matter reaching far beyond the visible edges of the galaxies. For our own Galaxy this hypothesis is supported by kinematical and dynamical studies of globular clusters in the outer Galactic halo.

The usefulness of globular clusters as test objects for probing the mass distribution in the outer part of the Galaxy is limited, however, for the following reason: The sample is small – the number of globular clusters with Galactocentric distances between 15 and 40 kpc, which can be used in a kinematical analysis, is 14. Furthermore, several recent remeasurements of globular cluster radial velocities have shown some of these to be substantially in error.

Lynden-Bell, Cannon and Godwin (1983) studied a sample of dwarf spheroidals situated at very large Galactocentric distances ( $\sim 100$  kpc). They found the objects to have quite low line of sight velocities (relative to the Galactic restframe) – the line of sight velocity

dispersion was found to be  $\sim 60$  km/s. Even if one assumes that the velocity distribution of these objects is isotropic, a mass of only  $M = (2.6 \pm 0.8) * 10^{11} M_{\odot}$  is inferred. This does not support the hypothesis that the mass of the Galaxy increases linearly with Galactocentric distance to distances  $\geq 100$  kpc.

In order to clarify further on the properties of distant halo objects we have identified and studied a sample of blue horizontal branch field (bhb) stars in the outer Galactic halo ( $r \leq 40$  kpc). The observations are described in section 2, and the results are discussed in section 3.

### 2. Observations and Data Analysis

We have carried out a search for hb stars at large Galactocentric distances. Part of the observations have been described in Sommer-Larsen and Christensen (1985 and 1986). The basic material was three stellar object catalogues, kindly provided by Drs. G. Gilmore and N. Reid. The catalogues cover three

fields located at the SGP ( $l, b = (38^{\circ}, -51^{\circ})$  and  $(l, b = (352^{\circ}, 52^{\circ})$ ). In total the catalogues cover 54 square degrees of the sky, and they are complete to  $V = 18.5$ . By observing spectroscopically faint blue stellar objects drawn from these catalogues, using the selection criterion  $0.0 \leq B-V \leq 0.2$ , a sample of 131 bhbf star candidates have been obtained.

The observations were done with the ESO 2.2-m telescope during a number of observing runs in the period 1984–1986. The observational setup and procedure were the same during all observing runs: The detector system consisted of a Boller and Chivens spectrograph together with the dual Reticon Photon Counting System (RPCS) (Christensen et al., 1984). The two decker holes, each projecting down onto its own Reticon-array, corresponded to an area of  $4 \times 4$  arcsec $^2$ . With a slit the aperture was reduced to 2 arcsec in the direction of dispersion. A 600 lines/mm grating blazed in the first order at 4200 Å was used yielding a reciprocal dispersion of  $\sim 1$  Å per channel. The wavelength range covered was

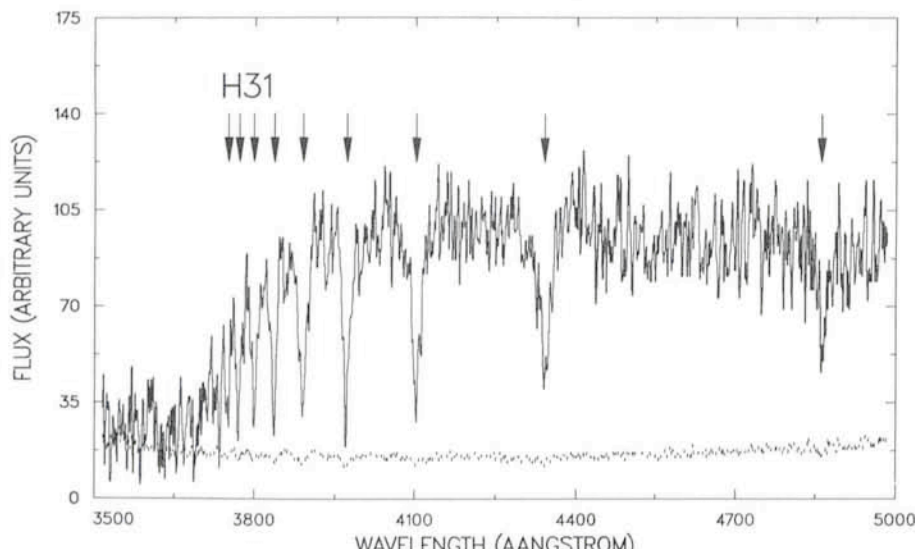


Figure 1: Part of the spectrum obtained for the bhbf object H31. The full drawn curve is the flux spectrum. The dotted curve shows the  $1\sigma$  level due to statistics. The magnitude of the object is  $V = 18.4$ , inferring a heliocentric distance of 29.6 kpc. The exposure time was 2,700 sec. The arrows show the positions of the Balmer lines  $H_{10}$  (3750 Å) to  $H\beta$  (4861 Å). The radial velocity of this bhbf star was determined to be  $20 \pm 20$  km s $^{-1}$ .

3200–5500 Å. The intrinsic resolution of the RPCS detector with this dispersion was  $\sim 2.0$  Å, but with the 2 arcsec wide slit, the resolution increased to 3.5 Å.

Each object was observed twice, focusing the object in the two decker holes subsequently. He-Ar calibration spectra were obtained after each pair of exposures. Every star which had an A-star type spectrum, and therefore was a potential bhbf star, was exposed until at least 100 (sky-subtracted) counts per channel had accumulated in the continuum in the centre of the array. No (double) exposure lasted more than 3,600 s. We were able to obtain such spectra for bhbf stars as faint as  $V = 18.7$  with this combination of telescope and detector. Such stars are located at Galactocentric distances  $r \sim 40$  kpc. A spectrum of a  $V = 18.4$  bhbf star is shown in Figure 1.

Radial (line of sight) velocities were obtained using the correlation tech-

nique. The rms error was 20 km/s for the brighter stars, increasing to 25 km/s for the faintest stars.

Balmer line widths were used to get a rough estimate of the surface gravities of the bhbf star candidates. 116 of the 131 candidates could unambiguously be identified as bhbf stars. The remaining 15 may have too high surface gravities to be bhbf stars and are tentatively identified as field blue stragglers.

### 3. Discussion

An analysis of the data obtained gives the following results: The system of bhbf stars in the Galactic halo is quite round with an axial ratio  $q \sim 0.8$ . The density distribution out to the limit of the sample ( $r \sim 40$  kpc) is well described by a power law with index  $\nu \sim -3$ . The system of bhbf stars does neither expand nor contract as would be expected for an old, well mixed system. It rotates, if at all,

very slowly relative to a Galactic rest-frame:  $v_{ROT} = 10 \pm 32$  km/s assuming  $v_\odot = 220$  km/s. This is consistent with what is found in general for metal poor stellar subsystems in the Galaxy. There are indications that the velocity distribution of bhbf stars is peaked in the radial direction (towards and away from the Galactic centre) everywhere in the inner Galactic halo.

The observed spatial and kinematical properties of the system of bhbf stars in the outer Galactic halo can be modelled without assuming that the Galaxy is embedded in an extended, massive halo characterized by an approximately flat rotation curve to  $r \geq 50$  kpc. If the Galaxy is embedded in such a massive halo then the motion of bhbf stars in the outer Galactic halo must be predominantly tangential (low eccentricity orbits). This contrasts with what is found for halo stars in the inner Galactic halo and tells us something about early Galactic history. It certainly does not support a rapid collapse picture for the outer Galactic halo. It may suggest that the bhbf stars in the outer Galactic halo were formed out of turbulent gas rather than out of gas with small macroscopic motions.

Our study of the inner and outer Galactic halo is by no means complete. Observations of bhbf stars in considerably more fields probing other parts of the Galactic halo would be of great interest in the light of the results obtained so far. Such observations are planned.

### References

- Christensen, P.R. et al., 1984, *The Messenger* **38**, 38.
- Lynden-Bell, D., Cannon, R.D., and Godwin, P.J., 1983, *Mon. Not. R. Astr. Soc.*, **204**, Short. Comm., p. 87.
- Sommer-Larsen, J. and Christensen, P.R., 1985, *Mon. Not. R. Astr. Soc.*, **212**, 851.
- Sommer-Larsen, J. and Christensen, P.R., 1986, *Mon. Not. R. Astr. Soc.*, **219**, 537.

## And then there were Three . . .

At the end of the article about the recovered minor planet MALLY (*Messenger* **46**, 11), the five remaining 'lost' minor planets were enumerated. Readers of this journal may be interested to learn, once more, that things move fast in astronomy nowadays, not only in front-line areas of high energy astrophysics, but also in the classical backwaters of celestial mechanics.

By early February 1987, two more lost minor planets had been 'shot

down'. Persistent efforts by Mr. Syuichi Nakano, who is spending one year at the IAU Minor Planet Centre in Cambridge, Mass., lead to the identification of (1026) INGRID with a minor planet observed in early 1986. He sent the resulting orbit to ESO, where no less than six further images of this planet were found on plates in the plate library.

The remeasurement at ESO of the original 1901 Heidelberg plates of (473) NOLLI, lost since that year, showed that

the published positions were somewhat in error (one by more than 30 arcseconds). Based on the improved measurements, Dr. Brian Marsden, who heads the Minor Planet Centre, was able to find identifications with minor planets, observed in 1940, 1981 and 1986. Three additional images were found in the ESO plate library, definitely confirming these identifications.

So, now there are only three left . . . (there are rumours that some of the MP-people are busy).

# Where Peculiars Turn Normal – IR Observations of CP Stars

R. KROLL, Universitäts-Sternwarte Göttingen

## Upper Main Sequence Stars

If you make all possible simplifications in the theory of stellar atmospheres – LTE, no convection, gas pressure two times the electron pressure, plane parallel atmosphere with solar composition, etc. – and look, where such a concept could actually work, you arrive at the upper main sequence stars. And in fact, there has been much progress in understanding such atmospheres, the model atmosphere grid calculated with Kurucz's famous ATLAS programme as an outstanding example.

Yet there is a large fraction ( $\sim 20\%$ ) of upper main-sequence stars that refuse to obey such simple physics. They show large metal overabundance, photometric variability, magnetic fields, breathtaking spectra or curious flux distribution. Following the systematic of Preston (1974) we call these stars 'chemical peculiar' or shortly CP stars.

Two mainstreams are distinguished, one that exhibits no magnetic fields and consists of the metallic line (Am) stars – nowadays called CP1 stars – and the Mercury-Manganese (HgMn or CP3) stars, and one that displays magnetic fields up to some 10,000 Gauss on the other hand. This article will mainly deal with these magnetic Ap stars, and reference them, more up-to-date, as CP2 stars.

Here the physical situation is complicated a little, namely by the strong magnetic field. This field in turn tries to be kind to the astronomer and keeps the second simplest form possible in most cases, that of a dipole, but inclined by some angle against the rotational axis. This working model – the oblique rotator – can explain most of the observed characteristics of CP2 stars, e.g. the photometric and spectroscopic variability, or polarity changes in the magnetic field, but the question remains, what causes the variety of abundance patterns in CP2 stars, which peak in objects like the famous and infamous Przybylski's star HD 101 065, where from the 15 strongest metallic lines 11 belong to Rare Earth Elements, 6 of these to the element Holmium, which is rarely encountered in any other branch of astrophysics.

Analysing the atmospheres of these stars is not a time consuming, unproductive work in some astrophysical

niche, but a necessity in understanding stellar evolution in the presence of magnetic fields, which is a commonly encountered configuration. The CP stars are not an accident in stellar evolution, but at least one possible branch, or maybe even a state that every upper-main-sequence star passes.

But the variety of phenomena is discouraging at the first glance; let us consider the most commonly observed phenomena. In most cases we find a flux deficiency in the ultraviolet spectrum and in turn a 'heating' of the visual part which is understood as a back-warming effect from the enhanced metal abundances found in CP2 stars. In other words, flux is redistributed from the UV to optical wavelengths. This process works according to the individual abundance pattern of the specific star, so all temperature estimates, photome-

tric calibrations, curve-of-growth analysis, etc. tend to produce rather uncertain, scattering results. Do we have any spectral window which is unaffected from the chemical peculiarity of the star, where we can find a stand?

## Infrared Observations of CP Stars

In 1983 the last hope, the infrared part of the spectrum, seemed to slip away. Large flux excesses at 5 microns were reported, measured at the ESO 1-m photometric telescope by Groote and Kaufmann. These observations pointed to the existence of considerable circumstellar matter around CP stars, with blackbody temperatures of 300 to 600 K, which must be connected to the CP phenomenon in one way, either being the cause of it, or an unavoidable result. Both could hardly be understood

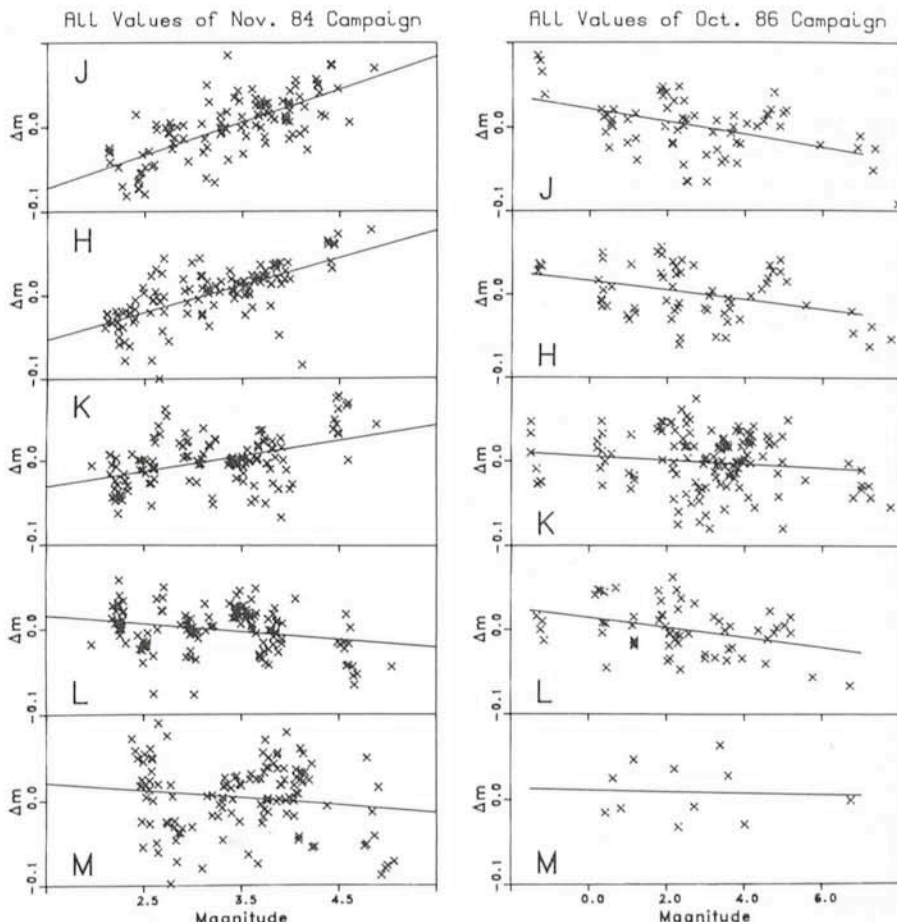


Figure 1a: Catalogue minus observed brightness versus intrinsic magnitude for all standard star measurements during the November 1984 campaign. The nonlinearity effect changes its slope continuously from J to M filter.

Figure 1b: Same as 1a, but for the October 1986 period. Note that the abscissa spans a double range compared to Figure 1a. Nonlinearity effects have been greatly diminished.

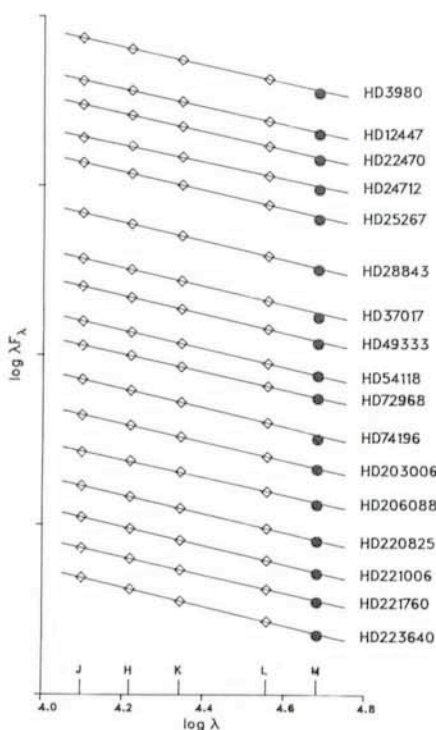


Figure 2: Rayleigh-Jeans diagnosis.  $M$  values above line would indicate flux excesses. All observed stars are normal.

with the most promising attempts to explain the forming up of chemical overabundances, like Michaud's diffusion theory.

But other researchers, like Bonsack and Dyck were unable to verify the claimed fluxes, so a careful reinvestigation of the subject was desirable. Franco Catalano from Catania/Sicily joined a group at Göttingen University Observatory in that attempt. Our first observing period dated November 19 (84 at the ESO 1-m telescope, equipped with its liquid nitrogen cooled IR photometer with InSb diode, which had undergone of course some minor changes since the time when Detlef Groote and Jens-Peter Kaufmann had made their exciting measurements.

In the first moment the observations made by Franco Catalano looked puzzling to us, when they were reduced in Göttingen. The calibration with standard stars from Koornneef's list was not satisfactory, because it showed a large scatter. During our attempts to localize the reason for that scatter, we plotted the difference between the expected and the measured brightness against the star's intrinsic magnitude in the specific filter. And here's the surprise (Fig. 1a)!

Instead of showing the expected scatter around a horizontal line, a clear correlation was seen, which – even worse – reversed its trend with increasing wavelength, from the J- to the M-filter. This effect may be called by defini-

tion a nonlinearity, whatever caused it. After carefully correcting for that effect, none of our programme stars showed any sign of flux excess in the M-band, though many had been found to be excessive in the Groote and Kaufmann survey. Figure 2 shows this in a Rayleigh-Jeans diagnosis. We fitted a straight line through the logarithmic fluxes in the J, H, K and L filter and plotted it against the logarithm of the wavelength. Now the  $M$  value is excessive against a blackbody flux distribution in the Rayleigh-Jeans approximation, if it lies above this line. But this is not the case for any of the programme stars.

### The IRAS View

Though the  $5\mu$  flux excess was disproven this way, we were sensitized for the possible existence of circumstellar matter and looked for it in the IRAS point sources catalogue. We found 40 CP stars of various types, for which good near IR data were present. From the CP 2 group none showed fluxes at the IRAS wavelengths – which are 12, 25, 60 and 100  $\mu$  – that would not fit to a blackbody flux distribution. Two objects were found where in fact circumstellar dust was indicated, but they belong to the He peculiar stars, or CP4 group, where we also find stars with Be characteristics. Dust shells are not uncommon for these objects. Positively spoken, our result from the IRAS data is that CP stars show normal main-sequence characteristics in the infrared as far as we can observe them. Figure 3 shows some examples for various CP types.

We may now safely conclude that all flux redistribution, caused by the curious chemistry of the CP stars has come to an end at infrared wavelengths, and hence the infrared fluxes are a superb indicator for the thermal properties of the atmospheres and a solid stand for further analysis.

### IR Light Curves

The next logical step is to get precise light curves in the infrared, which tell us what thermal changes take place, as the stellar rotation brings different parts of the atmosphere into the line of sight of the observer. For this project Franco Catalano and I got ten nights of observing time at the 1-m in October 1986. Unfortunately the delayed spring made this time shrink to merely four nights effectively.

Another handicap was that in the beginning we did not know which stars would show pronounced variability. Our compromise in having many data points per star as well as many stars checked,

resulted in sufficient data for about eight CP stars. Of course we had to restrict ourselves to objects with short periods.

First of all we checked whether the awful nonlinearity effect was still present – and were pleased to see that it had been nearly totally removed. Note that in Figure 1b the abscissa spans now eight magnitudes instead of four in Figure 1a.

Differently to the observations one year ago we performed differential photometry, taking comparison stars in the vicinity of the programme stars. This allows a much higher accuracy, be-

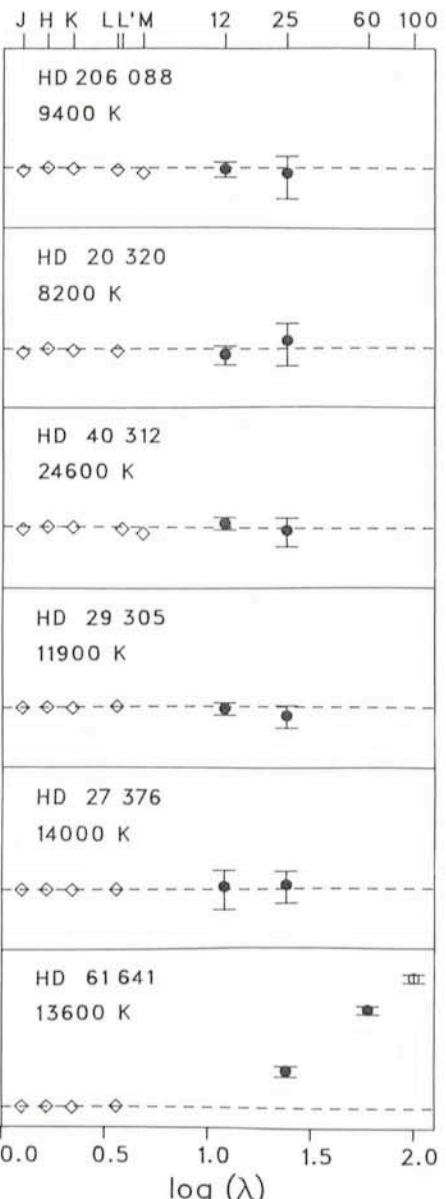


Figure 3: IRAS observations. Fluxes above dashed line are excessive against a blackbody with the indicated temperature, deduced from the near IR colours. The CP4 star HD 61 641 shows indications of a dust shell, which gives it Be type characteristics. All other stars show blackbody flux distribution (HD 206088 and 20320 are cool CP2 stars, HD 40312 and 29305 hot Si type CP2 stars, HD 27374 is a CP3 star). Error bars indicate  $3\sigma$ .

## HD 3980

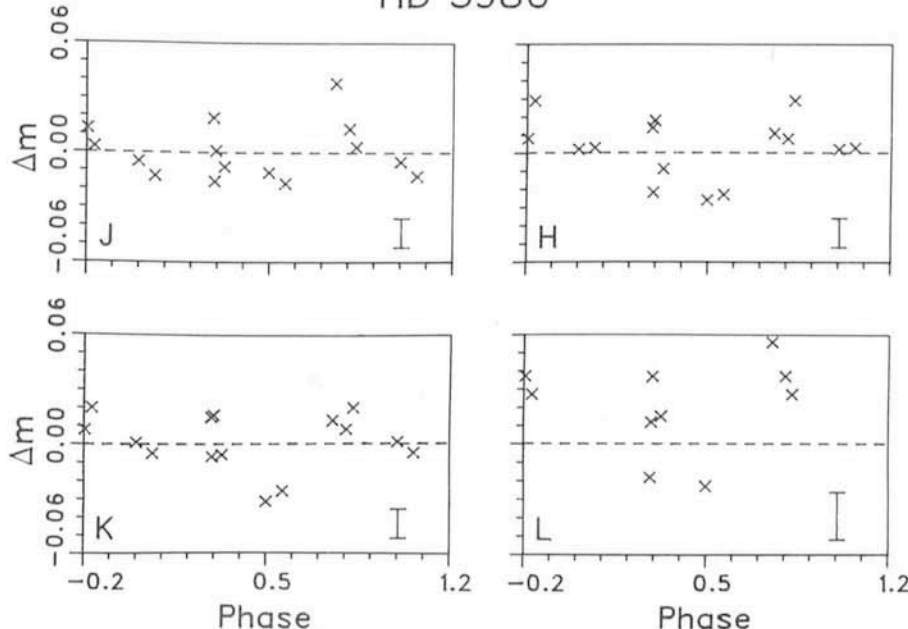


Figure 4: IR light curve of HD 3980 in four filters. No sign of periodic variability could be found. Mean errors are indicated by the error bars in the lower right corners.

cause the infrared sky is much more inhomogenous than the visual. We knew that high precision was needed, since our previous data showed that the expected amplitudes would be lower than about 0.03 magnitude.

The first results looked disappointing, one star after the other showed no clear sign of variability, like in the case of the well-known cool CP2 star HD 3980 (Fig. 4). So we reached the final star on our list,  $\alpha$  Doradi or HD 29305. Though we had only seven data points per filter, we observed in all filters a clear variation

with a mean amplitude of 0.028 magnitude (Fig. 5). The phase shifts and amplitudes are very similar in every filter but, because of the few data, the light curve must be confirmed by subsequent observations.

HD 29305 is a bright silicon type CP2 star, with an effective temperature of about 12,000 K. It has a high projected rotational velocity ( $v \cdot \sin i = 130$  km/s, but this value may be overestimated). Together with its rotational period of 2.95 days, this tells us that the rotational axis is tilted close to a right angle to the

line of sight. So we have a total exchange of the visible surface after half a period.

In the Rayleigh-Jeans regime, flux and temperature are linearly related, a 3% variation in flux corresponds to a 3% temperature change, which in the case of  $\alpha$  Dor gives 350 K. That means, the light minimum phase corresponds to an average temperature, which is 700 K lower than in the maximum phase. Remember, this value is an average over one hemisphere, so actual temperature differences may be much higher.

This observation implies that in this particular star the atmospheric variations may not be explained exclusively by the line blanketing mechanism, since this would leave the effective temperature unchanged.

Since any attempt to map the distribution of chemical elements on the surface of CP stars – and to relate that to the magnetic field configuration – needs a map of the physical parameters first, the infrared light curves may be of great value for such work. Till now, for such work the stellar atmosphere was always assumed to be homogenous in their physical parameters.

We will continue this work in July at La Silla.

### References

- Bonsack, W.K., Dyck, H.M., 1983: *Astron. Astrophys.* **125**, 29.
- Groote, D., Kaufmann, J.P., 1983: *Astron. Astrophys. Suppl. Ser.* **53**, 91.
- Koornneef, J., 1983: *Astron. Astrophys. Suppl. Ser.* **51**, 489.
- Kroll, R., Schneider, H., Catalano, F.A., Voigt, H.H., 1987: *Astron. Astrophys. Suppl. Ser.* **67**, 195.
- Kurucz, R.L., 1979: *Astron. J. Suppl. Ser.* **40**, 1.
- Michaud, G., 1980: *Astron. J.* **85**, 589.
- Preston, G.W., 1974: *Ann. Rev. Astr. Astrophys.* **12**, 257.

### ESO Press Releases

The following Press Releases have been published since the last issue of the *Messenger*.

PR 01/87: Possible Planetary System Photographed Around Nearby Star (31 December 1986; with B/W photo on request).

PR 02/87: Quasar-like Activity in the Outskirts of an Elliptical Galaxy (29 January 1987; with B/W photo and Colour photo on request).

PR 03/87: Bubbles From A Dying Star (20 February 1987; with B/W photo).

PR 04/87: Brightest Supernova Since Four Hundred Years Explodes in Large Magellanic Cloud (25 February 1987).

PR 05/87: Supernova in Large Magellanic Cloud: Overview of First Results (3 March 1987).

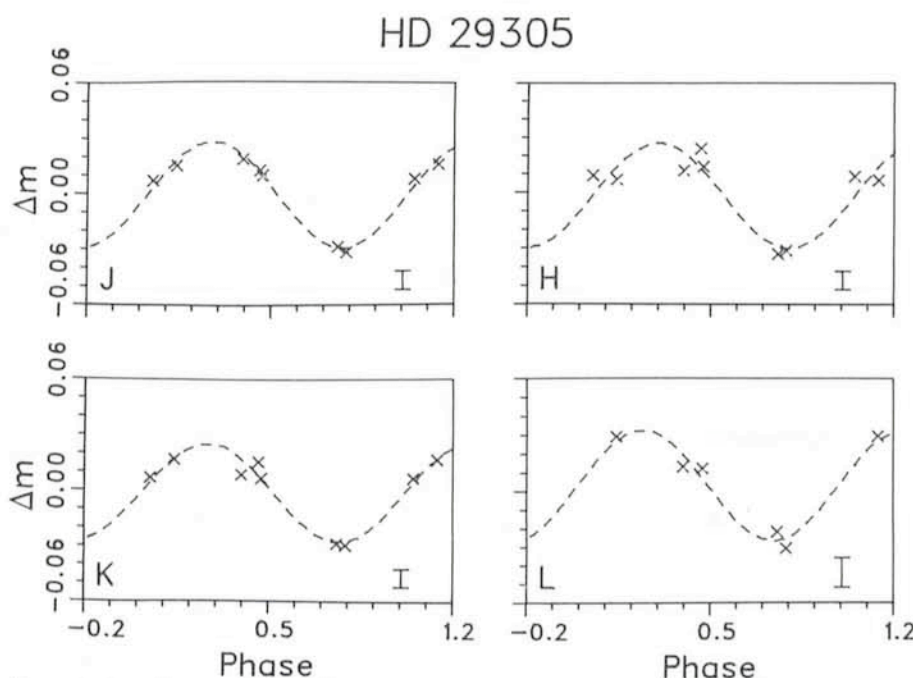


Figure 5: IR light curve of HD 29305 in four filters. The mean amplitude is 0.028 mag. Mean errors are indicated in the lower right corners.

# BD +03°740: a New Extreme Metal-poor Dwarf

P. MAGAIN, ESO

The analysis of the halo stars is an important tool, not only for tracing the chemical evolution of the Galaxy, but also for the understanding of the processes of star and galaxy formation. Although the models are able to explain a number of observed features, some basic problems remain. One of these problems is the absence of Population III stars, i.e. stars of the first generation, which would have formed out of the Big Bang matter (basically H and He) and would not contain any heavy elements (that is with atomic number  $Z \geq 6$ ) in their atmospheres. Recent models (Cayrel, 1986; Jones, 1985) seem able to explain the absence of these stars, basically by showing that massive short-lived stars are likely to form first and pollute the interstellar gas before the

formation of the long-lived lower mass stars that can be observed now. However, although these models are very attractive, they do not, for example, explain the presence of s elements (e.g. Sr, Y or Ba) in the atmospheres of the most metal-poor stars. These elements should be seen only in the atmospheres of the dwarfs of the third and subsequent generations: a first stellar generation is required to synthesize the "primary" elements (e.g. C, O, Fe, ...) from H and He, while the stars of the second generation, containing these primary elements, would be able to produce the "secondary" elements and, in particular, the s elements, which would thus appear in the atmospheres of the dwarfs of the third generation. (It should be pointed out that this problem is not par-

ticular to the new models mentioned here, but is common to most models of galactic evolution).

From the observational point of view, it is well known since the work of Spite and Spite (1978) that these s elements are overdeficient in the atmospheres of the most metal-poor stars. However, although low, their abundances are not zero, and this is the problem. Where would be the stars of the second generation?

In an attempt to clarify this problem, as well as other problems related to the early galactic evolution, I have observed a sample of extreme metal-poor dwarfs and subgiants during 4 nights (2 in May and 2 in October 1986) with the CASPEC at the 3.6-m telescope. These stars were selected mainly on the basis of their Strömgren colours indicating very low metal abundance. Some 25 stars were observed in two spectral regions, centred at 4300 and 5500 Å. A rapid inspection of the spectra immediately showed that one of these stars, namely BD +03°740, had extremely weak lines and should be one of the most metal-poor stars discovered so far. I would like to present here some results of a preliminary analysis of that star, based on the blue spectrum. This spectrum was obtained on the night 13/14 October, with an exposure time of 40 minutes, which gave a good S/N ratio for that 9.8-mag star. It was reduced using the MIDAS and IHAP facilities at La Silla. A portion of the spectrum of BD +03°740 is shown in Figure 1, while Figure 2 shows for comparison the same region in the spectrum of the classical extreme metal-poor star HD 140283. The extreme weakness of the metal lines in the spectrum of BD +03°740 is immediately obvious.

The analysis was carried out using the empirical models of Magain (1985). The effective temperature was deduced from the V-K colour index, indicating  $T_{\text{eff}} = 6,050$  K. The surface gravity was determined by forcing the Fe I and Fe II lines to give the same abundance, which led to  $\log g = 3.25$ . The microturbulent velocity was found equal to 1.5 km/s using the method of Magain (1984). The abundances were determined from a detailed line-by-line analysis, assuming, as usual, local thermodynamic equilibrium (LTE). The main results are shown in Table 1. As far as I know, only two stars are known with lower metal abundance, namely the giant CD -38°245 (Bessel and Norris,

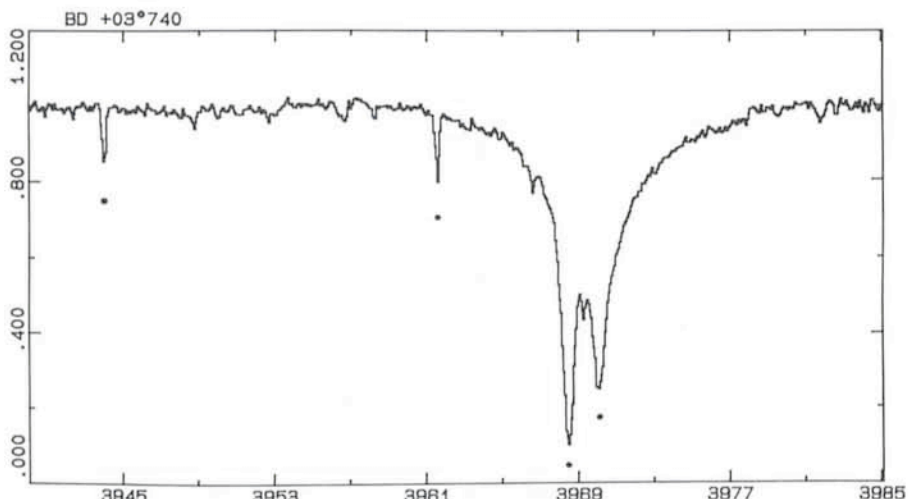


Figure 1: Portion of the CASPEC spectrum of BD +03°740. The dots indicate the two resonance lines of Al I, as well as the H line of Ca II and H<sub>i</sub>.

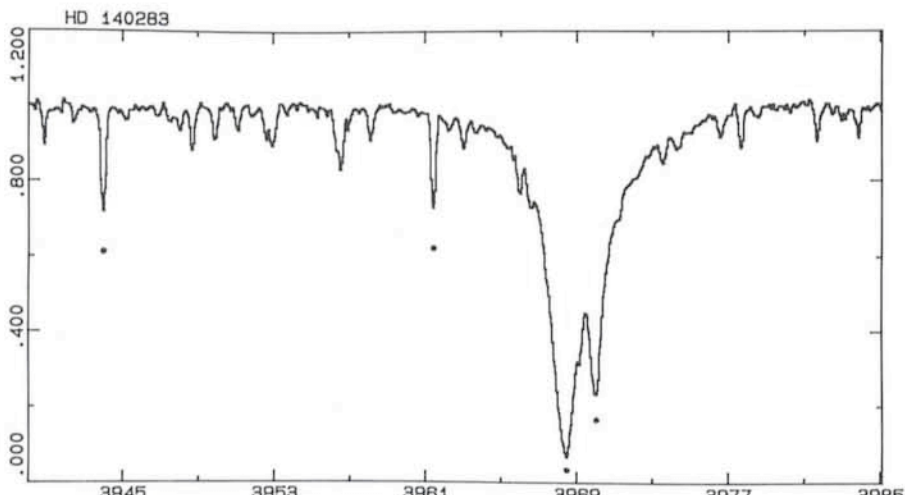


Figure 2: Same as Figure 1 for HD 140283.

Table 1: Relative abundances

[Fe/H]	= -3.13
[Mg/Fe]	= +0.59
[Al/Fe]	= -0.82
[Si/Fe]	= +0.50
[Ca/Fe]	= +0.50
[Ti/Fe]	= +0.38
[Cr/Fe]	= -0.18
[Sr/Fe]	= -0.22
[Ba/Fe]	= -0.62

1981) with  $[\text{Fe}/\text{H}] = -4.5$  and the turnoff star G 64-12 (Carney and Peterson, 1981) for which  $[\text{Fe}/\text{H}] = -3.5$ . Incidentally, BD +03°740 is also probably a star near the turnoff. The relative abundances confirm the general picture outlined in Magain (1985, 1987) and other papers, namely:

- overabundance of the “ $\alpha$  elements” Mg, Si, Ca and Ti by some 0.5 dex,
- overdeficiency of the s elements Sr and Ba,
- large overdeficiency of Al relative to Mg:  $[\text{Al}/\text{Mg}] = -1.4$ .

The behaviour of Al relative to Mg is subject to some controversy, some authors (e.g. François, 1986) suggesting that  $[\text{Al}/\text{Mg}]$  is constant in the halo, at roughly -0.5, while others (e.g. Arpigny and Magain, 1983; Magain, 1987) argue in favour of an increasing Al overdeficiency with decreasing metal abundance. The present analysis supports this last interpretation, as is shown in Figure 3, where the representative point of BD +03°740 is added to the  $[\text{Al}/\text{Mg}]$  versus  $[\text{Mg}/\text{H}]$  plot of Magain (1987). It should be pointed out, however, that the Al abundance in the most extreme metal-poor stars is determined from the

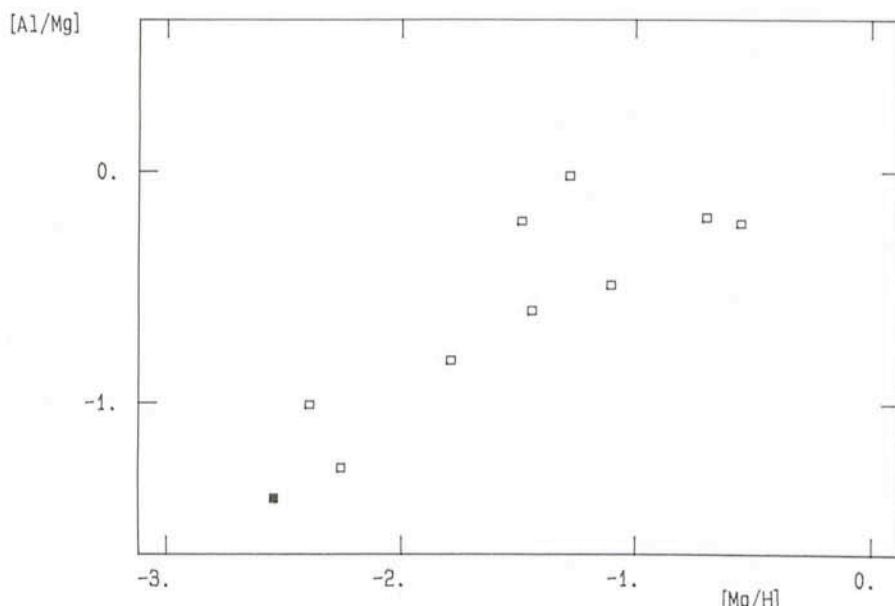


Figure 3: Plot of  $[\text{Al}/\text{Mg}]$  versus  $[\text{Mg}/\text{H}]$  for the stars of Magain (1987, open squares) and for BD +03°740 (full square).

single resonance line at 3961 Å, and would be in error if the latter was affected by departures from LTE.

Finally, the analysis of BD +03°740, which is the most metal-poor dwarf in which s element abundances have been determined, confirms the presence of these secondary elements in the atmospheres of the extreme halo dwarfs, in contradiction with the classical models of nucleosynthesis and galactic evolution.

#### Acknowledgements

I wish to thank T. Le Bertre and H. Lindgren for providing me some infrared and visual photometry of this star.

#### References

- Arpigny, C., Magain, P.: 1983, *Astron. Astrophys.* **127**, L7.
- Bessel, M.S., Norris, J.: 1981, IAU Coll. No. 68, p. 137.
- Carney, B.W., Peterson, R.C.: 1981, *Astrophys. J.* **245**, 238.
- Cayrel, R.: 1986, *Astron. Astrophys.* **168**, 81.
- François, P.: 1986, *Astron. Astrophys.* **160**, 264.
- Jones, J.E.: 1985, *Publ. Astron. Soc. Pacific* **97**, 593.
- Magain, P.: 1984, *Astron. Astrophys.* **134**, 189.
- Magain, P.: 1985, *Astron. Astrophys.* **146**, 95.
- Magain, P.: 1987, *Astron. Astrophys.*, in press.
- Spite, M., Spite, F.: 1978, *Astron. Astrophys.* **67**, 23.

## BD Pavonis, a New Double Lined Eclipsing Cataclysmic Binary

H. BARWIG and R. SCHOEMBS, Universitäts-Sternwarte München

Cataclysmic binaries are double stars consisting of a compact primary and a cool secondary component. They are so close that the surface of the secondary fills its so-called Roche limit and transfers matter towards the primary in a stream. Due to the system's orbital motion, however, the stream does not impact on the primary but forms an accretion disk around it. Where the overflowing mass hits the rotating gas, a hot bright spot is produced. The momentum of the disk material has to be separated before it can be accreted onto the pri-

mary. Magnetic fields can influence the structure of the disk, in some cases no disk exists at all and matter is forced to flow along the magnetic field lines producing extremely hot X-ray emitting spots above the magnetic poles.

Novae, dwarf novae, several X-ray sources like AM Her stars, intermediate polars, DQ Her stars and X-ray bursters are examples for the large group of CVs, and the variety of classes demonstrates their complex behaviour.

A unique member of this group, BD Pav, had been discovered by Boyd

(1939) on star plates taken in 1934. The object, never seen before, suddenly had brightened to 12.4 mag. After 20 days the star faded below detection limit (16.5 mag) again. This led to the classification as a classical nova, which was doubted already by Payne Gaposchkin (1977) because of consequences of the decay time scale on the absolute magnitude.

We observed BD Pav with the ESO 1.5-m telescope in June 1980 during a spectroscopic survey programme searching for cataclysmic systems with

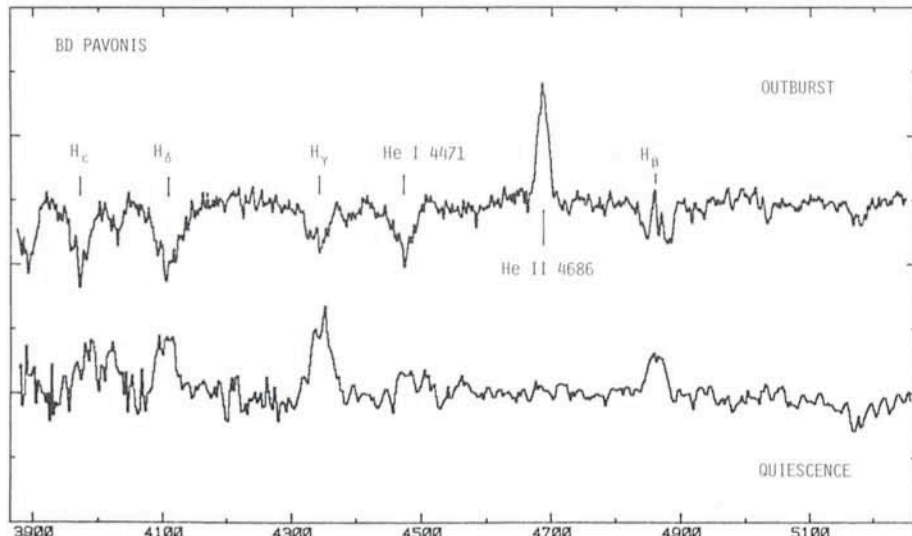


Figure 1: Averaged spectra of BD Pavonis during eruption and in quiescence. The outburst spectra (upper part) were taken at the ESO 3.6-m telescope with the B & C and CCD in 1985. Strong broad absorption lines of H and He I 4471 are shown together with He II 4686 in emission. The spectra in quiescence state (lower part), obtained with the 2.2-m telescope in 1986 mainly show the Balmer lines in emission.

high orbital inclination, i.e. with broad and double peaked emission lines. Due to its spectrum BD Pav was selected for further investigation.

Photometric light curves revealed strong flickering and eclipse like features (H. Barwig, R. Schoembs, 1981). The data had been seriously affected by variable extinction however. Since the object is well observable only during the season around June, known for its unfavourable weather conditions, several attempts to complete the observational material had to be made. A first analysis of the object was based on data obtained at La Silla in 1980 and 1981 (H. Barwig and R. Schoembs, 1983). This paper reported the orbital period ( $P = 4.3$  hours), the existence of a primary eclipse and strong effects from ellipsoidal distortion of the Roche lobe filling component. The secondary turned out to be unusually luminous. The complex double peaked emission line profiles were difficult to measure. Radial velocity variations of 600 km/s were determined by means of correlation techniques. These results considerably increased the interest on BD Pav. A further proposal for photometric observations in 1982, granted with 9 nights at the Walraven Photometer, was totally impeded by terrible weather. It was that period when a blizzard at La Silla stopped all astronomical activities.

Discussions on the most appropriate observing techniques convinced us that we would need a larger telescope for spectroscopy and a photometer totally different from classical single-channel instruments for observation of BD Pav and many other variable objects. Although at some other institutes first de-

1987). The instrument had been used at La Silla for the first time in 1983 (Schoembs et al., 1987) and for BD Pav in 1985.

Additionally, during the same observing period, two nights at the 3.6-m telescope had also been allotted to spectroscopy. When observations started, BD Pav appeared surprisingly bright on the TV screen, a phenomenon which first was attributed to its red colour, but when the first spectrum was displayed showing broad Balmer absorption lines instead of emissions, it became obvious that the object was caught during an eruption. This outburst is the first one known to us since discovery. It immediately confirmed our suggestion that BD Pav rather is a dwarf nova than a classical nova. Although it was great luck to encounter this outburst, we knew that because of the dominant radiation from the accretion disk during this active phase, there would hardly be a chance to find spectral features of the secondary, one important aim of our mission. Detection of the secondary spectrum in cataclysmic binaries is of fundamental importance. In that case much more reliable system parameters can be derived than from radial velocities of the emission or absorption lines originating in the complex primary accretion disk configuration. Typical spectra of BD Pav during outburst and quiescence are displayed in Figure 1 for comparison.

Immediately after the spectroscopic run, photometric observations at the 1-m telescope started for 8 nights. We were curious of the first light curve, in

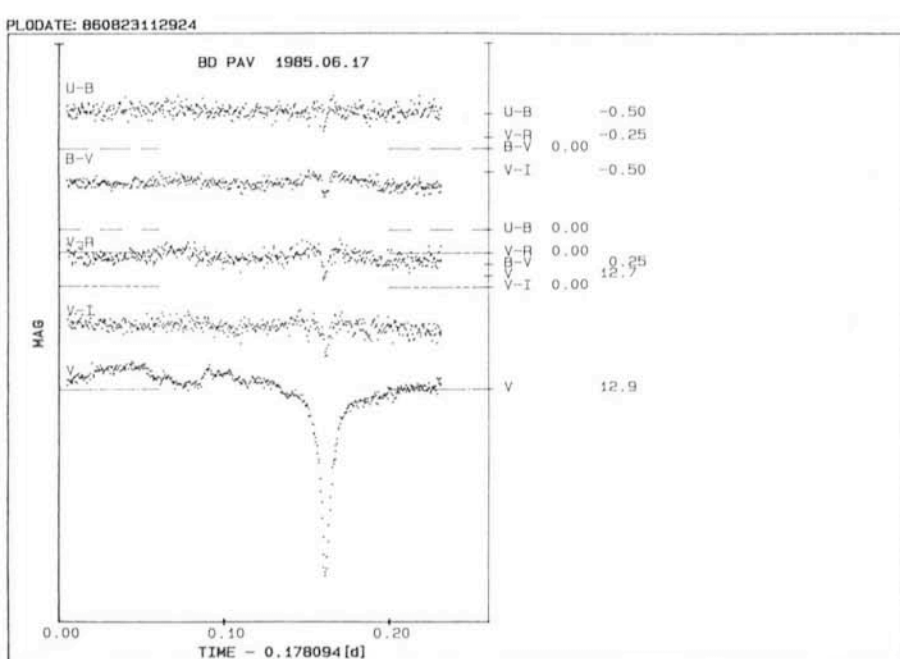


Figure 2: UVRI light curves of BD Pavonis during eruption taken in the first observing night at the ESO 1-m telescope with the multichannel photometer. The deep eclipse of a small blue primary and disk is shown and a shallow minimum of a larger redder object at orbital phase 0.5.

particular whether the eclipse feature visible during quiescent state would have disappeared or still exist. The latter case would mean that the orbital inclination is so large that even the bright central accretion disk, the main source of radiation during eruption, is eclipsed. Somewhat less than one orbital period after beginning of observation, when we already thought that the eclipse had disappeared, the intensity curve on the graphic screen suddenly began to drop while the comparison star stayed constant, indicating that no clouds were coming up. Some 20 minutes later the light curve had returned to its original level.

The reduced light curves of this night are displayed in Figure 2 while Figure 3 shows BD Pav during the last night of our observing period, when the star had almost reached its normal brightness. Figure 4 shows the recorded count rates of sky and comparison star for all nights. Cloudy skies yield comparison star counts ranging between their normal values and the sky counts, while clear nights only show the expected dependency on zenith distance super-

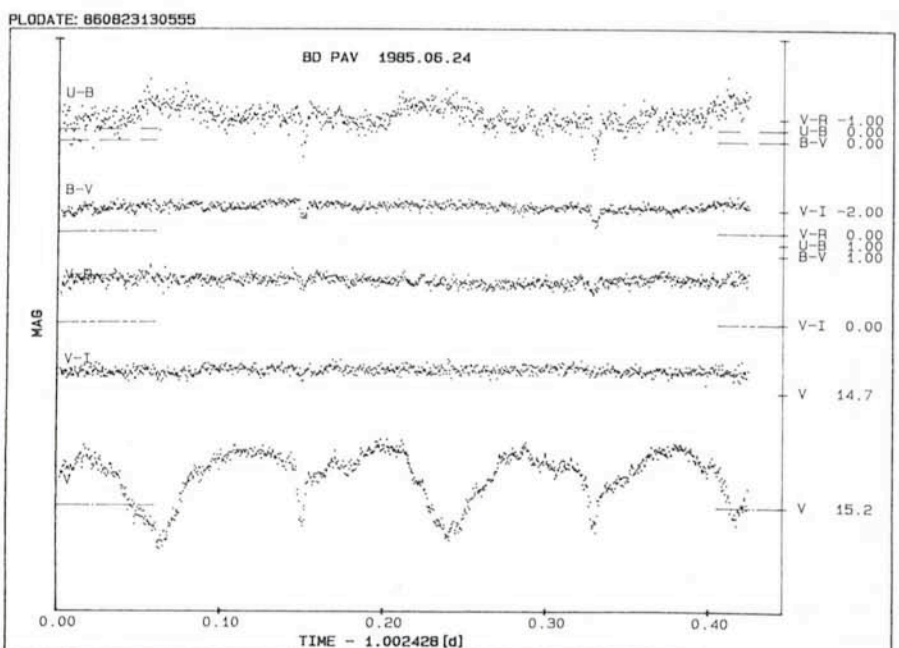


Figure 3: *UBVRI light curves of BD Pavonis at the end of eruption, obtained in the last observing night.*

posed by sky brightness variations (most pronounced in U during moon set at beginning of nights 7 and 8).

It is found that atmospheric transparency changes up to 80 % can be compensated applying the differential

PLODATE: 860822190255.

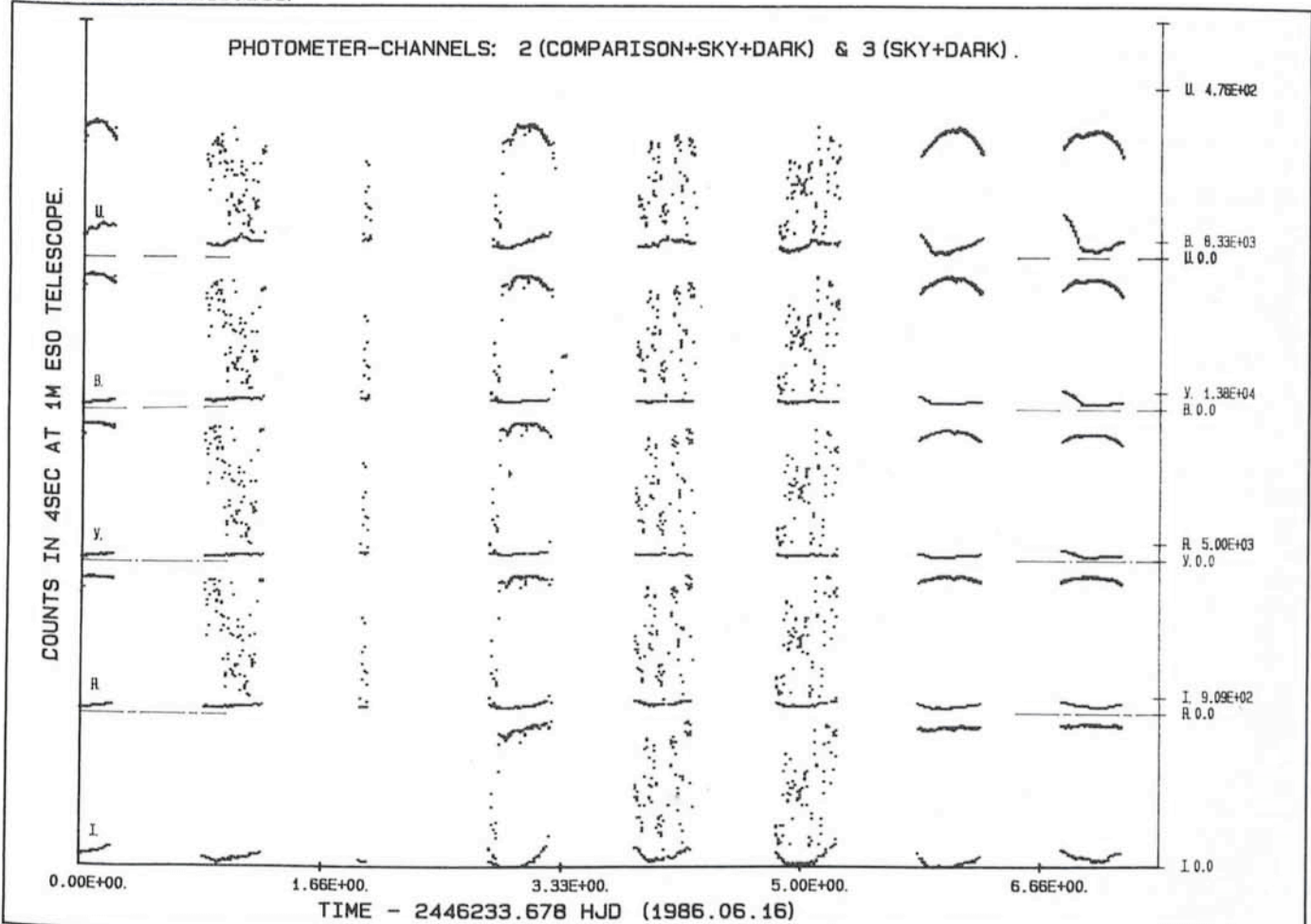
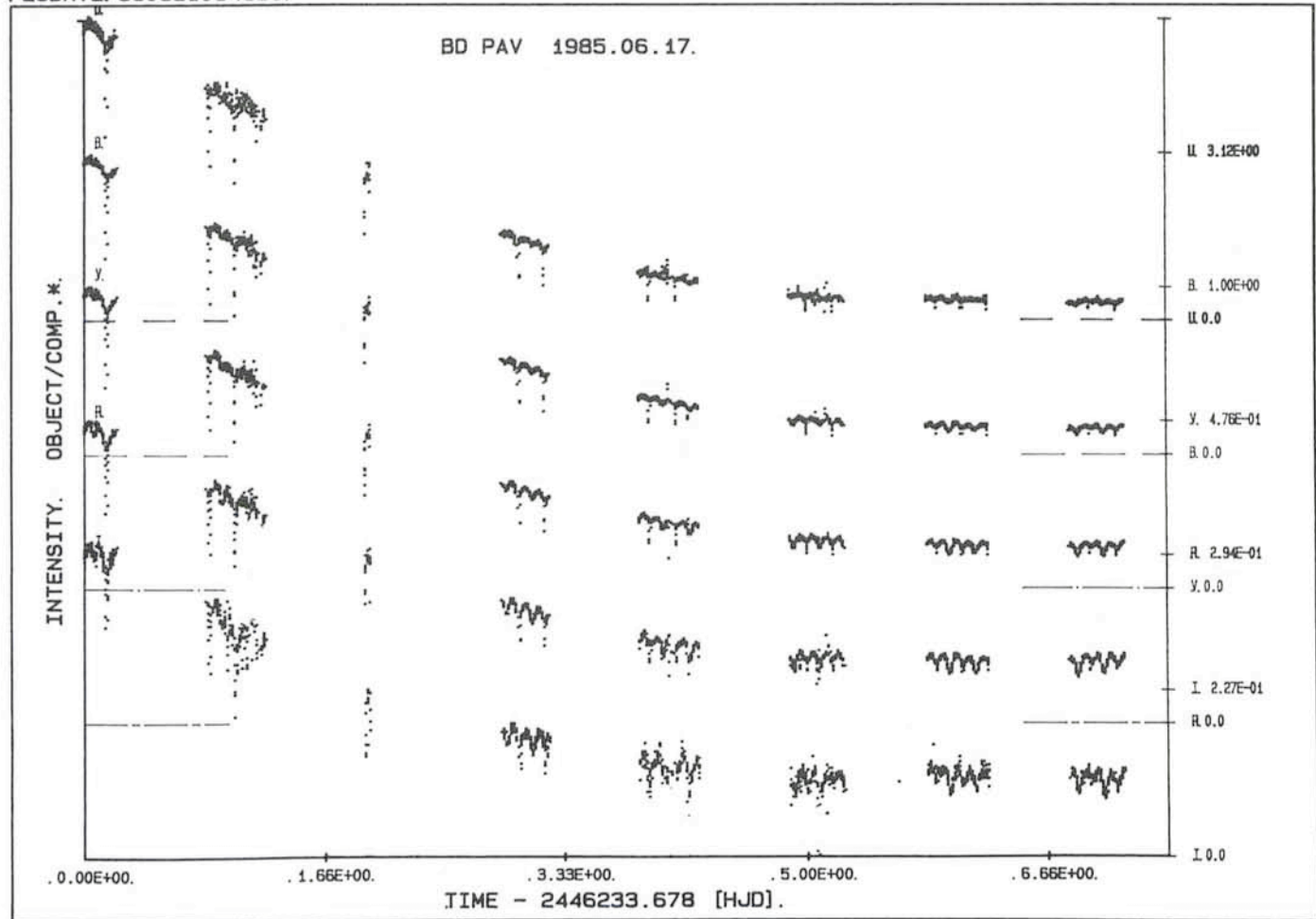


Figure 4: *Count rates for comparison star and sky simultaneously measured in UBVR with BD Pavonis during the whole observing period of 8 nights. In the pairs of curves the lower sky curve is the lower limit for the pure comparison star counts in case of zero sky transparency. Dark counts are negligible.*

BD PAV 1985.06.17.

Figure 5: The  $UBVRI$  intensity variations of BD Pavonis during decay from the eruption in 1985. Condensed representation.

measuring methode. Condensed light curves in Figure 5 reveal the behaviour of the intensities relative to the comparison during decay from eruption. During bright phases the primary eclipse is a prominent feature deeper at shorter wavelengths. Its relative minimum depth stays fairly constant throughout decay. There is a secondary minimum around phase 0.5 shown in Figures 2 and 3, which is stronger in the red. During the first two nights this minimum has an eclipse-like shape with sharp edges and flat bottoms. Later on it rather resembles variations caused by ellipsoidal distortion of the secondary. Again we found strong evidence for an unusual bright secondary which encouraged the attempt to obtain spectra during quiescence in order to detect the spectrum of the secondary.

Such spectra could be obtained with the ESO 2.2-m telescope in 1986. While observing, the 74 CCD spectra were sequentially arranged after each exposure into a two-dimensional frame displayed on the RAMTEK screen. Among the well-known emission line system of the primary disk configuration suddenly after a few integrations faint absorption

lines could be recognized to follow a sine like curve complementary to the emission lines (Fig. 6). – The secondary component had been detected! – The outburst spectra of 1985 had of course also been carefully checked earlier by plotting all traces in a single figure but no definite evidence for the companion star could be found. In the last weeks, a revision of the same spectra using the identical technique as in Fig. 6, revealed

the secondary component as well. A period analysis of the radial velocity variation yielded the photometric period.

In order to derive accurate system parameters from the observational data, several effects have to be taken into account as for example the non spherical shape and temperature distribution of the secondary and the distortion of the emission lines due to the complex velocity distribution of the line emitting

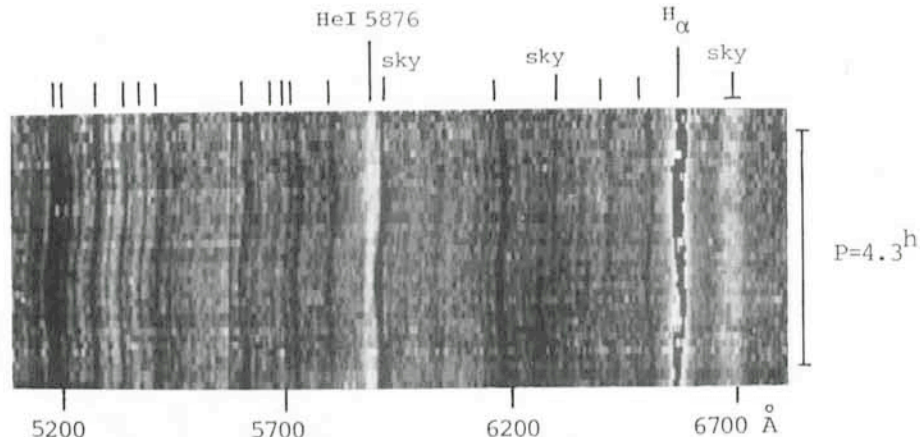


Figure 6: Sequential arrangement of 38 CCD spectra of BD Pavonis in quiescence taken with the 2.2-m telescope in 1986. The unlabeled tick marks indicate absorption lines of the secondary showing a sine like radial velocity variation.

material. Therefore the results obtained so far are still preliminary, however, it is obvious already that BD Pav has raised from a black dot on a plate in 1934 to an important star among the CVs.

#### References

- Barwig, H., Schoembs, R.: 1981, *Inf. Bull. Var. Stars* No. 2031.  
Barwig, H., Schoembs, R.: 1983, *Astron. Astrophys.* **124**, 287.  
Barwig, H., Schoembs, R., Buckenmayer, C.: 1987, *Astron. Astrophys.*, Main Journal, in press.  
Boyd, C.D.: 1939, *Harv. Ann.* **90**, 248.  
Payne-Gaposchkin, C.: 1977, in: *Novaes and related Stars*, p. 3.  
Schoembs, R., Dreier, H., Barwig, H.: 1987, *Astron. Astrophys.*, in press.

#### SUMMER SCHOOL ON

### "OBSERVING WITH LARGE TELESCOPES"

ESO and the Astronomical Council of the Academy of Sciences of the U.S.S.R. will organize a summer school during the period 21–30 September 1987 at the Byurakan Observatory near Erevan on the subject "Observing With Large Telescopes". A limited number of advanced predoctoral or recent postdoctoral participants from the ESO member countries will be invited to attend. Persons interested in participating should apply before 15 April 1987 to: Office of the Director General, ESO, Karl-Schwarzschild-Str. 2, D-8046 Garching b. München.

Applicants should give their main biographical data, passport number (incl. date and place of issue), a brief account of their scientific work and a list of publications. A letter of recommendation from their (thesis) supervisor should also be included.

## Strengthening Research Links Between Astronomy/Astrophysics and Computing/Statistics

F. MURTAGH<sup>1</sup>, Space Telescope – European Coordinating Facility, European Southern Observatory.

A. HECK, C.D.S., Observatoire Astronomique, Strasbourg, and

V. DI GESÙ, Dip. di Matematica ed Applicazioni, Univ. di Palermo, and IFCAI/CNR, Palermo.

In this article, a few current research directions are discussed, which relate to the common interfaces between astronomy/astrophysics, computer science and statistics. They relate essentially to organizational matters (working groups, conferences). Within the next decade contact between researchers over computer networks will become increasingly trouble-free, but for the present, contact between widely scattered researchers (and especially among those who straddle traditional disciplines) is necessarily in hard-copy form, as for example in this journal!

– Multivariate data analysis could be viewed as mid-way between statistics and graphics, and is an important part of the armoury of methods and tools available to the astronomer. Work to date in astronomy and astrophysics, using multivariate methods, has been surveyed (see Murtagh and Heck, 1986), and a text-book motivating methods, detailing the mathematics, and enumerating case-studies has recently become available (Murtagh and Heck, 1987).

– A working group was set up in 1985 to further contact between researchers with an interest in this, and related fields. It is the *Working Group for Mod-*

*ern Astronomical Methodology*, with a current active membership of a little under 100 worldwide. A bulletin is published twice yearly, and is currently contained in the *Bulletin d'Information du Centre de Données de Strasbourg* (C.D.S., Observatoire de Strasbourg, France). Further details may be obtained from André Heck or from Fionn Murtagh.

– Faced with ever-greater concentrations of astronomical data, new approaches to data handling and analysis need to be discussed and perfected. Recent years have seen the well-known workshops held at the Ettore Majorana Centre in Erice, Sicily (Di Gesù et al., 1984; 1986). The next workshop in the Erice series (*IIIrd International Workshop on Data Analysis in Astronomy*) will be held in June 1988. It will address advanced and unconventional data analysis methodologies; knowledge based systems; and parallel algorithms for data analysis. The use of fuzzy techniques and possibility theory is also an on-going topic of relevance, for low-statistics image data.

– A conference entitled *Astronomy from Large Databases: Scientific Objectives and Methodological Approaches* will be hosted by the ST-ECF in Garching on 12–14 October 1987. It functions as a follow-up conference to one enti-

tled *Statistical Methods in Astronomy* which was held in Strasbourg in 1983 (see Rolfe, 1983), and additionally addresses the topic of centralized data collections which are becoming increasingly important. The proceedings of this conference will be published by ESO.

– While it is important to focus efforts among astronomers and astrophysicists in order to tackle new problems in innovative ways, it is also important to mobilize computer scientists to bring increased efforts to bear on astronomical problems. A trend of relevance in recent years has been the increasing number of astronomical studies published in the mainstream pattern recognition literature. One important organ, internationally, in computing is the *International Association for Pattern Recognition* (IAPR). It is concerned with pattern recognition and image processing in a broad sense. It organizes major biennial conferences (the most recent in Paris in October 1986 had about 900 attendees), sponsors the journal *Pattern Recognition Letters*, and publishes a newsletter. Membership in the IAPR is by way of the relevant national pattern recognition or computing organization. The IAPR has a number of Technical Committees active in various fields of activity, and such a Technical Committee has recently been set up for astronomy and

<sup>1</sup> Affiliated to the Astrophysics Division, Space Science Department, European Space Agency.

astrophysics. Further details may be obtained from Vito Di Gesù or from Fionn Murtagh.

The foregoing trends serve to illustrate how "computational astronomy" has now become solidly established as a subdiscipline of importance in astronomy and astrophysics, closely following in the footsteps of its sister-subdiscipline, image processing.

#### References

1. V. Di Gesù, L. Scarsi, P. Crane, J.H. Friedman and S. Levialdi (eds.) (1984): *Data Analysis in Astronomy*, Plenum Press, New York.
2. V. Di Gesù, L. Scarsi, P. Crane, J.H. Friedman and S. Levialdi (eds.) (1986): *Data Analysis in Astronomy II*, Plenum Press, New York.
3. F. Murtagh and A. Heck (1986): An annotated bibliographical catalogue of multivariate statistical methods and of their astronomical applications (magnetic tape).

A conference, hosted by the Space Telescope – European Coordinating Facility, on

## Astronomy from Large Databases: Scientific Objectives and Methodological Approaches

will be held in Garching from 12 to 14 October 1987.

Topics will include statistical analysis of complex databases, object classification problems, astrophysics from large data collections, together with state of the art reviews of astronomical database technology and expert system applications.

The Proceedings will be published by ESO.

Further information may be obtained from F. Murtagh, ST-ECF, ESO, Karl-Schwarzschild-Str. 2, D-8046 Garching bei München, FRG.

*Astronomy and Astrophysics Supplement Series* (in press); ESO Scientific Preprint No. 465 (Sept. 1986).

4. F. Murtagh and A. Heck (1987): *Multivari-*

*ate Data Analysis*, D. Reidel, Dordrecht.  
5. E.J. Rolfe (ed.) (1983): *Statistical Methods in Astronomy*, European Space Agency Special Publication 201 (270 pp.).

## Crowded Field Photometry Using EFOSC and ROMAFOT

K.J. MIGHELL, Kapteyn Observatory, Roden, The Netherlands

### EFOSC

The ESO Faint Object Spectrograph and Camera (EFOSC), instrument of the ESO 3.6-m telescope, can be used as a very efficient CCD camera for wide-band photometry of crowded stellar fields. EFOSC was designed to match the RCA SID 501 EX CCD ( $320 \times 512$  pixels,  $30 \times 30$  microns pixel size). Each pixel corresponds to 0.675 arcsec and the total field of view is  $3.6 \times 4.7$  arcminutes (1). Using the instrument in direct imaging mode, the limiting magnitude of a 15 minute exposure with seeing of  $\text{FWHM} = 1.3$  arcseconds in the V band is about 25.5 for a signal-to-noise ratio of 3 (2).

A typical EFOSC field of the Small Magellanic Cloud will yield hundreds to thousands of stars in less than five minutes! In good seeing conditions the central cores of star images will be partially undersampled due to the 0.675 arcsecond per pixel scale. The combination of crowded stellar fields with partially undersampled data presents a challenge to the astronomer who wishes to do accurate stellar photometry with EFOSC data.

### DAOPHOT

In March 1986 I visited ESO Garching to see if the photometric reduction package DAOPHOT (3) was suitable for use with EFOSC data and CCD data

from the ESO 2.2-m telescope. Using both real and artificial data, I found DAOPHOT to be potentially useful for the 2.2-m data (0.35 arcsecond per pixel) and totally inadequate for the less well sampled EFOSC data (0.675 arcsecond per pixel). The results of this trial experiment do not bode well for the ability of DAOPHOT to work adequately with data from the Hubble Space Telescope.

### ELIA

ELIA (4) was developed at the Observatory of Rome specifically to do photometric reduction in crowded stellar fields – in particular globular clusters. I visited the Observatory of Rome in October 1985 and reduced some EFOSC images of an extremely crowded field in the SMC. Although the image was quite complex, ELIA made excellent fits to over 1,400 stars. ELIA employs a non-linear least squares fitting algorithm which was found to be remarkably successful at ignoring cosmic rays and other image defects.

### ROMAFOT and the Personal Astronomical Work Station

At the Rome Observatory, ELIA serves as a complete image processing system. Thus there are programmes to read and write FITS tapes, programmes to flat-field images, programmes to plot

data, etc. By using the ESO Munich Image Data Analysis System (MIDAS) as my main image processing system, I only needed to use the few programmes which actually did photometric reduction. I have converted these programmes to run on VAX computers and have renamed the package ROMAFOT.

I have also written a C language programme "Personal Astronomical Work Station" (PAWS) which effectively transforms a standard Commodore Amiga personal computer into a complete MIDAS work station consisting of emulations for (1) a VT-100 terminal, (2) a HP graphics terminal and (3) a DeAnza image display. By replacing the Tektronix terminal that ELIA previously required with an Amiga running PAWS, I have been able to substantially improve the performance of ROMAFOT. By judiciously using coloured images (instead of shades of green), ROMAFOT has been improved to make it easier for the user to quickly produce more accurate results. The combination of ROMAFOT with MIDAS provides the astronomer with a very powerful tool to do accurate photometric reduction of crowded stellar fields.

### ROMAFOT/MIDAS Features and Abilities

- Reads FITS tapes
- Automatic location of most stars on a CCD image

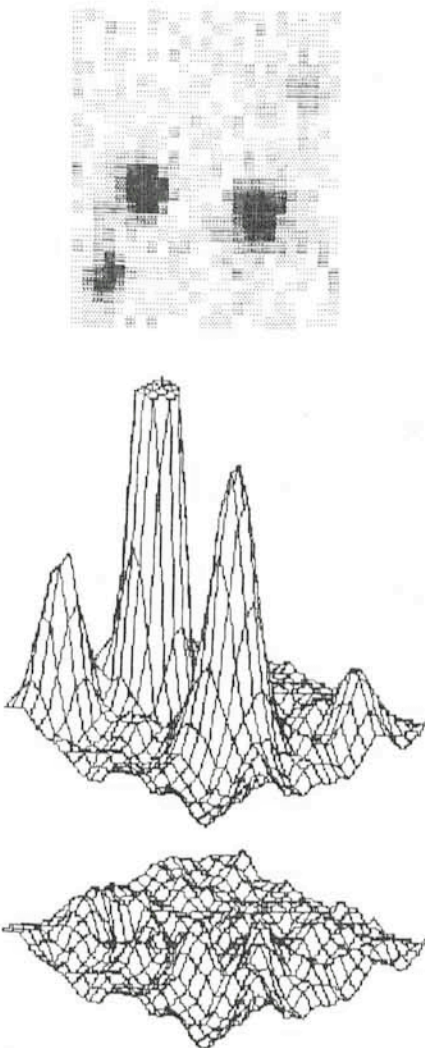


Figure 1.

- Examination of each stellar image to check for image quality, potential blending and missed fainter stars
  - Fast nonlinear least squares fitting routines that allow up to five blended components to be fitted simultaneously
  - Accurate and believable error estimates are determined for all fitted parameters
  - Examination of the final fits by displaying the original data and residuals
  - A proficient user can process 500 to 1,000 stars per day (depending on the crowding complexity of the field)
  - Transformation of coordinates from one CCD frame to the system of another frame
  - Transformation of instrumental magnitudes to a standard photometric system
  - Plots the results on a standard HR diagram
  - Artificial stars can be randomly inserted into the data at known flux levels to allow the user to find the systematic measurement errors.
- A visual example of how ROMAFOT and MIDAS can be used to do photo-

metric reduction in crowded stellar fields is shown in Figure 1 (all plots were made with PAWS).

Figure 1a shows a gray-scale representation of a crowded stellar field near the centre of Carina, a dwarf spheroidal galaxy in the Local Group. The data were collected with the ESO 3.6-m telescope using the EFOSC instrument with seeing of FWHM = 1.35 arcseconds in the V band. The integration time was 30 seconds. The subfield is 16.9 by 16.9 arcseconds in size. The intensity scale is linear with black representing the maximum and white representing the minimum intensity.

Figure 1b shows the same subfield in the form of a three-dimensional plot. The brightest star has a flat core because it was clipped for the plot to show better the fluctuation of the background. The second highest peak is composed of two closely spaced stars.

Figure 1c shows the residual field after all five stars were fitted. The visual magnitudes of the stars are  $19.16 \pm 0.01$ ,  $20.56 \pm 0.05$ ,  $21.38 \pm 0.11$ ,  $21.03 \pm 0.06$ ,  $22.00 \pm 0.16$ , respectively. The peaks of the two closely spaced stars ( $V = 20.31$ ,  $V = 21.13$ ) are separated by only 2.12 pixels. The full width at half maximum (FWHM) for these data is only 2.00 pixels, so these two stars are just barely resolved.

The above example shows how EFOSC can be used to obtain useful

photometry for many faint stars with short exposures. The ability to reach a visual magnitude of 22 in just 30 seconds will be very useful to those astronomers who would like to determine the colour-magnitude diagrams of globular clusters and stars in the Galaxy and nearby Local Group galaxies.

## The Future of ROMAFOT

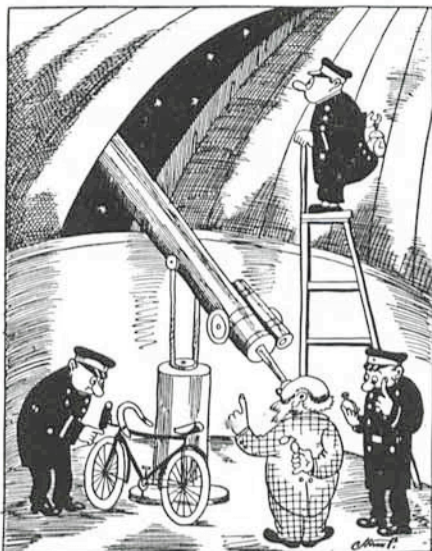
Roberto Buonanno (Observatory of Rome), Rein Warmels (ESO) and I will be working in the next few months to officially implement the ROMAFOT package as a part of MIDAS. The exact form of the MIDAS version of ROMAFOT has yet to be finalized but it will probably be very similar to the system I have described above.

## References

- (1) D'Odorico, S., Dekker, H., "The Five Observing Modes of EFOSC, the ESO Faint Object Spectrograph and Camera Designed Around a CCD Detector".
- (2) *The Messenger* 41, p. 26, 1985.
- (3) Stetson, P.B., "DAOPHOT User's Manual", Dominion Astrophysical Observatory, Herzberg Institute of Astrophysics, 5071 West Saanich Road, Victoria, British Columbia V8X 4M6, Canada.
- (4) Buonanno, R., Corsi, C.E., De Baise, G.A., Ferraro, I., 1979, in *Image Processing in Astronomy*, eds. G. Sedmak, M. Capaccioli, and R.J. Allen, Trieste, Italy, p. 554.

## Storm Petersen and Astronomy

Robert Storm Petersen (1882–1949) started his career as a butcher, but became a symbol of arch-Danish humour during his lifetime. Although *Storm P.* (as he is known by his countrymen)



*'The police now collaborates with the astronomers to determine the exact time when bicycle lights must be lit.'*

wrote prolifically, he is more famous for his drawings which appeared regularly in Danish newspapers from 1905 to his death. Many of the early drawings dealt with social injustice, but he soon found his own, less offensive way of expression. A museum dedicated to his works has been opened in Copenhagen and also exhibits many of his cartoons. Many of them concern the exact sciences which *Storm P.* approached with a sound measure of down-to-the-earth scepticism. But his dry humour always treated members of the astronomical profession and other employees of the state with due reverence . . .

## EDITOR'S NOTE

The information about the bright supernova 1987A in the LMC which is brought on the following pages was received on March 2, 1987. The publication of this issue of the *Messenger* was delayed in order to include a first overview of the exciting results.

# The Supernova in the LMC

During the night of 23/24 February, I. Shelton at the University of Toronto station at Las Campanas discovered a supernova in the Large Magellanic Cloud – the first naked-eye supernova to be seen since Kepler observed his “nova” in 1604. From the following night on, most ESO telescopes have been used to observe this object. The extraordinary brightness of this supernova for the first time allows very detailed observations to be made of the still mysterious supernova process, which involves the collapse and subsequent explosion of a star at the end of its evolution, and the probable genesis of a neutron star. In addition, this brightness allows studies to be made of the halo of our Galaxy and of the intergalactic medium by observations of absorption lines produced by the intervening matter. The absorption line data obtained with the High Resolution Spectrograph at the 1.4-m CAT have been unexpected and qualitatively superior to anything obtained before in the LMC.

In the last decades, supernovae have been observed in other galaxies; these supernovae, however, were always more than a hundred times fainter than the one in the LMC. While studies made with large telescopes at La Silla and elsewhere have yielded interesting data, no very high resolution studies were possible. With the full light gathering power of the VLT, however, fainter supernovae in other galaxies as well as some stars in the LMC will be observed with the same spectroscopic resolution as has been possible now for the LMC event. This supernova thereby gives us a preview of the discoveries that can be made with the VLT.

Following the discovery of the supernova, the telescope schedules have been changed and many planned programmes have not been executed. All observers at La Silla have switched over to the supernova with much enthusiasm. While for their coinvestigators it may be disappointing not to receive the data from their planned programmes, we expect that they will understand that it was not possible to continue business as usual in the light of this event. The initial data will be published very rapidly to ensure that the scientific community be fully informed.

L. WOLTJER, Director General of ESO

## The Initial Impact of the LMC Supernova

Between 2 o'clock and 7 o'clock universal time (UT) on Monday morning, February 23, 1987, a star in the Large Magellanic Cloud (LMC), at the position of the B3 I supergiant Sanduleak -69202, began to brighten rapidly. By 10 o'clock UT it had brightened by a factor of 200. And the next day it had increased in brightness by an additional factor of 10. As L. Woltjer notes above, this star is the first really bright supernova in the modern era. Because of its southern declination it can only be seen by southern observatories and space observatories.

The excitement generated by the supernova is intense. It is unusual in a number of respects and it is bright enough to be studied in great detail. It is nearly certain that the progenitor of the supernova is Sanduleak -69202. Since B supergiants were not believed to be evolved enough to undergo the core collapse necessary to produce a supernova, it had been thought that only M giants or supergiants could be the progenitors of supernovae. The LMC supernova is the first type II supernova to be seen in an irregular galaxy. It has long been a mystery why type II supernovae were not seen in irregular galaxies. Also this supernova is 2 to 5 magnitudes (up

to a factor of 100) fainter at maximum light than expected. This might be due to the fact that the progenitor is a B star rather than an M star. It has been suggested by Truran, Höflich, Weiss and Meyer (private communication) that the difference between this supernova and Type II supernovae in other galaxies is attributable to the low metallicity of the Large Magellanic Cloud. Brunish and Truran (1982, *Astrophysical Journal, Suppl.* **49**, 447–468) have shown that metal poor B stars may never become M supergiants prior to the onset of carbon burning. According to Peter Höflich at the Max Planck Institute for Astrophysics, the B star envelope has a steeper density gradient than the M star envelope. The denser inner envelope may trap the photons and result in a fainter maximum than would be the case if an M star had exploded. Because of this, more energy can be converted into kinetic energy in the outgoing matter. Since the LMC is metal poor, this model may explain the explosion of Sanduleak -69202. These authors also note further that it helps us to understand why we have not previously observed Type II supernovae in irregular galaxies. In any case, the future development of the supernova and more detailed modelling

can probably resolve these questions.

There is one characteristic of the LMC supernova that is not modest. The H $\alpha$  line shows structure 1000 Å wide. This corresponds to velocity outflow of 25,000 km/sec. If the envelope continues to expand at this rate it will subtend an angle of nearly 1/4 arcsec at the end of a year. When the VLT is completed about 10 years from now, the envelope will be big enough for detailed study by the VLT.

Early excitement was generated by CES spectroscopy of interstellar (and intergalactic) atomic lines. The CaII, H and K lines were broken into over 20 components with velocities ranging from the Galactic value to the velocity corresponding to the LMC, and numerous lines with intermediate velocities showed the presence of intergalactic clouds. When CES spectra are combined with far ultraviolet spectra taken with IUE it will be possible to determine the details of the ionization structure and abundances of the interstellar clouds in the line of sight to the supernova. The LMC supernova is already a bright radio source and it is very likely that it will become sufficiently bright for radio observations to determine the neutral hydrogen column densities in

these clouds. Such studies illustrate the value of exploiting a temporarily bright source in order to study the physics of the intervening material.

These reflections are being written one week after the explosion. We still have much to learn. Does the LMC supernova represent a new, previously unknown class of supernova? Will we see changes in the interstellar lines that will indicate the size of these gas filaments? Can model calculations together with early observations accurately pinpoint the moment the envelope began to expand? If so, what is the time delay between the beginning of the expansion and neutrino burst detected by

A workshop will be held at the ESO Headquarters in Garching from July 6–8, 1987 on

### "The Supernova in the LMC"

Data obtained during the first half year of the supernova will be presented and other evidence and theories about supernovae confronted with the data.

For further information please contact:

Dr. J.I. Danziger, European Southern Observatory, Karl-Schwarzschild-Str. 2, D-8046 Garching.

the Mont Blanc Neutrino Observatory? When will we be able to see the inner part of the expanding envelope with its rich soup of the products of nuclear

fusion? Surely this supernova will be one of the most actively studied objects in the sky for years to come.

J. Wampler (ESO)

## Walraven Photometry

The measurements were converted from log intensity to magnitudes.

UT	V	V-B	B	B-L	L	B-U	U	U-W	W
WAVEL. (Å)	5467		4325		3838		3633		3255
BANDW. (Å)	710		420		220		230		160
Feb.									
25.02	4.64	-0.19	4.83	-0.12	4.95	-0.13	4.96	-0.14	5.10
25.15	4.57	-0.19	4.76	-0.11	4.87	-0.11	4.87	-0.10	4.97
26.01	4.55	-0.26	4.81	-0.24	5.05	-0.31	5.12	-0.18	5.30
26.20	4.53	-0.26	4.79	-0.28	5.07	-0.33	5.12	-0.14	5.26
27.01	4.48	-0.39	4.87	-0.48	5.35	-0.65	5.52	-0.57	6.09
27.17	4.45	-0.40	4.95	-0.50	5.45	-0.71	5.66	-0.65	6.31
28.01	4.46	-0.56	5.02	-0.72	5.74	-1.26	6.28	-1.09	7.37
28.10	4.45	-0.54	4.99	-0.72	5.71	-1.27	6.26	-1.02	7.28
28.24	4.45	-0.56	5.01	-0.76	5.77	-1.35	6.36	-1.02	7.38
+/-	0.02	0.02	0.04	0.02	0.04	0.02	0.06	0.02	0.09

Observed by F. Steeman on the Dutch 91-cm telescope on La Silla.

P. Monderen, H.E. Schwarz (ESO), and F. Steeman (Leiden).

## Geneva Seven Colour Photometry

The Supernova 1987A in LMC was measured 46 times between February 25 and March 2 in the seven filter Gene-

va photometry (Golay, M., 1980, *Vistas in Astronomy*, vol. 24, 141) at the ESO La Silla observatory.

SN 1987A was measured together with the comparison star HD 37935, a Geneva standard star. It should be

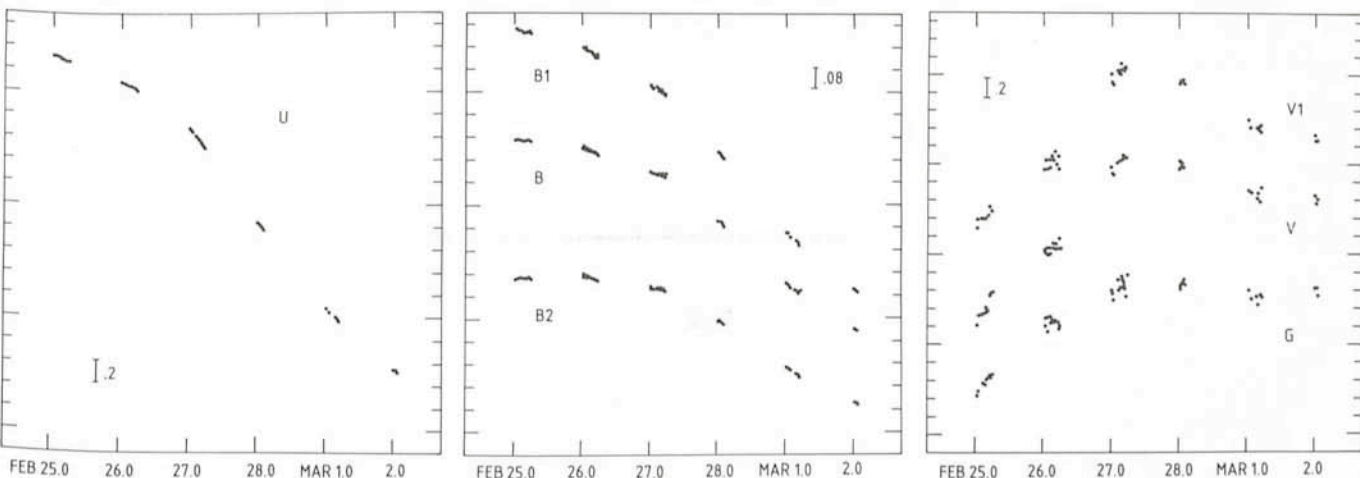


Figure 1: (a) U magnitude relative to the comparison star HD 37935; (b) B1, B and B2 magnitudes relative to the comparison star HD 37935; (c) V1, V and G magnitude relative to the comparison star HD 37935.

Table 1

Date	DV/DT	DU/DT	DB/DT
Feb. 25.0	-0.08	0.23	0.03
Feb. 26.0	-0.10	0.40	0.08
Feb. 27.0	0.01	0.83	0.18
Feb. 28.0	0.02	0.74	0.22
Feb. 29.0	0.01	0.55	0.17

noted that the values presented here are only preliminary, the final reductions will be performed in Geneva. Figure 1 shows the different magnitudes, relative to the comparison star. A first important feature to be noticed is the retardation of the intensity drop in the longer wavelength V1, V and G filters with respect to the B1, B and B2 and especially to the U filter, which was already decreasing significantly during the first night of observations. In Figure 1A, referring to the U filter, we see that after a strong decrease in brightness between February 27.0 and 27.9, the curve exhibits an inflection point. From the calculated gradients of the U light curve

(Table 1), we conclude that the curve became considerably smoother after the inflexion point.

The decrease in B1, B and B2 (Figure 1B) is much slower, the B2 curve even remains almost constant during the first two nights. Nevertheless, these curves too show an inflexion point. In contrast, the V1, V and G curves have a pronounced maximum during the third night (February 27.0) and a slow decrease afterwards. The V1-G index, in Figure 2, shows a completely different behaviour from the other colour indices. It has a strong peak towards the blue, coinciding with the time of maximum light in the V filter. This feature can be

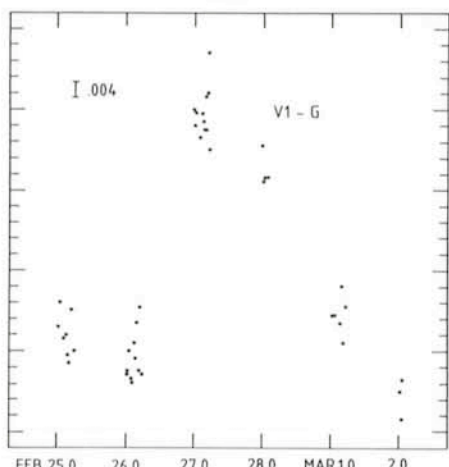


Figure 2: V1-G index relative to the comparison star HD 37935.

correlated with the disappearance of the P Cygni He I 5876 line observed simultaneously by Danziger, Fosbury and Dachs at the 3.6-m telescope.

J. Babel (Lausanne/Genève),  
D. Heynderickx (Leiden)

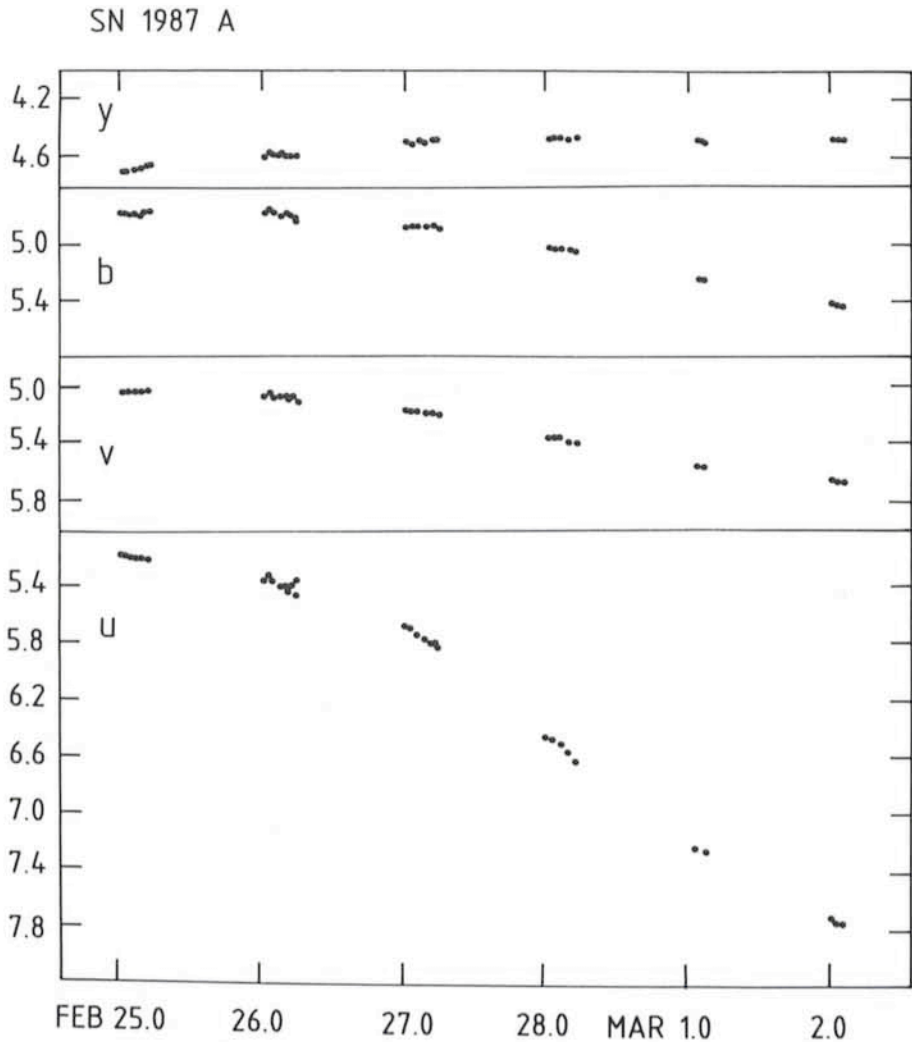
## Strömgren Photometry

As of March 2, the supernova SN 1987A was observed with the Danish 50-cm telescope on every night since its discovery. The Strömgren *uvby* intermediate band system was used. This combination of a small telescope and band widths of about 200 Å turned out to be ideal for observing such a bright star.

The bands in the *uvby* system are centred at 5490 Å (*y*), 4690 Å (*b*), 4110 Å (*v*), and 3500 Å (*u*). From spectra of the supernova obtained by other observers on La Silla we know that *y* essentially measures the continuum while both *b* and *v* fall on edges between emission lines and their P Cygni absorption throughs. The *y* magnitude is very similar to the visual *V* magnitude.

Preliminary light curves in the instrumental system are shown in the figure. It is obvious that *u* peaked before observations began and is now declining rapidly, while a maximum in *y* probably was reached around February 28, 1987. However, the changes in *y* are small. In addition to the *uvby* light curves, some Hβ observations are made to see whether changes in the Hβ structure can be detected by studying the flux through the narrow (30 Å) beta filter.

B.E. Helt (Copenhagen), L.P.R. Vaz (São Paulo) and H.E. Jørgensen (Copenhagen)



# Detection of the Diffuse IS Band at $\lambda$ 5780 Å in the Large Magellanic Cloud

The band at  $\lambda$  5780 Å is one of the 39 diffuse IS absorptions in the region  $\lambda\lambda$  4400–6850 Å which are generally correlated with the colour excess  $E(B-V)$  (Herbig, *Astrophysical Journal*, **196**, 129, 1975), and whose origin is still unknown. G. Vladilo (Osservatorio Astronomico di Trieste, Italy) took an exposure of  $1^h15^m$  of SN 1987A in the spectral range around  $\lambda$  5780 Å, with the CAT+CES+Reticon and a resolving power of 100,000. In Figure 1 one can see an expanded detail of the resulting calibrated spectrum. It is clear that two features have been detected: one close to the rest wavelength, which is interpreted of galactic origin, and the other displaced by a radial velocity of +261 km/s, i.e., in good agreement with neutral gas components previously detected in the LMC (de Boer, Fitzpatrick, and Savage, *M.N.R.A.S.*, **217**, 126, 1985). This is the first extragalactic de-

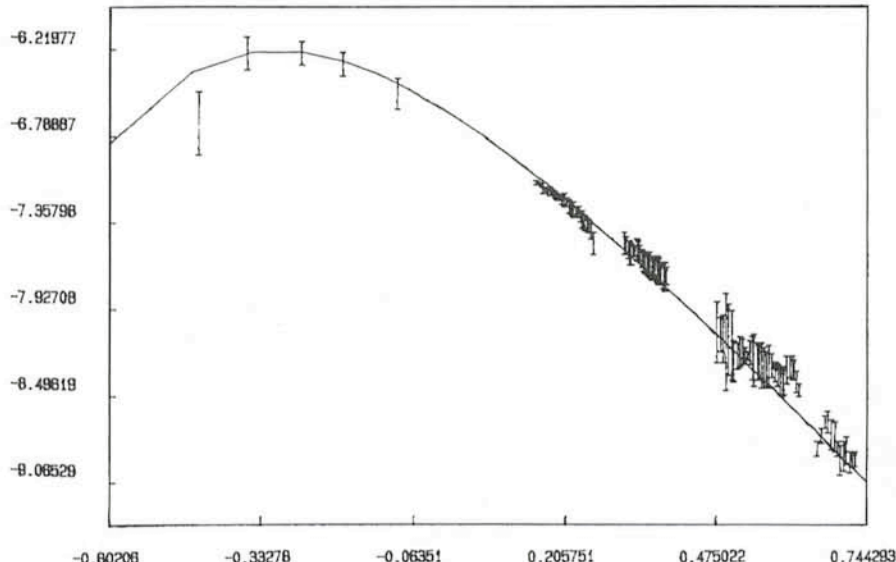


Figure 1: The 5780 Å feature, as observed in the spectrum of supernova 1987A. Note that the ordinate interval is less than 4 % of the continuum intensity.

tection of the  $\lambda$  5780 Å band. The central depths of the galactic and LMC components, once normalized to the continuum, are 0.023 and 0.018 respec-

tively, that is about one order of magnitude weaker than the typical values found by Herbig (1975) in his survey of galactic lines of sight. G. Vladilo (Trieste)

## The Temperature of 1987A



Visible photometry and infrared CVF scans. Data were collected on the night between February 28 and March 1, 1987, with the standard photometer attached at the ESO 50-cm in the broad Johnson bands UBVRI, and with the INSB detector at the 1-m telescope for the infrared, at La Silla. IR data have been collected by P. Bouchet and R. Stanga. The continuous line is the fit of a black body with a temperature  $T = 5900$  K. Vertical axis: Log (flux density ( $\text{ergs cm}^{-2} \text{s}^{-1} \mu\text{m}^{-1}$ )). Horizontal axis: Log ( $\lambda \mu\text{m}$ ).

## Fast Photometry of 1987 A

Fast photometry of the SN 1987 A has been carried out with the 1-m and the GMS 0.28-m telescopes at La Silla.

The 1-m telescope was equipped with the multi-channel photometer of the Universitäts-Sternwarte München. UBVRI data were obtained, observing sky and comparison star in two channels simultaneously with the object. Two photometric data sequences

were obtained with time resolution of 0.5 sec and 40 millisec respectively. Figure 1 shows a condensed version of the data plotted in bins of 8 seconds. The U-B decrease is due to the U fading of the supernova. B-V and V-R are almost constant during the night. The irregular variability in V-I is due to the I band and is probably caused by fluctuations of the comparison star. A preliminary

analysis does not reveal significant periodic or non-periodic variations on short timescales. The 3 sigma level for the detection of periodic variations was 0.0004 relative amplitude.

The system at the GMS telescope is normally used for monitoring gamma-ray bursters and has been described by Bouchet and Gutierrez (*Messenger*, **45**, 32). Thanks to the frantic work of J. Alonso and F. Gutierrez, it was possible to adapt it for monitoring the SN 1987 A on every clear night since the discovery, with a time resolution of 10 millisec and 1 millisec in the Johnson V band and in white light. It has not been possible to detect any periodical fluctuation in the frequency interval between 0.0003 and

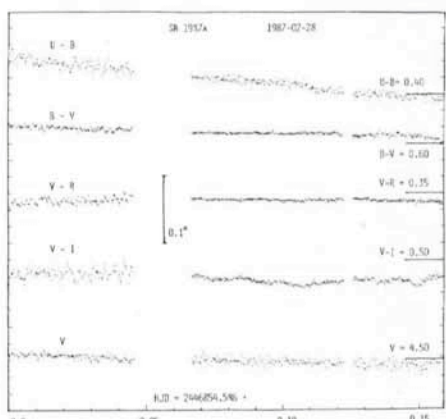


Figure 3: Condensed UBVRI (Kron-Cousins) light curves of the SN 1987 A, obtained on February 28. Each dot corresponds to an integration time of 8 seconds.



These two colour photos of the Large Magellanic Cloud show the sudden appearance of the bright supernova 1987A. They were obtained with a 6 × 6 Hasselblad camera mounted piggy-back on the GPO and Danish 1.5-m telescopes, respectively. The left-hand photo was taken on February 23, between 01 : 00 and 01 : 20 UT and is the last colour picture taken before the supernova exploded, probably a few hours later. The

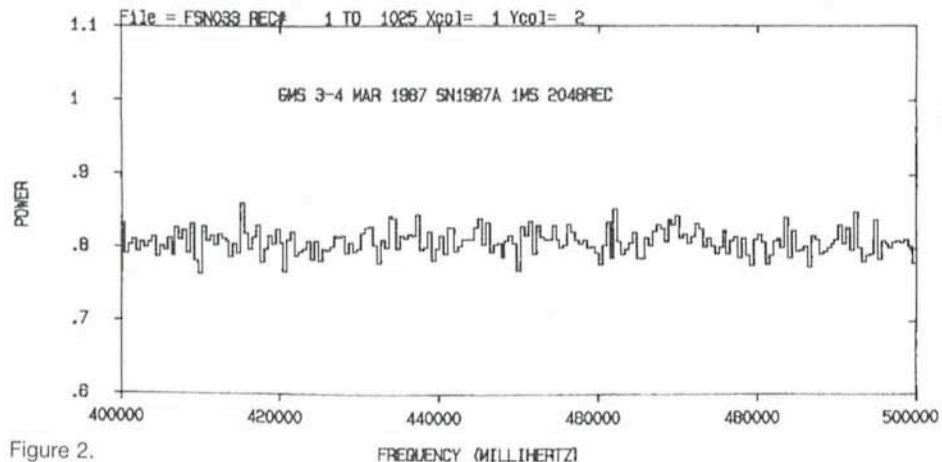


Figure 2.

500 Hz. In Figure 2 a portion of the Fourier transform of the GMS data is shown. Calibration of the system is in progress and the monitoring of the SN 1987 A will continue until it becomes too faint for this telescope.

H. Barwig, R. Schoembs (München)  
S. Cristiani, C. Gouiffes, J. L. Sauvageot  
(ESO)

## Chronology of a Once-in-a-Lifetime Event

Only 48 hours separate the two photos above, but during this brief interval an event happened that excited an entire generation of astronomers. Re-

flecting the importance of this supernova, the Central Bureau for Astronomical Telegrams issued no less than 15 IAU Circulars in the course of 9 days only, breaking all records in the history of astronomy. At ESO, these circulars were read through a computer link to the Headquarters in Garching as soon as they were issued, and immediately sent on to the observers at La Silla by telefax. In this way, and also by numerous telex messages and phone calls, the scientists were kept informed about what was going on in other places.

The time immediately following the discovery was particularly hectic. Here is a provisional compilation of the main events during the first hours, drawn from the information available on March 4:

UT

Feb.

22.4 Photos obtained with the University of Aston satellite tracking



right-hand photo was taken exactly two days later, on February 25, also at UT 01:00. On that date, the supernova had reached visual magnitude 4.5. It is well visible, left of the centre and above the LMC main body as the lower right (round) of the two bright objects. The other object, which is extended and more diffuse, is the Tarantula Nebula (30 Doradus). (Agfachrome 1000 RS emulsion, C. Madsen.)

- camera in Australia (R. H. McNaught) show the progenitor Sanduleak -69 202 at normal magnitude 12.
- 23.06 C. Madsen at La Silla obtains colour photo of LMC (above).
- 23.08 I. Shelton at Las Campanas obtains photo of LMC (not yet showing the supernova).
- 23.12 Five pulses, above 7 MeV, are detected during a 7 sec interval with the neutrino telescope in the Mount Blanc tunnel. This experiment is a collaboration between Istituto di Cosmogeofisica, Torino, Italy, and the Institute of Nuclear Studies in Moscow, USSR.
- 23.44 The supernova is recorded as a 6.1 magnitude object on plates taken with the satellite tracking camera in Australia, but it is not yet detected by the operators.
- 24.02 Shelton starts 3-hour exposure with the 25-cm astrograph of the University of Toronto station at Las Campanas.
- 24.2 Suspected visual sighting of the supernova by O. Duhalde, also at Las Campanas.
- 24.23 Shelton discovers the supernova on his plate after development. The IAU Telegram Bureau is informed soon thereafter.
- 24.37 Independent discovery by A. Jones, at Nelson, New Zealand, who estimated it at magnitude 5.1
- 24.4 A telegram announcing the discovery of the supernova, now designated "1987 A", is sent to all major observatories from the IAU Telegram Bureau.
- 24.46 McNaught estimates it at magnitude 4.8.
- 24.72 McNaught now thinks that it has brightened to 4.4
- 24.8 Spectral observations commence with the International Ultraviolet Explorer, a satellite telescope in orbit around the Earth, jointly operated by ESA and NASA.
- 24.8 Night falls in South Africa and multicolour photometry observations start at the SAAO.
- 24.9 A spectrum obtained with the 1.9 reflector at SAAO shows few features and appears to indicate that the object may be of Type I.
- 25.0 Night falls in Chile and observers at all telescopes on La Silla turn their attention to 1987 A . . .
- 25.05 The second colour picture of LMC, now with the supernova, is obtained by C. Madsen.

R. M. West (ESO)

# The Spectrum of Supernova 1987A

In the early phase of a supernova, the dense atmosphere of the progenitor star is blasted off with a high velocity. This surface radiates like a "black-body" and, as such emits a continuous spectrum which is essentially independent of the chemical composition and whose energy distribution is determined solely by its temperature: the light is radiated by charged particles as they scatter off one another.

As the "atmosphere" grows in size, the range of depths from which the photons can escape increases and the chemical composition becomes important in determining the opacity of the gas at different wavelengths. This is when spectral lines start to become apparent. But still, and indeed for a long time after maximum light, most of the energy is radiated as an approximately black-body continuum with a temperature – at least in type II supernovae, which are supposed to be hydrogen rich – corresponding to the layer where the hydrogen becomes fully ionized. The lines just impose a modulation on this underlying continuum. The outer part of the atmosphere, well above the continuum emitting surface, will radiate emission lines while that part between the surface and us will absorb the same lines. Since the atmosphere is expanding, the absorbing part will have the greatest component of velocity towards us and so will produce "blue-shifted" lines. Such an emission/absorption structure is known as a "P-Cygni" profile after the prototype Be star with an expanding atmosphere. Measurements of the positions (in wavelength), strengths and shapes of such profiles provide astronomers with the means to study the composition and the velocity evolution of the expanding shell.

The first optical spectra of SN 1987A obtained at ESO on the night of 24–25 February show very weak spectral features and an overall energy distribution which corresponds to that of a hot star. Over the next two days, strong, broad spectral features began to appear and by 27 February (Fig. 1a), strong P-Cygni lines are seen which correspond primarily to the Balmer series of hydrogen. The shift of the H-alpha absorption trough with respect to the rest wavelength corresponds to a velocity of over 17,000 km/s when the first measurements were made. The spectrum now appears to be evolving in the sense that the overall energy distribution is becoming redder (a cooling of the continuum emitting "photosphere") and the velocity shifts of the P-Cygni absorption components are slowly decreasing. The lines

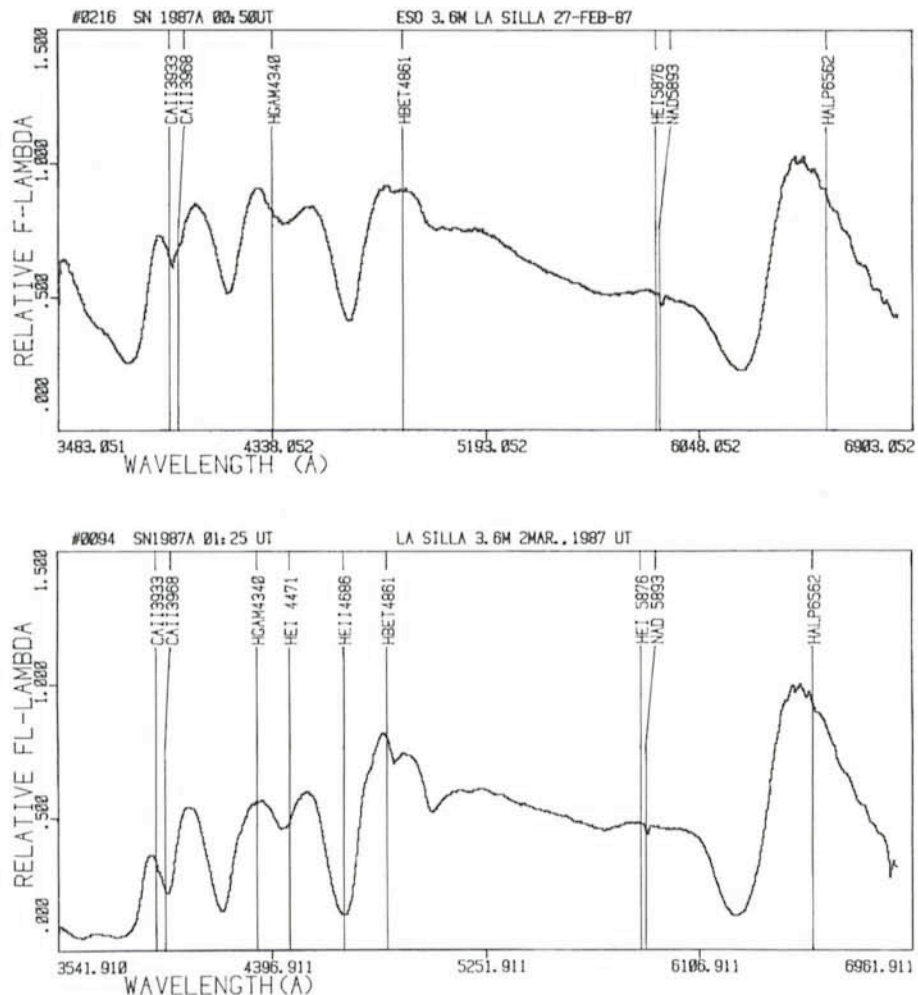


Figure 1: Spectra of 1987A, obtained by J. Danziger and R. Fosbury at the ESO 3.6-m telescope with the Boller and Chivens spectrograph. The upper spectrum (a) was obtained on February 27.05, four days after the explosion and already shows the strong P Cyg profiles mentioned in the text. The lower spectrum (b), although qualitatively similar, displays important changes in the amplitude and also in the velocities of the main features.

are also becoming stronger as the volume of the emitting gas increases and the temperature of the absorbing column decreases (Fig. 1b). There are

other, more subtle, changes as broad spectral features appear and fade as the ionization conditions in the atmosphere change. Because they are so broad,

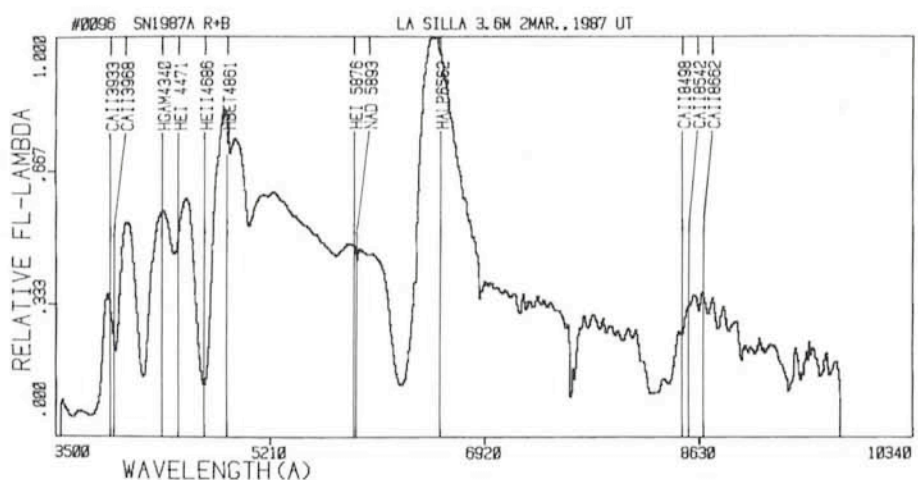


Figure 2: Spectrum of 1987A, obtained by R. Fosbury (3.6-m + B & C spectrograph + RCA CCD) on March 2.1 and covering the 350–950 nm spectral region.

these features are notoriously difficult to attribute to different chemical elements but it appears likely that the strongest of them can be identified with singly ionized calcium and iron. When the optical and infrared data are combined, the temperature of the "black-body" continuum is readily measured; it was 5900 K on the night of 1–2 March (see the plot of the infrared – optical photometry). The fact that this temperature

was higher in the initial phase was good news for the IUE for which the supernova now provides a greatly weakened source.

Another aspect of the spectroscopy which is causing great excitement is the possibility such a bright object in the LMC provides for the study of the interstellar/intergalactic medium between us and the supernova. Sight lines outside our own Galaxy have been studied be-

fore, using as background sources bright stars in the Magellanic Clouds and much more distant Quasars and Seyfert galaxies. These, however, are very faint objects and the opportunity presented by a naked eye supernova has already resulted in a Bonanza of results from the very high resolution spectrograph (CAT/CES) at ESO (see contribution by Andreani, Ferlet and Vidal-Madjar). *R. Fosbury (ST-ECF)*

## High-resolution Spectroscopy of 1987A

Observations at the 1.5-m CAT telescope with the Coudé Echelle Spectrograph and the Reticon Detector at resolution 100,000 (3 km/sec) have led to the identification of the following eleven in-

tervening main structures in the direction of the supernova: 7–22 km/s (heliocentric), strong Na I, Ca II, K I; 38 km/s, weak Ca II; 55–63 km/s, strong Ca II, weak Na I; 70–74 km/s,

same; 121–127 km/s, strong Ca II; 160–169 km/s, same; 206–218 km/s, strong Ca II and Na I; 248–253 km/s, weak Ca II and Na I; 264–269 km/s, same; 278–283 km/s, strong Ca II, Na I, K I; 293 km/s, weak Ca II. Many of these main structures are resolved into two or three nearby components. In particular, the 7–22 km/s structure clearly shows three distinct components.

In addition to the identification of a large number of intervening clouds, these observations establish with certainty that supernova 1987A is situated in the Large Magellanic Cloud, since no absorption lines are seen with velocities higher than that of the LMC.

*P. Andreani, R. Ferlet and R. Vidal-Madjar (IAP, Paris)*

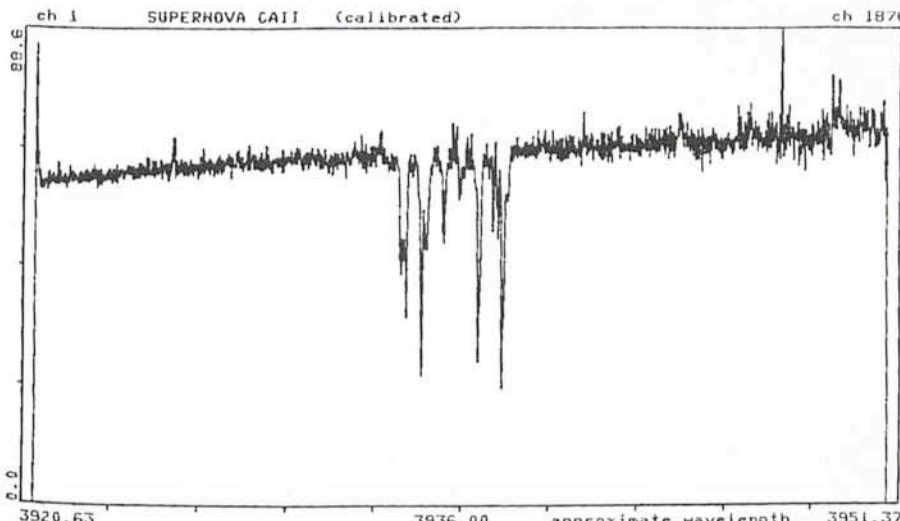


Figure 1: The spectrum of 1987A, around the Ca II (K) line at 393.3 nm, as obtained on February 25.05, with the CAT + CES + Reticon detector at resolution 100,000. The exposure time was 1,200 sec. This figure shows the main absorption structures only; up to 22 absorption lines from interstellar and intergalactic clouds were detected.

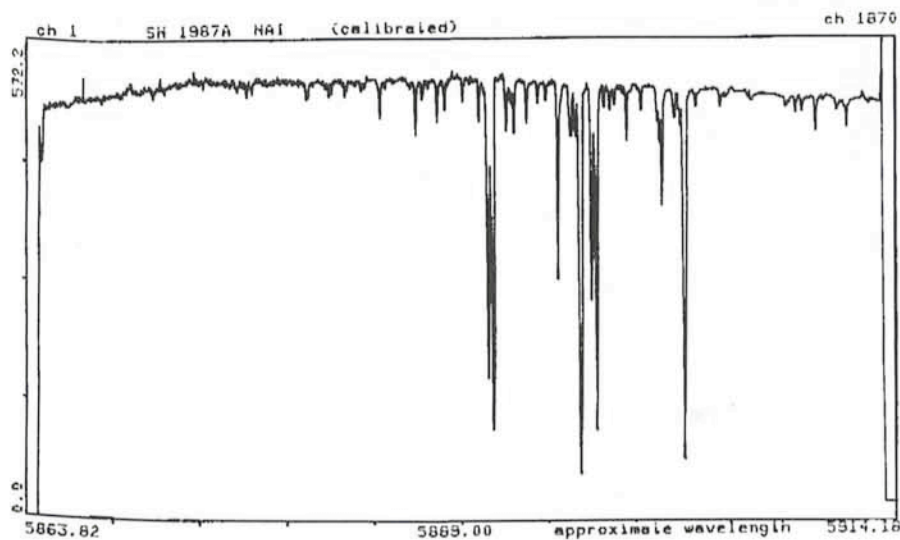
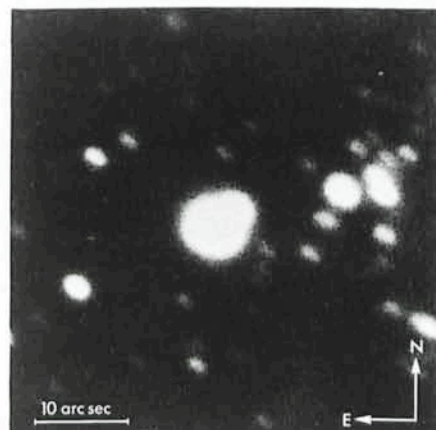


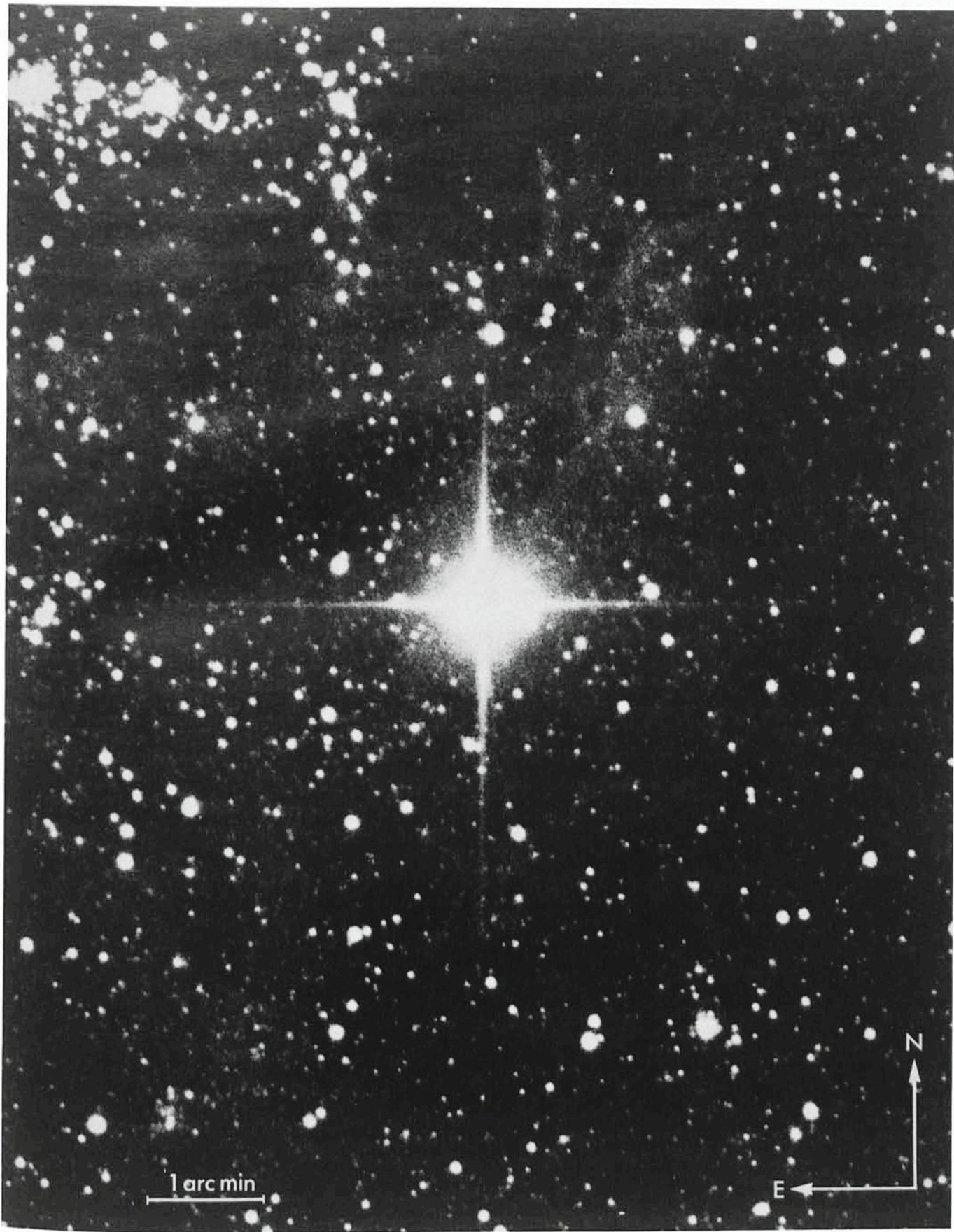
Figure 2: A spectrum taken by G. Vladilo on February 28 with the CAT + CES + Reticon detector, around the Na I doublet at 589 nm. The strongest lines correspond to absorption in the Galaxy and in the LMC.



This red photo (098-04 + RG 630, 60 min) of Sanduleak -69202, the suspected progenitor of supernova 1987A, was obtained with the ESO 3.6-m telescope on December 6, 1979. The star has at least two companions; one of them is clearly seen here (as a prominent bulge) to the northwest at a distance of only 2.6 arcseconds. It is not the progenitor, since its position does not coincide with that of the supernova. A third star lies about 1 arcsecond southeast of Sanduleak -69202, but it cannot be seen on this photo. The stellar images are very close to the edge of the plate and are somewhat elongated, due to less than optimal optical adjustment.



The star that exploded on February 23 in the Large Magellanic Cloud (the progenitor of supernova 1987A) has now been identified. It was catalogued in 1969 as an OB star of 12th magnitude and given the designation Sanduleak -69202. Observations at the European Southern Observatory in the mid-1970's allowed to classify it as of spectral type B3 I, that is a very hot, supergiant star. It is here shown on a photograph, obtained with the ESO Schmidt telescope in ultraviolet light on December 9, 1977 (IIa-O + UG1, 60 min). Closer inspection has now revealed that two other stars are seen very close to this star. On this photo, the image of Sanduleak -69202 is somewhat elongated towards northwest, since one of the companions lies in this direction at a distance of only 2.6 arcseconds. This companion cannot be the progenitor, since its position does not coincide with that of the supernova. However, there is a third star within 1 arcsecond, just southeast of the main star. Further investigations are needed to ascertain which of the two became the supernova. Observers: H.-E. Schuster and O. Pizarro.



This blue photo (IIa-O + GG 385, 15 min) of the bright supernova in the LMC was obtained with the ESO 1-m Schmidt telescope on February 26 at 01 : 25 UT. On this date, the supernova had reached visual magnitude 4.4. The photo should be compared with the ultraviolet photo showing the supernova progenitor which was taken with the same telescope in 1977. The enormous increase in brightness, around 2,000 times, is evident. The background nebulosity emits strongly in the ultraviolet and is therefore better visible on the ultraviolet photo. Otherwise more or less the same stars are seen on both photos. Note that the "cross" around the supernova is an optical effect in the telescope which is caused by the support of the plateholder. Observer: G. Pizarro.

# CASPEC Observations of sdO Stars: Are Some sdOs Lazy Remnants from the AGB?

U. HEBER and K. HUNGER, Institut für Theoretische Physik und Sternwarte der Universität Kiel,  
F.R.G.

The hot subdwarfs are ideal test objects for the theory of stellar evolution. Their core masses are pretty well known, as they originate ultimately from the horizontal branch,  $M_c \approx 0.5 M_\odot$ , and their envelope masses lie in the narrow range  $0 < M_{env} \leq 0.2 M_\odot$ . Moreover, their atmospheres are well understood through detailed NLTE model atmosphere analyses which appear especially suited to this class of hot high gravity objects. It appears from these analyses that the subdwarf B stars are extended horizontal-branch stars and thus have  $M_{env} \leq 0.02 M_\odot$ . The same is true for the subdwarf OB stars, only that the latter have even smaller envelope masses ( $\leq 10^{-3} M_\odot$ ). For both classes, further evolution proceeds directly towards the white dwarf domain. The subdwarf O stars, on the other hand, belong to the subgroup with envelope masses of the order of  $0.1 M_\odot$ . They reached their present position in the HR diagram along a rather complicated track (Fig. 1, for a detailed discussion see Groth et al., 1985). After they had left the horizontal branch they moved towards the AGB; there was not enough fuel remaining in the envelope for them to throw off planetary nebulae and thus to become central stars. They then contracted towards hotter temperatures, which are typically  $T_{eff} = 40,000 - 60,000$  K. Further evolution would again follow a direct track to white dwarf dimensions. So the small differences in the initial mass of the envelope decide whether a horizontal branch star evolves to either a subdwarf B (or OB) or to a subdwarf O star. Those with envelope masses exceeding

$\approx 0.2 M_\odot$ , finally, would be progenitors of the central stars of planetary nebulae.

This simple distinction, on account of the envelope mass is not actually quite correct; there are 8 newly discovered subdwarf O stars which seem to be of a particular nature and which seem to indicate that the above sketched picture may be too simple. But first let us report on the spectral analysis of these objects.

very weak ( $W_\lambda(4471) \leq 100$  mÅ) or even absent. This clearly indicates very high effective temperatures ( $> 55,000$  K) which are hotter than in any "classical" sdO star studied previously (Hunger et al., 1981).

The high spectral resolution (0.25 Å) also allows metal lines to be searched for and these have indeed been found in 6 objects. They are lines of highly ionized elements (e.g. CIV and NV). LSE 153, LSE 259 and KS 292 are remarkable in that they show a strong carbon spectrum. Surprisingly, some lines occur in emission (see Fig. 2) rather than in absorption. (Note that all emission lines are allowed transitions. No forbidden lines which are typical for nebula spectra are found.) The most extreme case in this respect is LSS 1362, the spectrum of which shows all metal lines in emission. In two objects, ROB 162 and LS IV-12°001, no trace of a metallic line can be found, in spite of the high spectral resolution. The discovery of faint metal lines, especially those in emission, is particularly valuable as it will supply the clue as to the nature of our programme stars.

## Data Reduction

The stars were observed with CASPEC in the blue spectral range (3900–4800 Å). In the beginning (1984), the 31.6 l/mm grating was employed while for the later observations the 52 l/mm was preferred because it yields wider separations of the orders. The spectra were reduced in two steps: first, the ESO-MIDAS software was used for both wavelength calibration and extraction of the Echelle orders. Then background correction and flat fielding were performed in Kiel using a computer programme written by G. Jonas. Data obtained with the 31.6 l/mm Echelle grating suffered from contamination of the background by scattered light from neighbouring orders, while no scattering was experienced with the 52 l/mm grating. The fraction of scattered light could be determined from the observations of standard stars (observed with both gratings). The last step of the data reduction procedure was the correction for the Echelle blaze. The Echelle blaze function ("Ripple function") was empirically determined for every order using the sdOB star Feige 110 plus the helium star BD-9°4395 as standard stars, since the spectra of the two stars are complementary: Feige 110 displays a line-poor spectrum, the only strong lines being the Balmer lines, whereas BD-9°4395 displays only very weak Balmer lines. The "Ripple function" was determined empirically from a least-square fit to the normalized continuum of BD-9°4395 for those orders containing Balmer lines, while for all other orders it was determined from the normalized continuum of Feige 110.

## Line Identification

Strong lines of ionized helium are present in all eight stars, whereas He I is

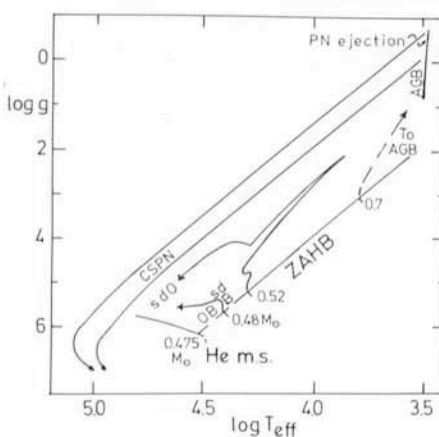


Figure 1: Post-horizontal-branch evolution (schematic).

## NLTE Analyses

NLTE analyses of the hydrogen and helium line spectrum were carried out with the Kiel programme (Kudritzki and Simon, 1978; Simon, 1980; Husfeld, 1986). For illustration, we have displayed the line-profile fits for the helium lines in ROB 162 (Fig. 3). The resulting atmospheric parameters, i.e. effective temperature, surface gravity and helium abundance, are summarized in Table I. Three programme stars have normal helium abundances, whereas the others are enriched with helium. In LSE 153, LSE 259 and LSE 263, no hydrogen is detectable and only upper limits to the hydrogen abundance can be derived. The position of our stars in the  $(g, T_{eff})$ -diagram is plotted in Figure 4, together with the position of previously analysed "classical" sdOs. Stars with normal helium abundance are shown as open circles, intermediate helium-rich stars as filled circles and extremely helium-rich stars (no hydrogen detectable) as crosses. The programme stars are indicated by error bars. Also shown are evolutionary tracks descending from the asymptotic giant branch for masses between

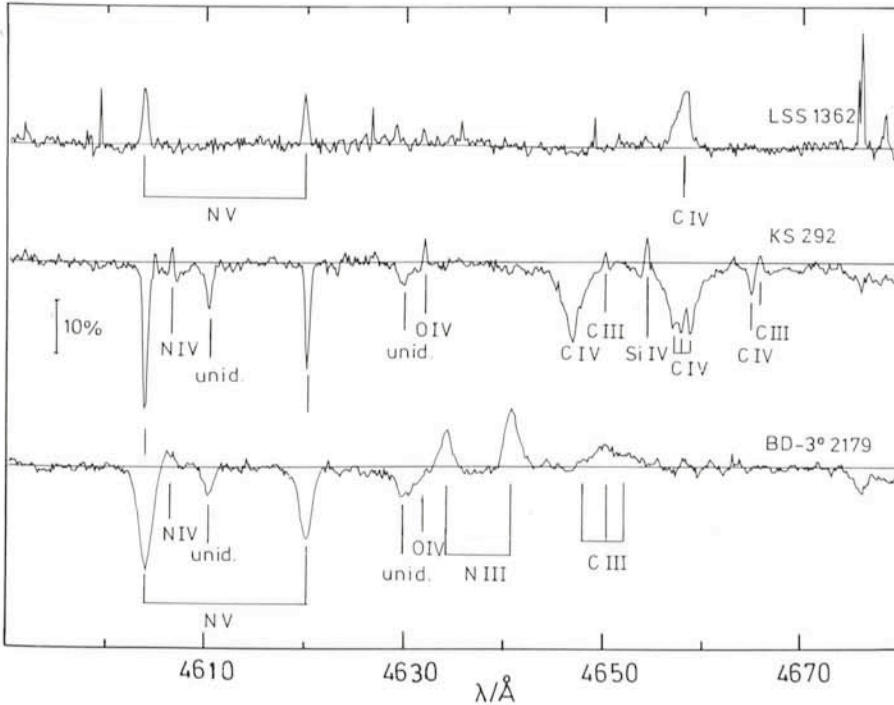


Figure 2: Caspec spectra of LSS 1362 (top), KS 292 (middle) and BD-3°2179 (bottom). Note the metallic emission lines. 10% continuum height is indicated by a vertical bar.

$0.546 M_{\odot}$  and  $0.76 M_{\odot}$  (Schönberner, 1979, 1983; Faulkner and Wood, 1984).

As can be seen from Figure 4, our stars (as well as BD+37°442, Giddings, 1980) do not lie in the region where the classical sdO stars are to be found. Instead, they can be identified with post-AGB tracks of about  $0.6 M_{\odot}$  and with a mean luminosity of about  $10^{3.8} L_{\odot}$ . These masses and luminosities are typical for central stars of planetary nebulae (CSPN) and, indeed, the spectra of our programme stars reveal a further similarity to CSPN, i.e. the presence of the metallic emission lines, for similar emission lines can be observed in some CSPNs (Méndez et al., 1981). Hence, spectroscopically, the programme stars may also be termed as CSPNs except that they lack the nebulae (or perhaps it wasn't noticed?). A careful inspection of the ESO sky survey plates did in fact reveal the existence of a very extended faint nebulosity around LSS 1362. All other stars, however, do not show nebulosities. Why is this the case?

According to the theory of evolution the age of our CSPN candidates, after they had left the AGB, should not have exceeded a few thousand years; if they had ejected nebulae at the tip of the AGB, they should still be visible. The question arising from these facts is whether there are further parameters which distinguish our stars from CSPNs. There are three conceivable reasons why no nebula can be detected:

(i) The stars simply left the AGB with-

out ejecting a nebula. This is not a satisfactory answer (at least for helium rich stars) since it cannot explain the enrichment of helium and carbon.

(ii) After ejection of a nebula, our stars evolved much more slowly than the other CSPNs and, therefore, the nebulae had already been dispersed before the stars became hot enough to ionize it. Calculations (Schönberner, 1979; Iben, 1982) show that there may be a discriminating factor: the metallicity. The rate of evolution, namely, is slow for post-AGB stars when the metallicity is low and vice versa. The effect, however, is small. It might explain the cases of ROB 162 and LSIV-12°001, as ROB 162 belongs to the metal-poor cluster NGC 6397 ( $[Fe/H] = -1.83$ ) and LS IV-12°001 has a metal-poor line spectrum (see above). The latter has an unusually large radial velocity ( $-178 \text{ km/s}$ ) and, therefore, is probably also a population II star. For the other 6 candidates, this hypothesis does not apply.

(iii) The third and most interesting explanation is the concept of "born again"

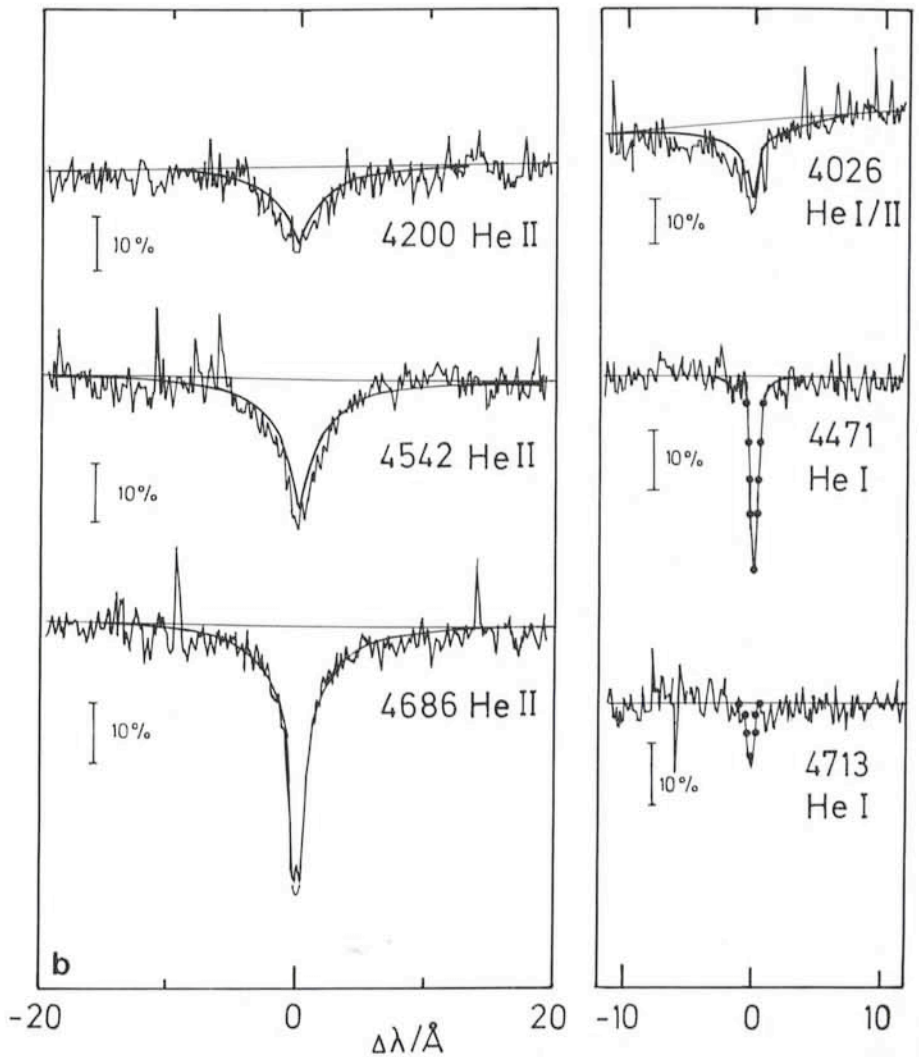


Figure 3: Comparison of observed and theoretical helium line profiles for ROB 162 ( $V = 13.23$ ).

Table 1: NLTE analyses of sdO stars

Star	$T_{\text{eff}}/\text{K}$	$\log g$	$n_{\text{He}}/(n_{\text{H}}+n_{\text{He}})$	Carbon line spectrum	Reference
BD+37°442 <sup>a</sup>	55000	4.0	1.0	+	Giddings (1980)
LSE 153	70000	4.75	$\geq 0.9$	+	
LSE 259	75000	4.4	$\geq 0.95$	+	
LSE 263	70000	4.9	$\geq 0.9$	-	
BD-3°2179	62000 <sup>b</sup>	4.5 <sup>b</sup>	0.25 <sup>b</sup>	-	Husfeld, Heber, Drilling (1986)
LS IV-12°1	60000	4.5	0.1	-	
KS 292	75000	4.7	0.33	+	
LSS 1362	100000	5.0	0.1	-	
ROB 162	51000	4.5	0.1	-	Heber, Kudritzki (1986)

<sup>a</sup> based on photographic spectra    <sup>b</sup> preliminary values, analysis is not completed

+: carbon strong lined    -: carbon weak lined

post-AGB stars. After ejection of a nebula, such a star crosses the HR diagram in the usual way, i.e. as a true CSPN, and finally reaches the hot end of the cooling sequence of white stars. According to Schönberner (1979) and Iben et al. (1983), a last thermal pulse may occur in this phase. Such a pulse brings the star back to red giant temperatures and dimensions. During the pulse, most of the hydrogen left to the star at the onset of the pulse is mixed into the helium-burning convective shell and thus is completely burned. The star is now almost devoid of hydrogen and proceeds to burn helium in a shell. The evolutionary track in the  $(g, T_{\text{eff}})$  diagram is approximately the same as that for hydrogen-burning post-AGB stars (CPNs). However, no new nebula is expelled and the old one has long since disappeared.

This scenario can also solve the riddle of the helium and carbon enrichment (the latter is found only in a few cases, see Table I). The theory of evolution does not predict any helium enrichment for "normal" CSPN since the hydrogen rich envelope is too massive ( $\approx 10^{-4} M_{\odot}$ ) to allow any helium to be seen at the surface. Indeed most of the CSPNs studied so far, have a normal helium abundance. However, the situation is different for post-AGB stars that experience a final thermal pulse when they already have reached the cooling sequence. Theoretical calculations (see Iben et al., 1983), namely, predict a final hydrogen burning episode during the peak of the final thermal pulse and a mixing episode during the giant phase. Both mechanisms can mix processed material (He and N from the CNO-cycle; C from the 3  $\alpha$ -process) to the surface.

## Conclusion

The NLTE analyses have revealed the existence of a new group of sdO stars

that were once CSPNs but were born again just before they reached their final destiny, the white dwarf cemetery; a last thermal pulse brought them back to life as a post-AGB star. While the true CSPN lives on H-burning, the reborn post-AGB star lives on He-burning, which prolongs the active lifespan by some 10,000 years, a good fortune that only a small fraction of the central stars will experience.

## Acknowledgement

We thank D. Ponz (ESO) and G. Jonas (Kiel) for their kind assistance in various aspects of the data reduction.

## References

- Faulkner, D.J., Wood, P.R.: 1984, Proc. ASA **5**, 543.
- Giddings, J.R.: 1980, Ph.D. thesis, UCL, London.
- Groth, H.G., Kudritzki, R.P., Heber, U.: 1985, *Astron. Astrophys.* **152**, 107.
- Heber, U., Kudritzki, R.P.: 1986, *Astron. Astrophys.* **169**, 244.
- Hunger, K., Gruschinske, J., Kudritzki, R.P., Simon, K.P.: 1981, *Astron. Astrophys.* **95**, 244.
- Husfeld, D.: 1986, Ph.D. thesis, München.
- Husfeld, D., Heber, U., Drilling, J.S.: 1986, Proc. IAU Coll. No. 87, p. 353.
- Iben, I.Jr.: 1982, *Astrophys. J.* **260**, 822.
- Iben, I.Jr., Kaler, J.B., Truran, J.W., Renzini, A.: 1983, *Astrophys. J.* **264**, 605.
- Kudritzki, R.P., Simon, K.P.: 1978, *Astron. Astrophys.* **70**, 653.
- Méndez, R.H., Kudritzki, R.P., Simon, K.P.: 1981, *Astron. Astrophys.* **101**, 323.
- Schönberner, D.: 1979, *Astron. Astrophys.* **79**, 108.
- Schönberner, D.: 1983, *Astrophys. J.* **272**, 708.
- Simon, K.P.: 1980, Ph.D. thesis, Kiel.

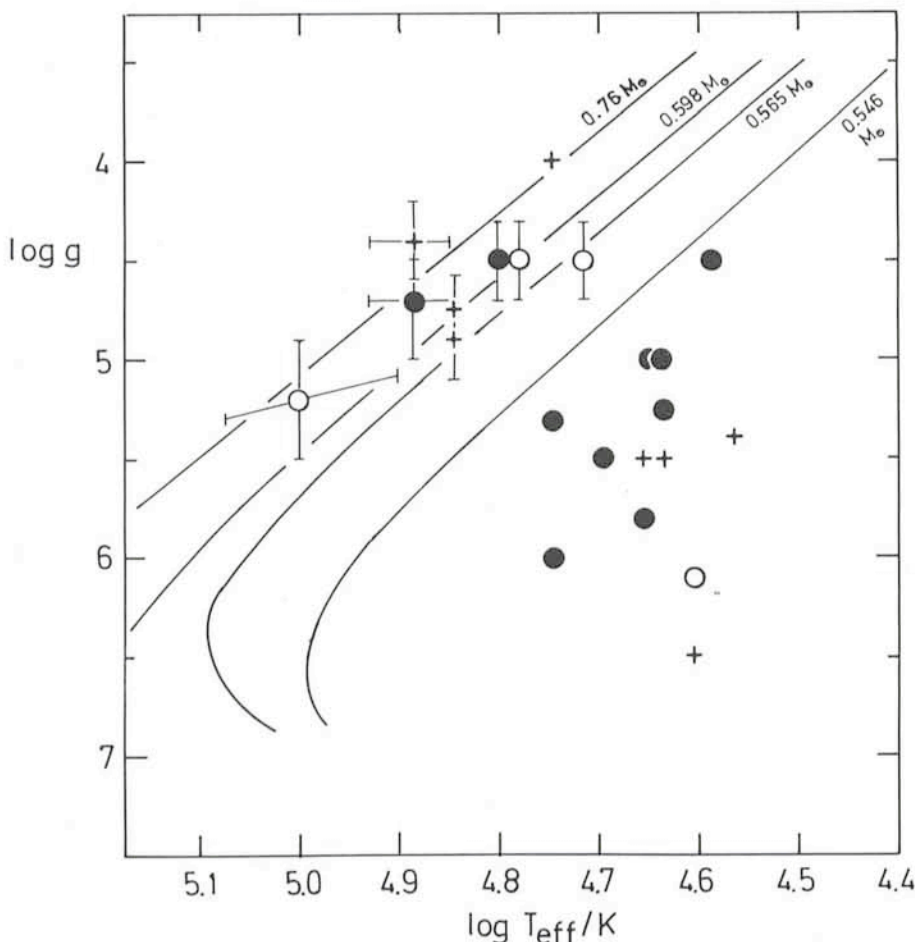


Figure 4: Position of subluminous stars in the  $(g, T_{\text{eff}})$ -diagram. The programme stars are marked by error bars. The dashed lines are theoretical evolutionary tracks for stars of  $0.546 M_{\odot}$ ,  $0.565 M_{\odot}$ ,  $0.598 M_{\odot}$  (Schönberner, 1979, 1983) and  $0.76 M_{\odot}$  (Faulkner and Wood, 1984) descending from the asymptotic giant branch.

# P/Halley: Characterization of the Coma Dust by Polarimetry

A. DOLLFUS and J.-L. SUCHAIL, Observatoire de Paris

The new photopolarimeter of Observatoire de Paris, at Meudon, was first used on Comet P/Halley with the 100-cm telescope of Meudon Observatory from September to December 1985. After full tests were secured and comet polarization measurements recorded, the instrument was packed and shipped

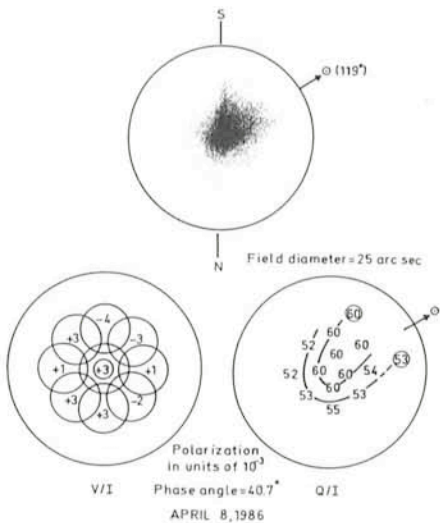


Figure 1: Comet P/Halley. Polarization over the inner coma. Photopolarimeter PPHR of Observatoire de Paris, with the 1.52 m ESO telescope at La Silla. April 8, 1986, phase angle  $40.7^\circ$ , field diameter 25 arcsec. Top: Aspect of the inner coma and dust streamers. Bottom left: Positions of the hole and degree of circular polarization  $V/I$  in units of  $10^{-3}$ . Bottom right: Degree of linear polarization  $Q/I$  in units of  $10^{-3}$  and isophotes for  $53 \times 10^{-3}$  and  $60 \times 10^{-3}$ .

to La Silla for an intensive polarization analysis of the comet with the 1.52-m ESO spectroscopic telescope. Nine nights were allocated from 7 to 16 April, 1986. Of these, eight nights showed a perfect sky with exquisit seeing! In addition, the telescope, perfectly well adapted for the purpose, was accurately operated by Messrs. Miranda and Borguez, under the supervision of Mr. Le Saux.

Figure 1 shows the first of our polarization mappings over the inner corona on April 7–8, 1986. At the top, the coma is seen at the eyepiece with a magnification of 1,000, in a field of 25 arcseconds diameter. A dust streamer is ejected toward south, at  $45^\circ$  from the direction of the Sun. The sizes and the successive positions of photopolarimeter holes over this field are shown at bottom left in the figure, together with the values measured for the degree of circular polarization  $V/I$ , expressed in units of  $10^{-3}$ . At bottom right, the measurements of the degree of linear polarization  $Q/I$  are given, also in units of  $10^{-3}$ , together with the approximate isophotes for the two values  $53 \times 10^{-3}$  and  $60 \times 10^{-3}$ . The azimuth of the polarization was everywhere almost perpendicular to the direction of the Sun (meaning that the Stokes parameter  $U/I$ , which is at  $45^\circ$  from  $Q/I$ , is negligible). A wide band colour filter was used, centred at 500 nm (circle and dashed line in Fig. 9).

We have eight such maps. After April 10, we extended the coverage to a wider field of 120 arcseconds in diameter, and expressed the linear polarization by segments giving the azimuth and the degree  $P$  of polarization which is  $P = \sqrt{Q^2 + U^2}/I$ . As the phase angle decreased with time, the polarization decreased also and the effect of deflection in the azimuth of polarization took more significance. Figures 2, 3 and 4 show at top the full development on the fountain-line dust ejection by the nucleus toward the direction of the Sun and at bottom right the linear polarization which decreases with phase angle and also progressively wanders in its azimuth. On April 16 it is almost randomly oriented; at the corresponding phase angle of  $21.6^\circ$ , the polarization produced by isotropic scattering is almost zero and the polarization effect produced by anisotropies in the dust configurations remains almost alone. The small and variable circular polarization  $V/I$  which is recorded probably results also from such dust shape anisotropies.

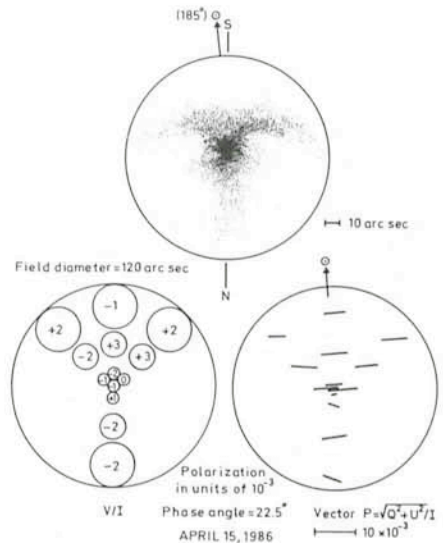


Figure 3: Same as Figure 2 but for April 15, 1986, at phase angle  $22.5^\circ$ .

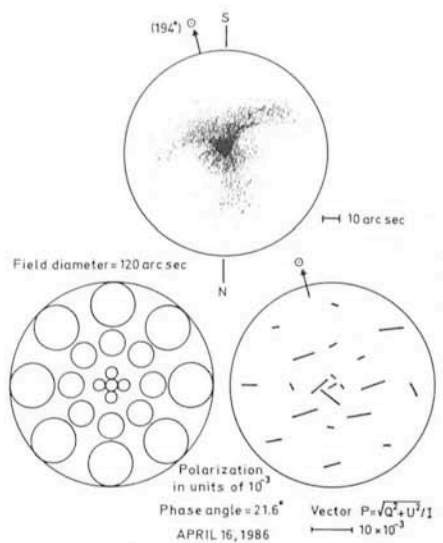


Figure 4: Same as Figures 2 and 3 but for April 16, 1986, at phase angle  $21.6^\circ$  for which the linear polarization produced by isotropic scattering is almost negligible. The linear polarization which remains is largely produced by orientations and anisotropies in the dust shapes.

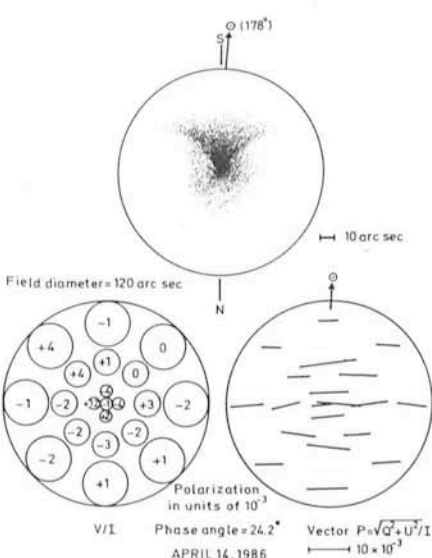


Figure 2: Same as Figure 1 but over a larger field of 120 arcsec. diameter on April 14, 1986, at phase angle  $24.2^\circ$ . The linear polarization is expressed by segments giving the azimuths and the degree of polarization (see scale).

We detailed also the polarization in the inner part of the coma within 3,000 km from the nucleus, by using concentric holes centred at the nucleus. The measurement with a hole is then corrected by those with smaller size. The smallest hole had 2.1 arcseconds diameter, or a radius of 300 km around the nucleus. Figure 5 shows the luminescence (in relative units) and the degree of polarization (in units of  $10^{-3}$ ) so deduced, as a function of the distance of the nucleus, given in arcseconds and in

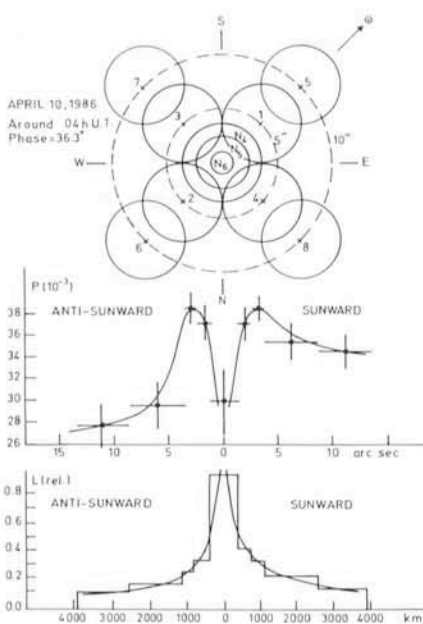


Figure 5: Detailed analysis of the polarization over the inner part of the coma, close to the nucleus. April 10, 1986, at phase angle  $36^{\circ} 3$ . Top: Positions and sizes of the holes. Middle: Degree of linear polarization with distance to the nucleus, sunward and anti-sunward. Bottom: Same, for the luminosity.

kilometres, for the observation of April 10, 1986, at phase angle  $36^{\circ} 3$ . A very bright point source, almost star-like, was seen around the nucleus (within hole N6). It corresponds to a sort of permanent envelope surrounding the nucleus. At the apparent distance of 4,000 km from the nucleus in the direction opposite to the Sun, the polarization is  $28 \times 10^{-3}$ . Approaching the nucleus,

the polarization increases up to  $38 \times 10^{-3}$ . Then the envelope discloses a completely different and smaller polarization. Towards the Sun, the fountain of fresh dust maintains a high polarization. On April 13, at phase angle  $36^{\circ} 2$  (Fig. 6) a gust of fresh dust ejected towards the observer screened completely and temporarily the bright envelope around the nucleus which disappeared. The polarization then uniformized all over the field. Next day, on April 14 (Fig. 7), the dust streamer having spread out, the envelope was seen again with its anomalous polarization, now observed at phase angle  $24^{\circ} 2$ .

Our data include 9 documents such as those of Figures 5, 6, and 7, and 8 maps like those of Figures 1 to 4, plus measurements directly recorded around the nucleus. With these data, we derived the Figure 8 showing the curve of variations of the degree of polarization as a function of phase angle, for the dust at 3,000 km (dots), for the fresher dust at 1,000 km (crosses) and for bright envelopes around the nucleus (circles). These measurements have been subjected to a slight correction due to the smaller polarization produced by the emission lines partly included in the spectral band isolated by our filter. The effect is to increase the polarization for the largest phase angles. The uncorrected data are given in the Figure 5 of the paper by Dollfus et al. (1987) cited in reference. Our measurements with narrow colour or interference filters, such as those of Figure 9, indicate also that there is only a small variation of the continuum polarization with wavelength.

Curves of polarization are related to the nature of the dust particle responsible for the scattering; they help to characterize their physical properties. Without entering here into the details of the interpretation, which is still under

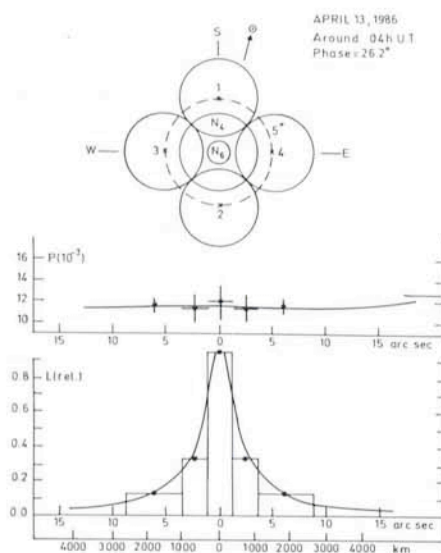


Figure 6: Same as Figure 5 but for April 13, 1986, at phase angle  $26^{\circ} 3$ . A dust streamer ejected in the direction of the Earth has temporarily masked the bright envelope around the nucleus and uniformized the polarization over the field.

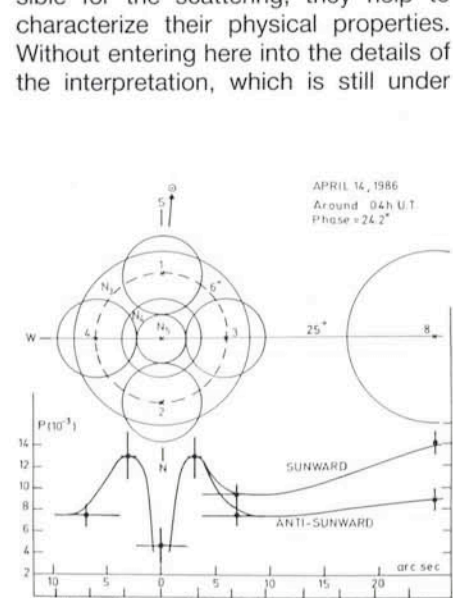


Figure 7: Same as Figure 6, but next night. The dust streamer has spread out, the bright envelope reappears and its polarization is now observed at phase angle  $24^{\circ} 2$ .

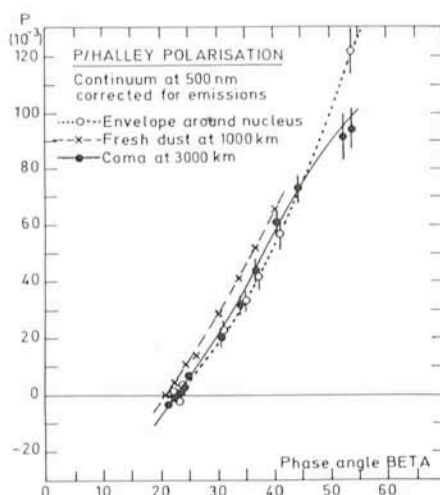


Figure 8: Degree of linear polarization as a function of phase angle: curves of polarization for the coma dust at 3,000 km from the nucleus (dots), for the freshly ejected dust observed at 1,000 km (crosses) and for the bright envelope around the nucleus (circles). The measurements have been corrected for the polarization produced by the gas emissions included in the spectral band transmitted by the filter.

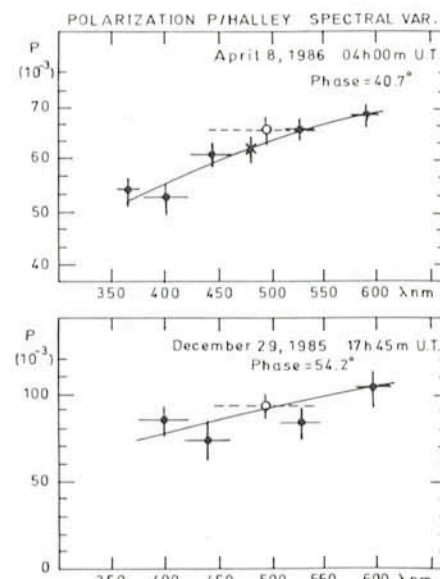


Figure 9: Spectral variation of the polarization in the range from 360 to 600 nm. Top: for phase angle  $40^{\circ} 1$ . Bottom: for phase angle  $54^{\circ} 2$ . Measurements corrected for gas emission polarization when relevant.

progress, we note that curves such as those for crosses and dots in Figure 8, are compatible with, and even suggestive for, a model of grains made of fluffy aggregates of small particles. The grains have to be very dark and neutral in colour. These structures, fragile and uncompacted, may be somewhat elongated or filamentary, as suggested by the deflected and the circular polarizations.

The polarization by the bright halo

which is enveloping the nucleus (circles in Figure 8) does not fit as easily with such a model. Other types of grains may be required, perhaps of higher albedo. Water ice may be considered.

#### Reference

Dollfus, A., Suchail, J.-L., Crussaire, D., Killinger, R. (1987): Comet Halley: Dust characterization by photopolarimetry. To be published in Proc. ESA Symposium Exploration of Halley's Comet, Heidelberg, FRG, 27–31 Oct. 1986.

## MESSENGER INDEX

An index of all contributions published in the Messenger from No. 1 to No. 46 (1974–1986) has been compiled and will be distributed with this issue of the Messenger.

The index consists of three parts. The first part – the Subject Index – lists the contributions grouped by 20 subject titles. In the second part – the Author Index – the articles are listed by authors, in alphabetical order. The third part contains the Spanish summaries, grouped by subject titles and in chronological order.

Although the division of the contributions into 20 subjects and their assignment to these subjects may not be perfect, it is hoped that the index will help the reader to obtain a better overview of the articles which have appeared in the Messenger and permit him to find them more easily.

In the future, annual indexes will be compiled.

# Multiple Object Redshift Determinations in Clusters of Galaxies Using OPTOPUS

A. MAZURE and D. PROUST, DAEC, Observatoire de Meudon, France

L. SODRE, IAG, São Paulo, Brasil

H. CAPELATO, São Jose dos Campos, Brasil

G. LUND, Département d'Astrophysique de l'Université de Nice, France

#### Introduction

From recent developments of observational astronomy, the overall view of the structure of the universe appears to be very different from the homogeneous and isotropic one claimed by traditional cosmology. The hypothesis of long, interconnected linear filaments or even large "bubbles" characterizing the concentration of galaxies now seems to be well established, these regions being separated by large voids empty of bright galaxies.

One of the fundamental factors in the understanding of such formations is the determination of their structure in the third dimension as opposed to their flat "projected" appearance.

If the redshift determinations represent virtually the only tool giving access to the third dimension, they are also essential to the understanding of structural dynamics because they provide us with a wealth of information concerning the velocity dispersion in particle systems. Radial velocity measurements are essential to the understanding of structures such as galaxy clusters, as dynamic analysis of their velocity distribution can lead to mass determinations and to an estimate of the missing mass in the universe.

Analyses of some Abell clusters have recently been published; as an example it has been shown that the A496 cluster has a complex structure formed essentially by a main cluster (or main sub-cluster), and another small sub-cluster,

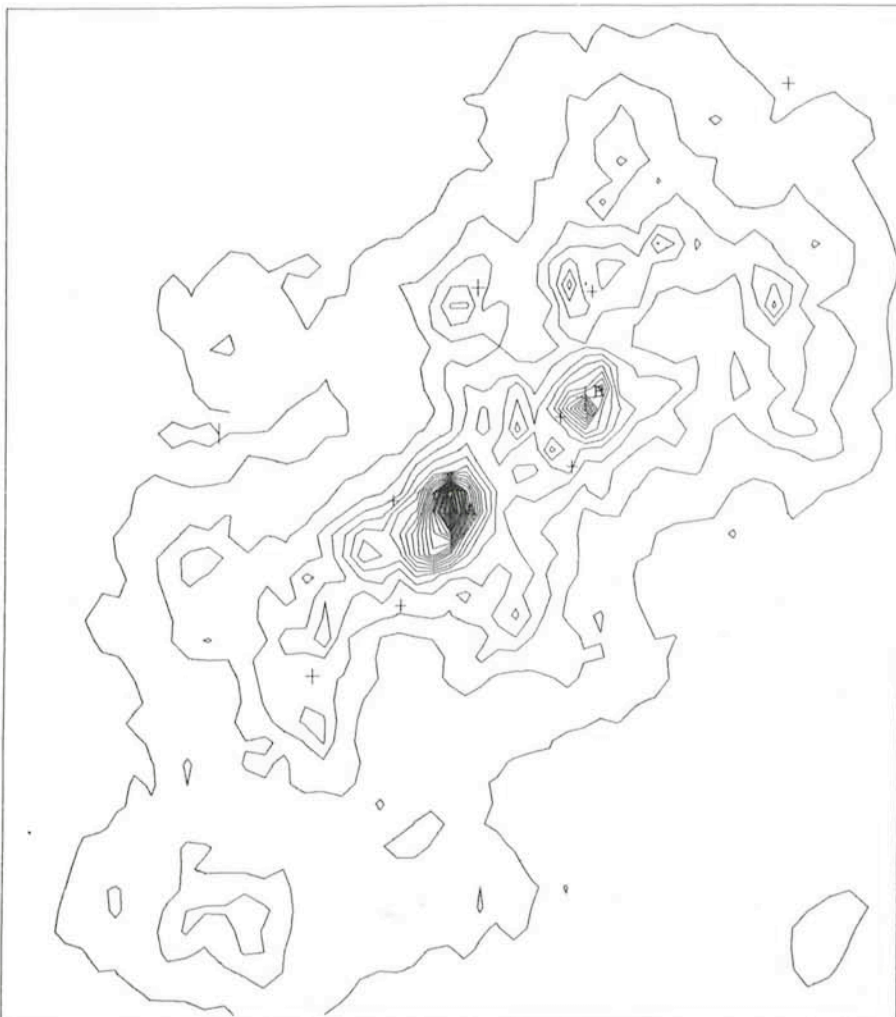


Figure 1: Isocontours of SC2008-565. The ten brightest galaxies are plotted. The radial velocities of A and B are 16,490 and 16,890 km/s.

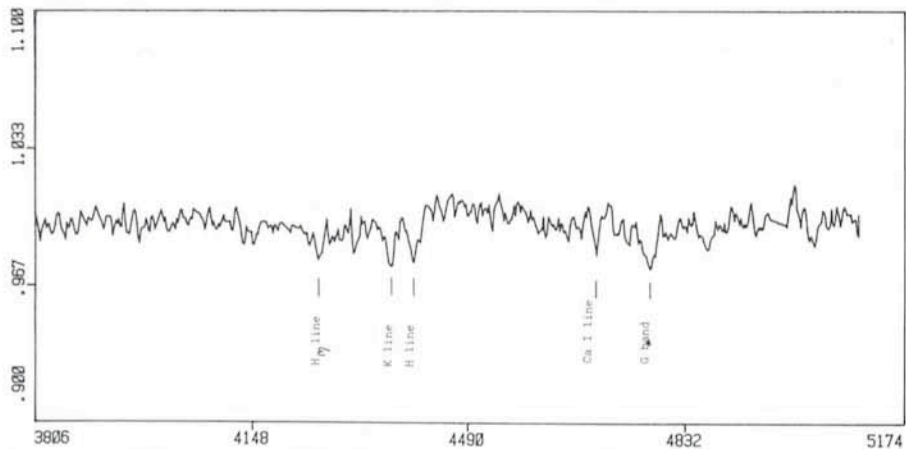


Figure 2: Spectrum of an elliptical mb 17.26 galaxy in the SC0004.8-345 cluster.

with the cD in its centre, at the same distance (Mazure et al., 1986).

The well-known Coma cluster has also been reinvestigated by Mellier et al. (1987). The isopleth map of 'sequence' galaxies determined from a colour-magnitude strip (Visvanathan and Sandage, 1977) to magnitude 20 shows the presence of several secondary density peaks in the vicinity of bright galaxies and a double structure in the core of the cluster. The distribution of velocities relative to the brightest galaxies indicates also a composite population, one with a velocity dispersion as small as  $\sigma = 350$  km/s.

Using the ESO multi-object facility, OPTOPUS, we have observed a sample of galaxy clusters such as SC2008-565 (Fig. 1) in order to collect a large set of individual radial velocities, and to pursue similar analyses.

## Instrumentation

The observations were carried out during two nights at the end of July 1986 at the 3.6-m telescope, using the multi-object spectrograph OPTOPUS. The characteristics of the instrument are

summarized in the *Messenger* No. 41, page 25 and No. 43 p. 1, and in the corresponding ESO Operating Manual. For each exposure, 32 separate optical fibres were available due to the use of an f/2.5 dioptric camera, slower than the usual Schmidt camera, in a field of 33 arcminutes diameter. The aluminium starplates were prepared at ESO Garching using X-Y Schmidt plate coordinates measured with the Optronics-3000 facility, converted into (1950) alpha, delta coordinates using the POS software and standard stars from the Perth 70 catalogue. At least 3 stars were selected on each plate, in order to check its position and orientation, and the rms residual position error corresponded to 0.25 arcsec.

A dispersion of 114 Å/mm was used, providing spectral coverage from 3800 to 5180 Å. With the fibre spaghetti correctly entangled with the appropriate plates, cooking times ranging from 90 minutes to 150 minutes were needed, according to the average blue magnitude of each cluster.

In all cases, observations were made in the vicinity of the meridian plane in

order to minimize refraction effects which can lead to small fibre/image offsets during the course of observations. The second half of the last night was almost completely lost because of cloudy conditions.

## Data Reduction and Results

Data reduction was carried out using the IHAP image-processing software at ESO Garching. The programme automatically identifies the positions of the spectra on the CCD frame and extracts them by adding the contribution of the brightest columns. Wavelength calibration was performed using the He-Ar lamp reference exposures obtained immediately after each cluster exposure through the same OPTOPUS configuration, at the same sky position. The redshifts were determined by measuring the most prominent absorption lines and systematically cross-correlating them with a template spectrum of known radial velocity.

For a cluster like SC0004.8-345 (Carter, 1980), we derived 28 reliable redshifts from 32 raw galaxy spectra ranging in blue magnitude between 17.0 and 18.8, obtained with an exposure time of 150 minutes Figures 2 and 3 show two spectra of resp. mb 17.26 and 18.79 galaxies of this cluster. The signal-to-noise ratio in the latter case is around five. It represents the extreme case of redshift determination using the cross-correlation procedure. The same number of redshifts was achieved for the galaxy cluster DC1842. However, in the case of SC2008-565, the poorly known photometry of this cluster led to an underestimation of the required exposure time, and thus to a considerable degradation in the proportion of accurately determined redshifts. We were nevertheless extremely pleased to obtain a total of 100 well-determined redshifts from 1½ nights of observation.

In conclusion, OPTOPUS appears to be a particularly well-adapted instrument for the rapid and simultaneous determination of redshifts in catalogued galaxy clusters.

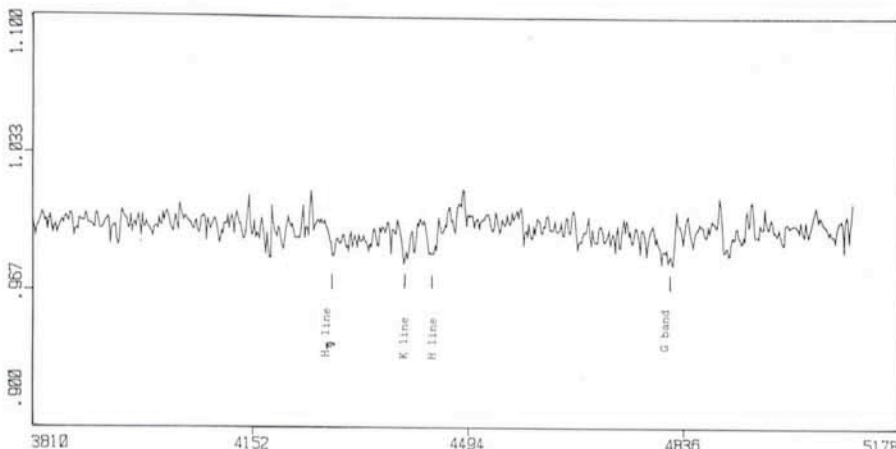


Figure 3: Same as Figure 2 for an mb 18.79 galaxy.

## References

- Carter, D.: 1980, *Mon. Not. Roy. Astron. Soc.*, **190**, 307.
- Mazure, A., Gerbal, D., Proust, D., Capelato, H.V.: 1986, *Astron. Astrophys.* **157**, 159.
- Mellier, Y., Mazure, A., Mathez, G., Chauvineau, B., Proust, D.: 1987, preprint.
- Visvanathan, N., Sandage, A.R.: 1977, *Astrophys. J.*, **216**, 214.

# Coronography at La Silla: High Resolution Imaging of Faint Features Near Bright Objects

F. PARESCE and C. BURROWS, Space Telescope Science Institute, Baltimore, USA, and Astrophysics Division, Space Science Dept. of ESA

## Introduction

Some of the more interesting astronomical sources happen to lie very close to bright objects. If the source is very faint, it becomes extremely difficult to discern it against the glare of the bright object. This situation arises, for example, when attempting to image the ionized tori around satellites such as Io, protoplanetary or circumstellar systems of nearby stars, accretion disks within close binaries, faint emission nebulosities in the vicinity of old novae and possible fuzz around bright quasars. In all these cases, it is imperative to reduce dramatically the scattered light in the wings of the bright object seeing disk and/or to prevent the bright object from saturating the detector and thereby disabling it in the adjacent areas. The latter effect can be important even for relatively faint objects such as 15th magnitude quasars if long integration times are required.

Accomplishing this objective would open up a very fertile field of inquiry; one that is ideally suited to the performance characteristics of modern high resolution, large aperture telescopes and detectors. Success requires a well-designed coronograph coupled to a high quality photon collecting device located on a site with excellent seeing conditions. This note briefly describes the techniques we have devised in our first attempts with a simple coronograph mated to the 2.2-metre MPI Cassegrain telescope at La Silla and some of the results obtained in the first year of operation. A more complete description of the experimental and data analysis techniques and the scientific results can be found in the references at the end

of this article and available from the authors.

## Experimental Setup

The optical configuration of our observational setup at La Silla is shown schematically in Figure 1. Light from the object under investigation is gathered and focused by the f/8 MPI 2.2-metre Cassegrain telescope onto a blackened photoetched mask located in the focal plane. This occulting mask is shaped in the form of a long thin wedge which can be moved longitudinally by a micrometer in order to vary its projected width in the sky from 2 to 10 arcseconds depending on seeing conditions, source brightness, etc. It can also be moved transversely to occult any desired portion of the field of view. Following the mask, an achromatic doublet reimages the telescope focal plane with a magnification of 5 onto the detector so that the effective focal ratio of the system becomes f/40.

An apodizing mask especially designed to reduce diffracted stellar light from the 2.2-metre telescope pupil is located in the exit pupil and is rigidly attached to the lens mount to ensure that it remains there as the coronograph is focused. The mask obscures 30 per cent of the exit pupil close to the images of the entrance pupil edges. After this mask, the light passes through optical filters in a rotating commandable two-wheel assembly mounted just in front of the detector. In our two runs of September and November 1986 at La Silla, we employed the  $512 \times 320$  30 micron square pixels RCA CCD. In this particular configuration, each pixel corre-

sponds to  $5 \cdot 10^{-3}$  square arcseconds in the sky with a total rectangular field of view of 22.5 by 35.9 arcseconds.

The optical and detector system just described was calibrated absolutely using bright, stable stars as calibration sources. Using standard Johnson B, V, and R and Cousins I filters available at La Silla (ESO filter numbers 445, 446, 447 and 465), we obtained overall peak counting efficiencies between 4,000 and 8,000 Å of 0.2 to 0.4 CCD counts per photon depending on bandpass. The transmission of the achromatic doublet decreases rapidly below 4000 Å and is essentially opaque below 3500 Å. Thus for U band measurements the lens should be replaced by a singlet of fused quartz or silica and the detector changed to the UV sensitive GEC CCD available at the 2.2 metre.

## Observing Methodology

First, the coronograph is focused by adjusting the position of the lens mount until the image of the occulting wedge under flat field illumination comes into sharp focus. The coronograph comes equipped with internal LEDs to provide such illumination so that the focusing can be carried out even when the telescope is not in operation. Second, a suitable star is made to fall somewhere on the unocculted area of the detector through a broad band filter and the resultant image is used to focus the telescope secondary. The coronograph need not be refocused if a filter is changed since the filters are in an f/40 beam. Third, a suitably opaque neutral density filter (ND3 or 4) is moved into the beam and the bright primary source acquired.

Using the telescope TV autoguiding system described by Duchateau and Ziebell in the *Messenger* No. 45, 1986, the source is placed behind the occulting wedge in a series of short acquisition exposures. With a series of increasingly smaller offsets, the source is precisely centred behind the occulting wedge. This is accomplished by making the spillover light distribution above and below the wedge obtained with progressively less ND attenuation as symmetrical as possible. Finally, any ND filter remaining is removed and the long exposure in the specified bandpass be-

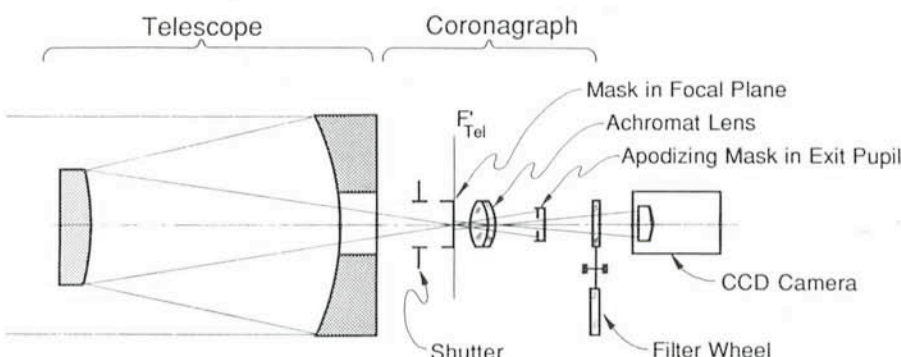


Figure 1: Optical configuration.

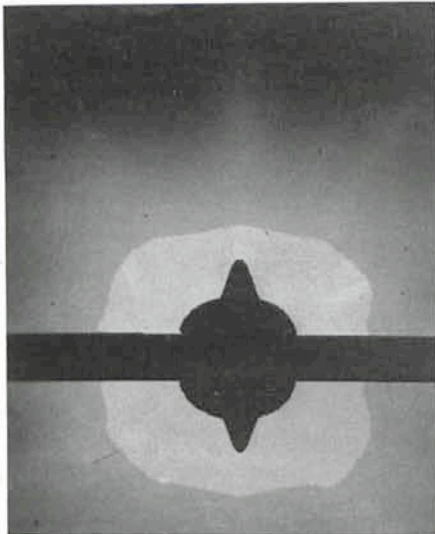


Figure 2: Image of Alpha Pictoris. The image has been flat fielded, and minor blemishes have been removed. The horizontal bar is the occulting mask and has been masked black. The masked circular area in the centre with triangular appendages is due to saturated and bleeding pixels. The deviations from circular symmetry are due to instrumental scattering and diffraction effects. The image is truncated at 5,000 counts, and has been displayed with the image greyscale changed to give equal numbers of pixels at any given intensity. (Histogram equalization.)

gun. If a faint feature is expected to be lost in the light from the wings of the bright object seeing profile, the telescope is moved to a control star nearby and the procedure just described repeated. After some practice, the overhead time used to acquire and precisely register the source can be kept within approximately 20 minutes. This time is

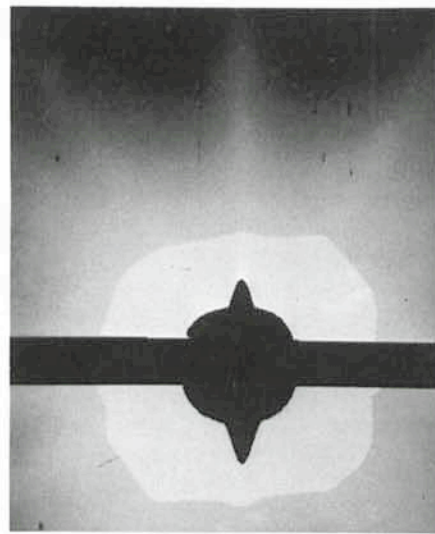


Figure 3: An image of Beta Pictoris with truncation at 3,000 counts. It is otherwise treated identically to that of Figure 1. All instrumental effects are similar but there is an additional bulge in the image at bottom left (NE) through top right, due to the circumstellar disk.

set mainly by the time necessary to read out, process, and display the relevant CCD acquisition images. A detector with real time display capabilities or a faster data handling system for the CCD would obviously shorten considerably this set up period and allow a faster turn around. This is a critical factor for a lengthy survey programme.

### Data Analysis and Results

All the raw images are processed in a standard way to prepare them for scientific analysis. The CCD bias level and the variations in response across the detector area are removed by subtracting a constant bias level and dividing by an appropriate flat field. Overclocked, saturated pixels, and bad columns are easily located and masked out so that they will not contribute to the rest of the process-

ing. Cosmic ray events and local CCD defects are also located by comparison with neighbouring pixels using standard statistical tests and iterating to avoid including bad pixels in the averaging process. Finally, the edges of the occulting mask are defined interactively and stored in a file associated with the image. No further user interaction is required in the subsequent processing which can proceed automatically.

The results of this process are shown in Figures 2 and 3 that represent images of Beta and Alpha Pictoris, respectively, taken with the system we have just described with the R band filter on the night of November 27, 1986. Beta Pictoris is a star suspected of having a giant protoplanetary system seen edge-on in emission surrounding the central star while Alpha Pictoris is used as the reference star. Both images are mainly

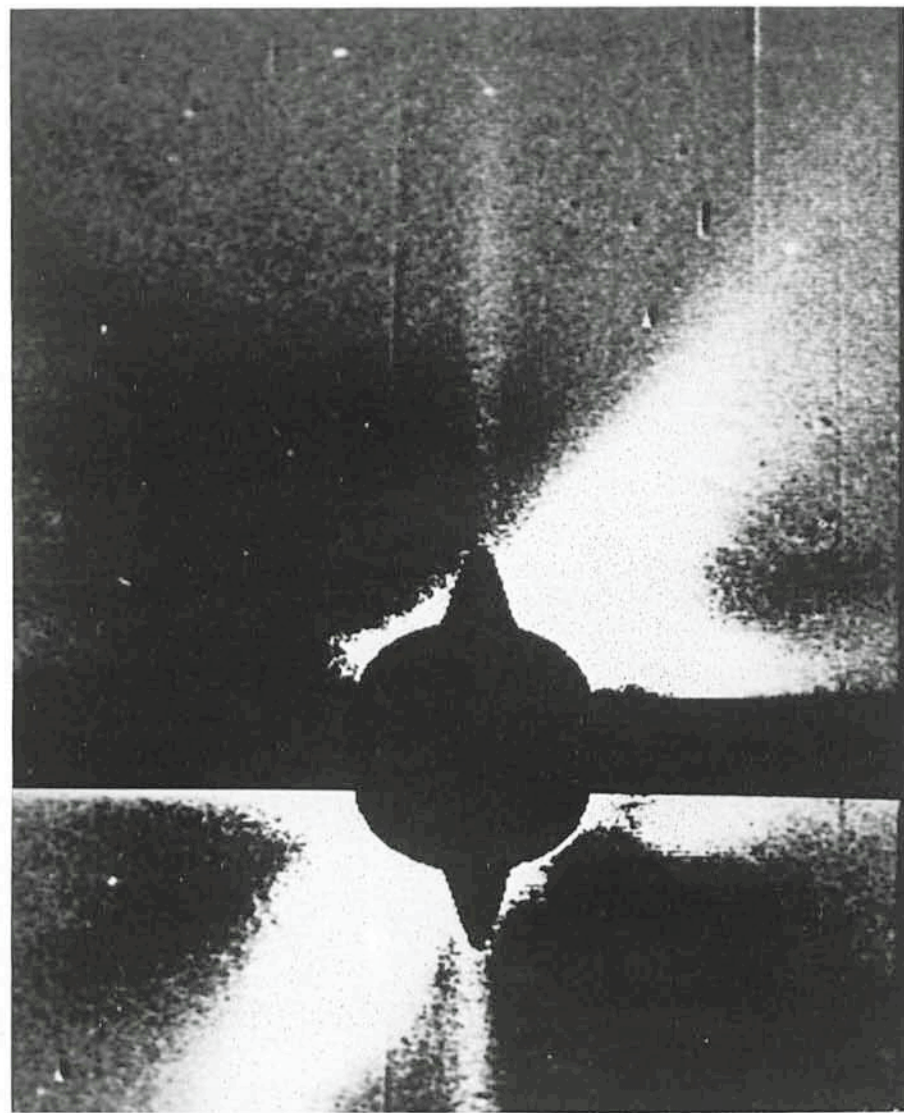


Figure 4: R band image of Beta Pictoris circumstellar disk obtained as a difference image of Figures 2 and 1. North is up and East is to the left. The image displayed is about 23 arcsec in width. The disk extends diagonally from NE to SW. The dark portions of the image are due to saturated pixels or the focal plane mask. The bright line running vertically through the frame centre, and light close to the mask particularly to the right of centre are due to residual diffractive scattering.

composed of the stellar seeing disk with small contributions due to scattering within the instrument and, of course, for Beta Pictoris, the circumstellar disk. This feature, however, is almost lost in the image shown in Figure 2 without benefit of a direct comparison with the reference image shown in Figure 3.

Although a feature running in a roughly NE to SW direction through the Beta Pic image, without a corresponding one to be discerned in the control image, stands out rather clearly in the image shown in Figure 2, considerably more analysis effort has to be expended in order to generate a photometrically true or correct image of the immediate surroundings of Beta Pictoris. Details of the complex data processing techniques used to subtract the reference image of Alpha Pic shown in Figure 3 from that of Beta Pic in Figure 2 are given in Reference 1. The basic problem to be solved is to make the result of the analysis as free as possible from assumptions, biases and subjective judgements as possible. In other words, it was taken as axiomatic that no user interaction would be permissible and no assumptions about the characteristics or even the existence of circumstellar features would be allowed. This is a crucial but often neglected attribute of any method applicable to the interpretation of astronomical data of this type. The best algorithm chosen essentially consisted of a truncated least squares fit between the two images allowing the relative intensity, overall background and spatial registration to vary. The best values for these parameters obtained this way were then used by the programme to subtract the reference from the Beta Pictoris image.

The result of this procedure for the Beta Pictoris case is shown in Figure 3. This figure dramatically illustrates the power of the technique briefly described here. The image is photometrically accurate in that counts at any point in this image are linearly related to the true emitted intensities of the protoplanetary disk through the absolute calibration of the optical and detector system used. A standard ratio image, for example, would not satisfy these basic requirements and, thus, cannot represent a true image of the stellar surroundings dependent as it still is on spurious and contaminating effects of the specific detecting system employed in the investigation. This and other images of the Beta Pictoris disk taken at La Silla in the B, V, R and  $I_c$  bands represent the first visible images of this fascinating feature.

The physical implications of these measurements on Beta Pictoris and other candidates are described in detail in Reference 2. For Beta Pictoris, the

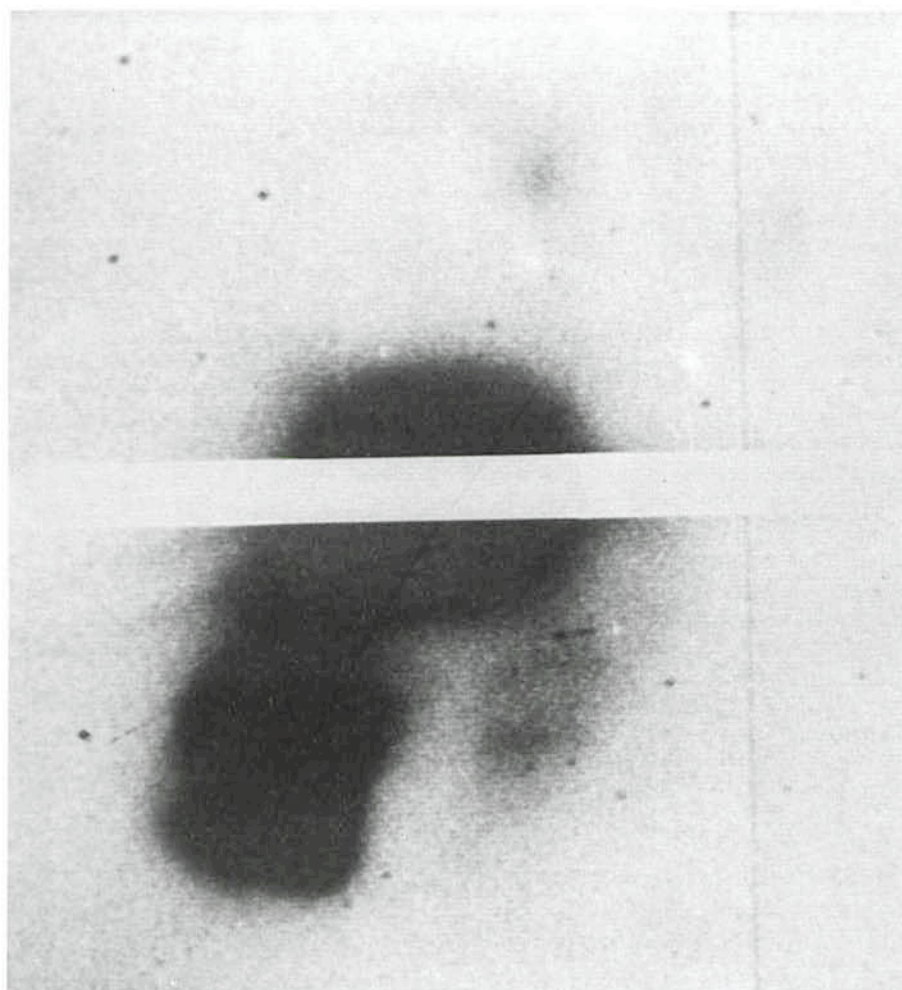


Figure 5: A narrow band NII image of R Aquarii, a variable binary with known emission of ionized knots along a collimated axis. The knots are resolved clearly in the raw data but are overexposed in this image to reveal the presence of faint loops of material to the North of the star. The directions are the same as in the previous figures.

fact that the variations in brightness of the disk in the broad B, V, R and  $I_c$  bands quite closely mimic the stellar spectrum, almost certainly implies that the emission we detect is due to scattering of the stellar radiation from particles of average size much larger than one micron diameter. This, in turn, indicates that some sort of accretion process has been active in the protoplanetary nebula to form large grains from the approximately 0.1 micron sized particles commonly found in interstellar space. It should be noted that the IRAS infrared excess emission reported for this star by Gillett, 1986 (Reference 3) that initially triggered interest in this particular system does not necessarily have to originate from the same material responsible for the scattering observed in the optical.

A slightly different application of the coronographic technique just described is shown in Figure 4 wherein an area around the symbiotic Mira variable R Aqr is investigated in some detail. This fascinating system is quite likely to consist of a mass losing Mira variable and a

hotter blue companion accreting a portion of that mass via an accretion disk (see Solf and Ulrich, 1985, and references therein). Although this system is known to be one of the most complex observed so far, probably, mainly because it is so close (200–300 parsecs by most estimates), some of the most exciting phenomena occur deep within the inner nebulosity extending out to 10–15 arcseconds at most from the central object. The morphology and physical characteristics of this nebulosity are not well known, principally because of the difficulty of imaging accurately and reliably within a few arcseconds of the bright Mira whose visual magnitude varies periodically from  $m_v = 6$  to 11 in 387 days.

An obvious solution to this problem is offered by the coronographic technique whereby the bright Mira is occulted by the 2 arcsecond wide wedge as shown in Figure 4. This allows long integration time exposures through narrow band filters tuned to bright emission lines such as H $\alpha$  and the forbidden [NII] 6583 Å. Short duration broad band R

exposures appropriately subtracted from the narrow band images allow an even better view of the line emission region around this object. The image shown in Figure 4 also illustrates graphically the potential of this technique as both previously known and unknown bright and faint features throughout the inner nebulosity can be readily discerned and accurately measured down to approximately one arcsecond of the Mira without much trouble. Especially obvious is the famous jet made up of several knots extending in a generally northern direction towards the bottom of the figure but faint wisps, knots, and a counter jet extending to the limits of our image in the southwest are also clearly discernible against the sky background. Direct comparisons of images taken in the light of several emission lines of elements in varying ionization stages show remarkable differences revealing a complex temperature and electron density structure within the nebulosity. These data should prove quite useful in

establishing and elucidating the mechanism responsible for the observed activity in this enigmatic system.

More observations of a number of interesting objects with this technique at La Silla are being planned for the near future. The authors welcome suggestions from readers of this publication for improvements, additions to and ideas for new applications of the basic technique described here. If you have a favourite object that might benefit from an investigation with our coronograph, please contact us so that we may explore the feasibility of a joint effort.

### Acknowledgements

None of this work would have been even remotely possible without the enthusiastic support of Daniel Hofstadt and his operations group at La Silla, in particular Paul Le Saux, Gerardo Ihle, Michel Maugis, and A. Urquieta. We are especially grateful to Anatoli Evzerov for

construction and calibration of the coronograph, to B.G. Taylor, F. Macchietto and H.S. Stockman at ESA and the ST Scl for constant encouragement and financial support, to P. Bély, R. Prangé, R. de Grijp and A. Vidal-Madjar for assistance in many aspect of this programme. We also wish to thank S. di Serego Alighieri for the flat field he kindly supplied and F. Noriel, for expert editorial assistance.

### References

1. Burrows, C., F. Paresce, and A. Evzerov, Instrumentation and Data Reduction Techniques for the Detection of Circumstellar Material, *B.A.A.S.*, **18**, 1027, 1986.
2. Paresce, F. and C. Burrows, Wide Band Imaging of the Beta Pictoris Circumstellar Disk, *B.A.A.S.*, **18**, 1027, 1986.
3. Gillett, F.C., "IRAS Observations of Cool Excess around Main Sequence Stars", in *Light on Dark Matter*, ed. F.T. Israel, D. Reidel, **61**, 1986.
4. Solf, J., and H. Ulrich, "The structure of the R Aquarii Nebula", *Astron. Astrophys.*, **148**, 274, 1985.

## Search for Supernovae in Distant Clusters of Galaxies

L. HANSEN, Copenhagen University Observatory

H.U. NØRGAARD-NIELSEN, Danish Space Research Institute

H.E. JØRGENSEN, Copenhagen University Observatory

### Supernovae and Cosmology

One of the main problems of cosmology today is to determine whether the universe is open or closed, i.e. if it will continue to expand for ever or if it will recollapse in a far future. The classical attempt to settle the question is to observe some kind of standard candle out to large redshifts,  $z$ , and measure the positions of the objects in the Hubble diagram ( $\log(z)$  versus apparent magnitude). The brightest galaxies in rich clusters have for example been used for this purpose, but significant evolution corrections are expected which are hard to determine with the required precision, and no firm conclusion has been reached as yet.

A more promising candidate for a standard candle is the type I supernova (SN I). SN I events show spectra and light curves which are very alike, and the intrinsic scatter in peak brightness is less than 0.3 magnitude. SNe I occur in spirals as well as in elliptical galaxies. Events in elliptical galaxies are not expected to suffer from any significant interstellar extinction in the parent galaxy, which would otherwise be difficult to correct for with the necessary accuracy.

SNe I near maximum rival with galaxies in brightness ( $M_V = -19.7$  for  $H_0 = 50 \text{ km s}^{-1} \text{ Mpc}^{-1}$ ). At a redshift of  $z = 0.5$  the expected peak magnitude in V is about 22.7 depending on K-correction and the cosmological model assumed. For Friedmann models with  $q_0 = 0.0$  (open) and  $q_0 = 0.5$  (transition to closed) the difference is 0.28 magnitude. A modest number of SN I events could therefore provide the evidence for an open or closed universe. Notice, that neither  $H_0$  nor the absolute peak magnitude need to be known.

SNe I as standard candles are not supposed to be plagued by uncertain corrections, as are other candidates. The K-corrections can be accurately determined from nearby SNe I, and no change of the supernova characteristics with look-back time is expected.

A well-developed theoretical model for SNe I assumes the deflagration of a white dwarf which is pushed to the Chandrasekhar limit by mass accreted from an evolving companion. In this picture virtually the same event happens every time with no variation of mass and chemical composition. This explains the reproducibility of the phenomenon.

It has recently been realized, however, that a subgroup named SNe Ib exists in spiral galaxies. This subgroup is characterized by the absence of the  $\lambda 6150$  absorption feature in the spectra. SNe Ib will hardly cause any major problem for cosmological applications as they are about  $1^m.5$  fainter than the majority of SNe I. If they are not discriminated by other means they may be discarded because of gross deviations from the predicted apparent magnitude.

### The Search Programme

With the launch of the Hubble Space Telescope (HST) it will become possible to do photometry on distant SNe to magnitudes fainter than 25, and the cosmological goal is then within reach. The first and difficult problem is to find the SNe I. G.A. Tammann (1) estimates that a Coma-like cluster at  $z = 0.5$  will show a rate of 0.5 SN I per year within the field of the Wide Field Camera of the HST. However, observing time on the HST is very expensive, and fortunately the job can be performed from the ground. The Danish 1.5-m telescope at La Silla is ideal for the task. The observing time is

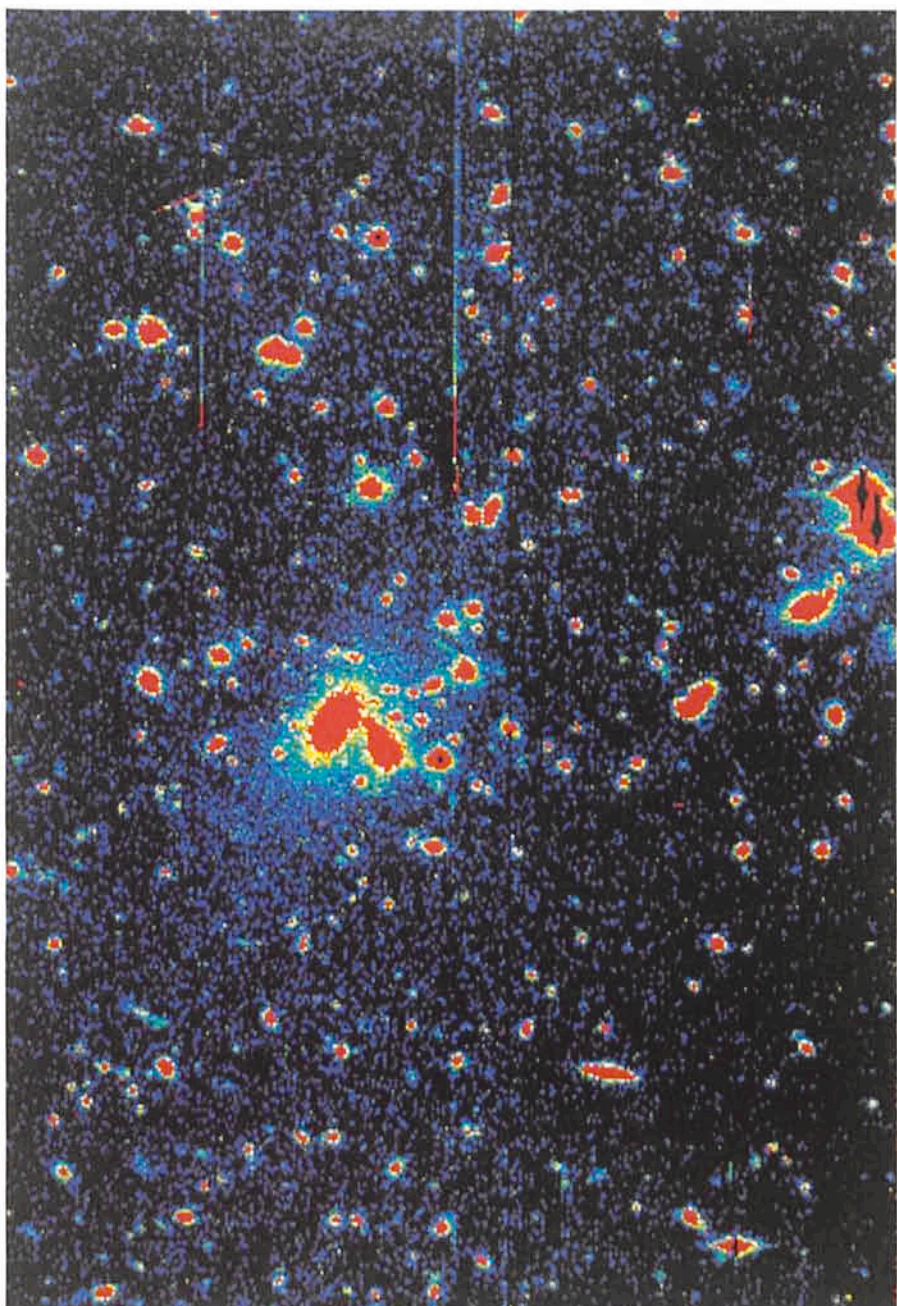


Figure 1: A 1-hour CCD exposure in the V-band of the cluster AC 114 ( $z = 0.31$ ) obtained with the Danish 1.5-m telescope. The seeing was  $0.9'$  (FWHM). The field is  $2.5' \times 4'$ . Most of the objects seen are galaxies.

relatively cheap, the field of view somewhat larger than for the Wide Field Camera, it has a large number of nights with good seeing, and it is known for its high image quality. Photometry on stars of  $24''$  can be made with a CCD camera from 30-minute exposures (2). As explained in the text of Figure 2 we have performed realistic simulations of a supernova event and demonstrated the feasibility of our methods. We have, therefore, initiated a major campaign in September 1986 with the aim to find distant SNe I in elliptical galaxies.

Our plan is to observe rich clusters of galaxies with redshifts from 0.2 to 0.6 if

possible each month from September through April with the Danish 1.5-m telescope. A SN I remains within 1 magnitude of its maximum brightness for about 25 days, but because of relativistic effects (time dilation) time intervals are stretched by a factor  $1+z$  when observed at the redshift  $z$ . This means that for  $z = 0.5$  and less a SN I remains above our detection limit of approximately  $24''$  for more than a month, and it cannot avoid discovery if it occurs within the half year period of our watch. If, say, 20 clusters are searched every month we expect 5 SNe I per year to be found.

## The Procedure

During the last part of 1986 we observed using the old ESO CCD camera with a pixel size corresponding to  $0.47''$ . The old CCD has many defects and a rather large read-out noise. From 1987 we will use a new one with twice as much spatial resolution, few defects and reduced noise. Of great importance is also the availability of the ESO image processing system, IHAP.

Our exposure time is 45 minutes to 1 hour, and generally we use the V-band, although some exposures have been obtained in Gunn R. However, interference fringes from night sky emission lines are very prominent in the R-band and hard to correct for in a satisfactory way.

As soon as a new exposure has been started, the previous exposure is reduced. This is only a matter of a few minutes. We then start a large BATCH procedure that compares the new images with a standard exposure of the field. A number of common objects are identified, and the new image is rotated to coincide with the standard within 0.05 pixel. The seeing is determined, and the image of best seeing is Gauss-smoothed in order to match the seeing of the other. After scaling the intensity of the objects to the same level in the two images the standard is subtracted from the new, and a difference image is obtained.

The next step is the exciting evaluation of the difference image. The standard frame is displayed in the first quadrant of the colour screen, while the three other quadrants show 1/15 of the field in the new, the standard, and the difference image. With the special colour scale we use, the noisy difference image will look greenish. Pixel-values deviating more than about  $2.5\sigma$  will appear either black or red. A stellar image of  $24''$  and average seeing  $1.5''$  covers some 10 pixels (old chip). If such a star appears between two exposures it will stand out very prominently in the difference as black or red.

When we examine the field in 15 steps we notice a number of black or red features from well-known bad pixels and columns of the CCD. Often we find that a few stars are too bright to cancel when the difference between two large count-numbers are taken. These stars are then checked for variability by one or more procedures for magnitude determination. We will also find a number of cosmic (radioactive) events in the CCD chip. This is a problem which worries our sceptic colleagues more than it worries us. Cosmics have a very narrow energy distribution, and the large majority of events are easily distinguished

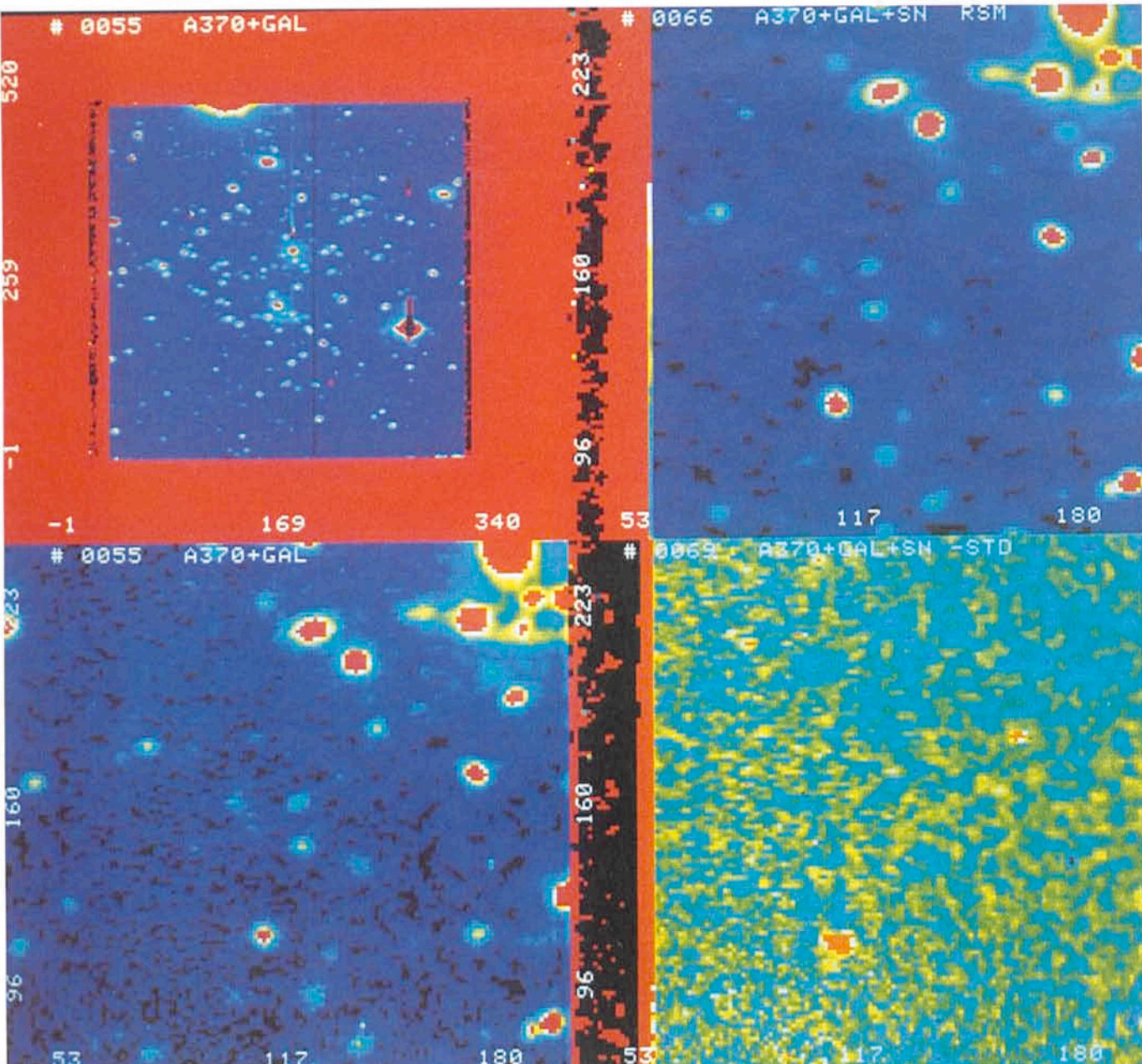


Figure 2: The colour screen during one of the 15 comparison steps. Part of a new (upper right) and a standard (lower left) exposure of the cluster AC 370 ( $z = 0.37$ ) is shown. The lower right shows the difference. In the upper left a compressed image of the whole field is displayed. The standard image is of rather poor seeing ( $1.9''$ ), and the new exposure has been rotated, smoothed and scaled to match the standard. A SN I event has been simulated in the following way: A B-exposure of SN 1985 I in a galaxy of  $z = 0.03$  obtained by J. Teuber was "zoomed" out to  $z = 0.37$ , smoothed to match the seeing and added to the new image. The magnitude of the supernova at  $z = 0.37$  is 22.0. Similarly, an image of the parent galaxy cleaned for the supernova was added to the standard image of AC370. The "event" appears to the left of and below the centre in the difference. The fake is quite realistic as the noise is always dominated by the background.

by the experienced eye or by comparing the profile with that of a star.

In rare cases cosmics may simulate a SN event, e.g. by falling on top of an object in the image. Therefore, a promising SN candidate must be confirmed. We planned that the whole comparison procedure should take less than 30 minutes. A candidate can then be confirmed by a second observation the very same night. This is important for the follow-up. In practice it is no problem to do the comparison within 30 minutes – at the computer centre! The computer on the Danish 1.5-m turned out to be

too slow because it lacks a floating-point processor. At present we must accept a delay of one day, which may have sad consequences if a candidate appears on the last night of observing.

### Preliminary Results

Until now we have had 5 runs on the Danish 1.5-m. We have paid most attention to the clusters in the range  $0.2 < z < 0.4$  because (a) HST is not yet in orbit, (b) we want to be sure of our methods, and (c) ground-based spectroscopy can be made for SNe I at these

redshifts. We cooperate on the project with R.S. Ellis, University of Durham, and W. Couch, Anglo-Australian Observatory. They have supplied us with a number of distant clusters, and they have obtained over-head time on the Anglo-Australian 3.9-m telescope and the Isaac Newton 2.5-m telescope with the possibility to do spectroscopy with short notice of events down to about  $V = 22''$ .

Our survey supplies us with a steadily increasing list of faint blue variable objects. One of the objects for example is apparently an active galaxy possibly at

the cluster redshift ( $z = 0.3$ ). Most likely the majority of the variables are faint QSO's roughly in agreement with statistics of QSO's around  $22''$  (3) predicting approximately 1/3 object per CCD-frame.

After the first 5 runs we have been able to do 48 comparisons of fields. The expected number of SNI events in 2 according to the supernova-rate given above, but we have found none until now. Why? Part of the answer may be that although many of the clusters are really impressive some are less rich than

Coma. One should also notice that the local supernova-rate is uncertain with a factor of 2 according to Tamman (private communication). Further, there is at present no evidence of the rate at earlier epochs of the universe.

This campaign will at the very least put important limits on the supernova rate at cosmological distances. A valuable spin-off will also be the nice selection of high quality cluster images, because sub-arcsecond seeing is not an unusual event at the Danish 1.5-m. However, the primary purpose is to dis-

cover SNe. The first season has convinced us that our technique works. If a supernova appears we will find it!

## References

- (1) Tamman, G.A.: 1979, in *Astronomical Uses of the Space Telescope*, proceedings from the ESA/ESO workshop, ed. Macchetto et al.
- (2) Stobie, R.S., Sagar, R., and Gilmore, G.: 1985, *Astron. Astrophys. Suppl.* **60**, 503.
- (3) Koo, D.C., Kron, R.G., and Cudworth, K.M.: 1986, *Publ. Astron. Soc. Pacific* **98**, 285.

## NEWS ON ESO INSTRUMENTATION

### On the Rates of Radiation Events in ESO CCDs

Radiation events (cosmic rays and local radiation) stand out in exposures taken with thinned CCD devices as spikes covering 1–4 pixels. Their intensities vary from about one hundredth electrons (the lower detection limit) above the background to a few thousand for the most energetic events. In front-illuminated, thick CCDs energetic particles can produce a short track of electrons as they cut diagonally through the silicon layer.

The number of radiation events per unit time is such that they contribute in a significant way to the noise in the astronomical data extracted from the CCD frames. In direct imaging they can be distinguished from stars on the basis of the point spread function. The problem is more serious for spectroscopic observations. In long-slit spectra where the dispersion direction is aligned with the rows or the columns of the CCD, the area where the sky is sampled can be efficiently cleaned with a median filter running in a window which moves perpendicular to the dispersion (RBLEMISH command in the ESO IHAP data reduction system). For spectra in the echelle format, the only effective way to identify the radiation events is by comparison of two, or possibly more, spectra taken with an identical configuration. Pixels affected by a cosmic ray in a single exposure can be sorted out and rejected when their signal value is compared with that measured on the average frame. Routines operating on this basis exist in both the MIDAS and IHAP data analysis systems. To achieve good cleaning without degradation of the astronomical data, it is necessary that pa-

rameters like sky transparency, seeing and sky emission line intensities do not vary too much during the sequence of exposures.

Billions of radiation events have been duly recorded by CCDs used for astronomy in the last 10 years, but being considered essentially a nuisance, little has been published on their rate or energy distribution. As a step towards a better understanding of this phenomenon, we have counted radiation events in a number of long (typically one hour) dark exposures obtained in the last four years with ESO CCDs both in the Garching lab and at different instruments at La Silla. We list in Table 1 the event rates derived from these exposures. Typical values for some of the ESO CCDs have

been reported occasionally in the Operating Manuals of the instruments (CASPEC, EFOSC). The data collected here are more systematic and give the possibility to draw a few simple conclusions. A batch programme based on a filtering technique was used to identify the events with intensities larger than about  $5\sigma$  of the background noise. The rates are not very sensitive to the value of this lower cut, most of the events being of sufficient energy to be detected. No systematic difference is found between measurements at Garching and La Silla, with variations being observed in both directions at the 10–20 % level. The rates do not seem to correlate with the telescope or the instrument type. It is worth noting that

Table 1: Radiation event frequency in CCDs

ESO CCD Number	Type	Telescope	Instrument	Number $\text{cm}^{-2} \text{min}^{-1}$	No. Exposures
3	RCA SID 501 EX (thinned)	3.6 m	CASPEC	5.8	3
3	RCA SID 501 EX (thinned)	3.6 m	EFOSC	5.2	5
3	RCA SID 501 EX (thinned)	2.2 m	B & C	5.7	3
5	RCA SID 501 EX (thinned)	3.6 m	CASPEC	6.6	4
5	RCA SID 501 EX (thinned)	2.2 m	Imaging	6.1	3
6	GEC 8603*	2.2 m	B & C	1.2	2
7	GEC 8603*	2.2 m	B & C	2.1°	3
7	GEC 8603*	3.6 m	CASPEC	2.3°	2
8	RCA* SID 006 ES	3.6 m	EFOSC	5.2	2
12	TEK 512 M – 11*	3.6 m	CASPEC	1.4	3

\*  $15 \mu\text{m}$  pixels   \* Coated to improve UV-blue sensitivity

° Possibly contaminated by electronic noise

the same CCD #3 was used with dewar windows made of two different types of fused silica when on CASPEC or EFOSC (see Table 1). Event rates in RCA CCDs are relatively constant and a factor of 3–4 higher than in GEC and TEK CCDs. As the dewars are the same for all CCD types, the high rates are probably related to some radioactive component in the RCA CCD package, the support glass being the most likely candidate. It is not clear whether the difference be-

tween GEC and TEK is significant. The count rates in GEC CCDs may have been slightly affected by electronic noise which can imitate radiation events.

The values are very close to the low limits quoted by C.D. Mac Kay in his review article in the 1986 Annual Review of *Astronomy and Astrophysics*. The question remains open as to whether a fraction of these counts observed in GEC and TEK CCDs is still of local ori-

gin, and further tests are planned in the near future.

Astronomers who have measured or suspect that the event rates in their CCD exposures are significantly different from the values given in Table 1 are strongly encouraged to send their data to ESO for further analysis. It would be of particular interest to measure using the same algorithm rates from CCDs of different types and/or located at other Observatories.

S. D'Odorico and S. Deiries

## New Technology Telescope Taking Shape

M. TARENghi, ESO

As an intermediate step towards a very large telescope (VLT), ESO decided to design and build a New Technology Telescope (NTT) with a mirror measuring 3.5 m in diameter. This telescope will help reduce demand on the 3.6 m telescope and will offer an opportunity for practical testing of new ideas for telescope design.

The NTT project includes a number of innovations:

- (i) thin primary mirror with active optical control of the mirror geometry,
- (ii) active control of the collimation and of the focusing of the secondary mirror,
- (iii) maximum exposure of the telescope to the external environment during observations (better seeing),
- (iv) fast switching of the light beam between two different instruments,
- (v) alt-azimuth mount with high pointing and tracking accuracy,
- (vi) flexible and easy control system,
- (vii) remote control,
- (viii) rotating compact building.

The optical system is a Ritchey-Chretien type. The primary M1 as well as the M2 and M3 mirrors consist of Zerodur glass ceramic manufactured by Schott Glaswerke, Mainz, FRG. The meniscus shape and the diameter-to-thickness ratio of only 15 of the primary mirror is thinner than that of any other large optical telescope built in recent years.

The optical figuring is now being carried out by Carl Zeiss, Oberkochen, FRG. The optical quality specification to the manufacturer for the combined optical train (Nasmyth image) is 80% of the geometrical optical energy within 0.4 arcsec. However, after correction with the ESO active optics support, the optics should maintain an image quality of

80% of the geometrical optical energy within 0.15 arcsec.

The telescope mechanics is made of box-shaped parts in order to achieve high stiffness with low mass. The NTT is expected to have an eigenfrequency of about 8 Hz. The result is a structure with the turning part weighing approximately 110 tons. The manufacturing of the main steel structure and the assembly in Europe of the complete telescope is being carried out by Innocenti-Santeustachio, INNSE, Brescia, Italy.

The azimuth axis is mounted on an axial multipad hydrostatic bearing of 3.5 metre diameter. The radial location is defined by an axially pre-loaded angular contact ball bearing. The altitude axis is mounted on large self-aligning internally pre-loaded ball bearings.

The function of the azimuth axial hydrostatic bearing system is to provide a stiff support and to allow the accurate and low-friction rotation of the telescope fork on the supporting ring. This is accomplished by using an oil low-pressure, multipad (24), hydrostatic bearing with a large carrying surface. In addition to the low-pressure design of the hydrostatic supports, which allows for a low consumption of oil and a limited temperature increase of the oil in the pads, an active, high-accuracy oil temperature control system avoids major exchanges of heat between oil, telescope structure and environment.

The two axes of the telescope are both controlled by a group of four servodrives. The altitude drive system is composed of two toothed wheels, one

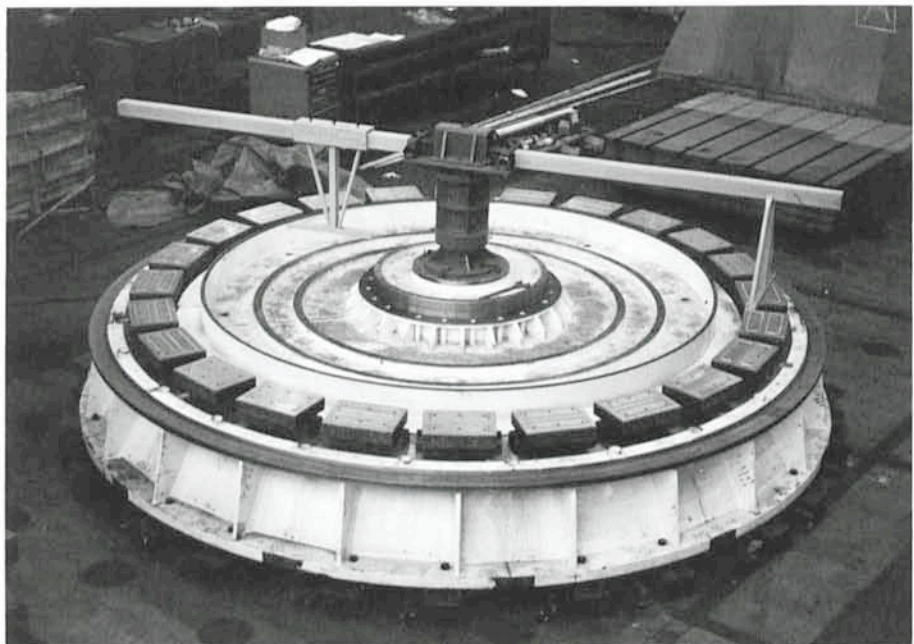


Figure 1: The supporting ring with 24 hydrostatic pads in the workshop INNSE, Brescia, in February 1987. This is a first element of the European pre-assembly of the NTT.



Figure 2: The fork arms on the reference plane. The seats (holes) for the drive units and for the big ball-bearing of the elevation axis are clearly visible.

at each end of the altitude axis, each driven by two servodrives via two pinions. The azimuth drive system consists of a stationary toothed wheel on which four pinions, one for each servodrive, are engaged.

The absolute position of the telescope is measured by two directly coupled absolute encoders. The tracking is controlled by two friction-driven incremental encoders. Each axis is provided with one absolute and one incremental encoder.

An important aspect in the design is the maximum exposure of the telescope to the external environment during observation. This approach has been selected in order to provide maximum ventilation to the structure, thus allowing for thermal stabilization of the telescope to night conditions and avoiding the trapping of layers of air at different temperatures in the path of the optical beam, which would cause blurring of the image. The building floor is actively

cooled, as are all heat sources located on the telescope.

The mobile part of the building is octagonal, has three storeys and rotates on a cylindrical concrete base.

The instrument rooms are on both sides of the telescope behind the side walls of the telescope room. The control equipment occupies a separate lower floor. At this level is also a room for the technical services of the building.

In order to keep high pointing and tracking accuracies with good ventilation at the same time, the telescope is protected at the front and back by permeable wind-screens which control the wind speed in the chamber where the Telescope tube sits.

The temperature in the telescope room and in the instrument rooms is maintained at the level of the outside temperature at night, achieved by means of an appropriate thermal insulation and air conditioning system.

## NTT Control/Acquisition Software

G. RAFFI, ESO

In these months, while the main mechanical and optical components are being prepared for the NTT, the control software has also to meet its first deadlines. In a few months, members of the Electronics Group will be testing the main telescope movements at INNSE in Brescia.

This will be the first result of a preparatory work, which started a couple of years ago. The present description should highlight new aspects of the NTT software with respect to the control/acquisition systems presently in use at La Silla.

The NTT control system design in general (electronics and software) was designed by the TP Electronics Group. People who are specifically working at the NTT software (some part-time or for a limited period of time due to other ongoing projects) are P. Bierreichel, B. Gilli, B. Gustafsson, J. Marchand, G. Raffi, K. Wierenstrand from the Electronics Group and L. Noethe from the NTT Group.

In this issue of the *Messenger* the general structure of the NTT control/acquisition system is summarized. In future issues some areas will be expanded more in detail, like: user interface; pool; parameter data base; microprocessor software, and active optics software.

### Computers

Figure 1 shows the NTT control computer configuration. As the control electronics of the NTT was designed to be distributed, in order to reduce cabling and therefore increase reliability, a number of crates (based on the VME standard) are used for the telescope control functions. The VME crates incorporate microprocessors of the Motorola 68000 family and are all linked via a Local Area Network (LAN) of the Ethernet type.

The control computer of the NTT is a Hewlett Packard A900, which has the function of coordinating the distributed control system, perform data acquisition, accommodate user interface and image processing and support remote control. The A900 minicomputer is the newest member of the HP1000 family based on newer and more compact technology and with computational performances a factor of two better than HP1000 F computers.

### Software

Software control and data acquisition systems serve the purpose of managing telescope, instrument, detector, image processing operation in a way which

has to be comprehensive and clear for the user. The need for a data acquisition system has been recognized and implemented at La Silla already some years ago. The NTT, however, is the first case where a comprehensive system design has been done right from the beginning.

The main requirements of the NTT system were to accommodate distributed control electronics and two instruments which will be permanently connected. This in turn led to specify that the software should allow multi-instrument operation and multi-user operation (or multi-station) as a consequence of the simultaneous use of more than one instrument and of remote control.

Additional needs, which had a large impact on the design, were remote control and user interface. Finally, during the whole design phase of the NTT system, much attention was paid to see that the present design work could also be used for the VLT and thus represent a first test bench for this instrument.

Altogether the NTT control/acquisition system can be characterized in the following way:

– *Distributed system:* Programmes can be either on the A900 or on any

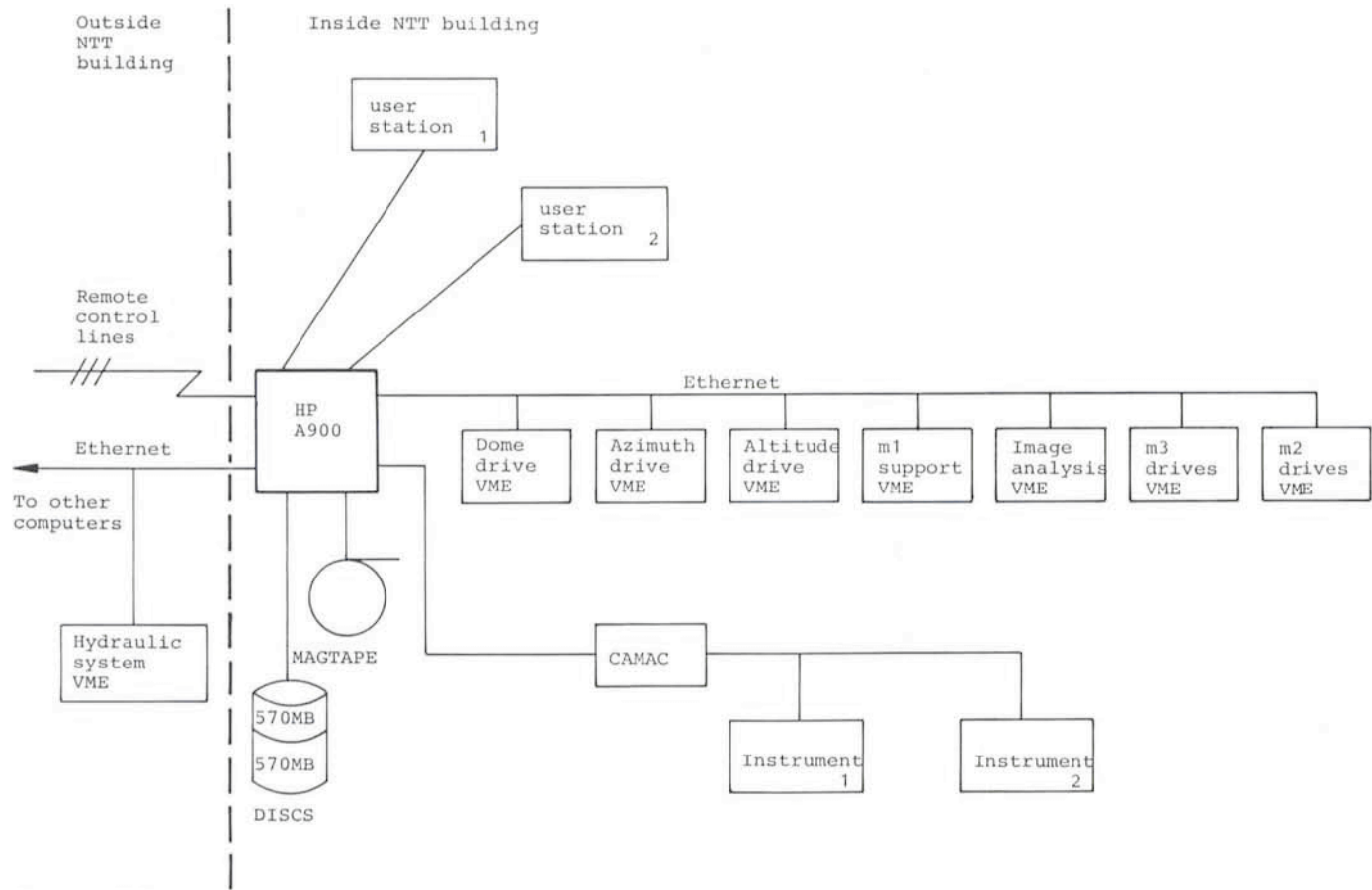


Figure 1: NTT control computer configuration.

microprocessor connected to Ethernet. Rules and protocols had to be designed so that commands/replies and data could be exchanged transparently, i.e. without differences due to where the programme is running. So one can visualize the NTT software as distributed on many CPU's, while up to now microprocessors were always used as "black boxes", with a special protocol with every one of them. A very relevant activity in this area was to define and implement a suitable real-time system for the microprocessors and adequate cross-support tools. Then interfacing both with Ethernet and with the control electronics had to be coped with, namely the writing of corresponding drivers, which is still an on-going activity.

– *Multi user/instruments system:* Many operational environments can run at the same time (not only one as at present), though clearly certain parts like the control of the light beam will belong to one instrument only at one given time. Booking of devices enforces protections and interlocks and separates users. Image processing can be done with IHAP on many independent data bases. Multidetector operation, like in the case of EMMI, is also implicitly included into this concept.

– The system can accommodate several user stations, where users will be doing simultaneously different ac-

tivities. Stations are identical in hardware and software. In practice different users will choose different tables and menus in accordance with the work they are doing, namely: active use, monitoring, off-line work.

– *User interface:* This had to be updated not only because of the inadequacy of the present terminals, but mainly for the need to have a more flexible and easy to modify user end. To improve the physical user end, the display information was brought to a large colour monitor (with softkey, tables, graphics, etc...) of the Ramtek type (with the advantage that this is interchangeable also for image processing use). To improve the operational aspects, the user sees now a unique set of commands for different purposes (telescope control, instruments, detectors, image processing), rather than a set of terminals. The layout of the user end can be easily modified, as this layer of software does not belong to any specific control package and basically sends commands to any control programme, receives and displays replies.

– *Pool:* To enforce complete independence of control modules for multi-instrument operation and to detach the user end from the rest, it was not enough to define interface rules and protocols. A lot of information has to be exchanged between various modules

(e.g. between instrument and telescope) and a large number of parameters needs changing/updating as soon as new modules are added. It has in fact to be remembered that a control/aquisition system has to be open to allow additions. For this purpose a data base, named Pool, has been implemented, where the time critical files are kept in memory. Tools will be available to read and display what it contains, easily monitoring an operation going on in the system (e.g. monitoring from a remote site control operations).

– *Remote control:* For a description of the last tests on R.C. see the article in the *Messenger* No. 44, June 1986. R.C. concepts have been embodied in the design of the NTT control/aquisition system and it will benefit from the features described before. One relevant example of the impact of R.C. on the design is the Pool, where local files are residing on one computer while global files are kept updated on two computers (local and remote). Meanwhile R.C. will be operational on the 2.2-m and on the CAT telescopes starting with July 1987, so that more experience might be acquired before installing it on the NTT.

So far all the basic elements of the system have been implemented, while work is still proceeding on the specific control programmes for the different telescope components.

# MIDAS Memo

## ESO Image Processing Group

### 1. Application Developments

The plotting facilities have been upgraded with many new features such as negative increments on axes and overplot of error bars. The INTAPE/FITS command was updated so that it now reads blocked FITS tapes according to the agreement of the FITS committees i.e. a physical blocking factor of up to 10 is allowed. The Dicomeds commands have been upgraded to allow for spooling of the output files. That means the B/W and colour mode can be used simultaneously at ESO/Garching.

The FILTER SMOOTH command now employs an algorithm which is nearly independent of the window size. A boxcar filtering of 1024 \* 1024 image with a 15 \* 15 window takes now 13 sec CPU-time versus 211 sec CPU-time before (these are VAX 8600 times, approximately 2.3 times faster than a VAX 11/785). The FFT routines were modified to get rid of the excessive paging observed with large images. For a 1024 \* 1024 image the FFT needs now 54,000 page faults (with a working set size of 1024 pages) and 6 : 30 min CPU-time (VAX 8600).

It is now possible to run several parallel MIDAS sessions from the same disk directory by using the MIDAS login command INMIDAS PARALLEL. The DEFINE/Parameter was added for definition of parameters in MIDAS procedure files. This command replaces the commands DEFAULTS, TYPES and LIMIT which have been removed. NOTE: if you have used any of these commands they must be substituted by the DEFINE/PARAMETER.

### 2. Support of MIDAS at External Sites

The MIDAS system has now been exported to a large number of external sites (i.e. more than 40 sites on 3 continents). In order to give these sites a first class support, a new MIDAS Hot-line service will be started from April 1, 1987.

This service will provide an answer to MIDAS related questions received through either Telex no. 528 282 22 eo d (attn.: MIDAS HOT-LINE) or electronic mail (SPAN: 'ESOMC1::MIDAS' or EARN/BITNET: 'MIDAS@DGAESO51'). Requests and questions received before noon will be answered not later than the next normal working day.

In addition, a special telephone no. +49-89-320-60-456 will be created for general MIDAS questions and prob-

lems. This extension will be connected to the MIDAS support person on duty.

### 3. MIDAS Workshop

The next Data Analysis Workshop, arranged by the ST-ECF, will take place in Garching in the week of May 4-8, 1987. The very positive response to the introduction of a MIDAS Workshop has meant that it will be continued. It will again be arranged just after the Data Analysis Workshop on May 7, 1987. The programme will include sessions on general developments, new applications and the status of the portable MIDAS version in addition to a MIDAS Users meeting. A tentative agenda will be sent out together with other material for the Data Analysis Workshop. People interested in participating in the Workshop should contact either the Image Processing Group or ST-ECF.

### 4. Measuring Machines

The mechanical and optical modification of the OPTRONICS measuring

machine took place as planned during May 1986. The machine has since been used for manual measurements of stellar positions with the old HP 1000 system. Due to problems in the electronics for reading the diode array and delay in the software developments, it has unfortunately not been possible to offer the scanning mode yet. Most of the problems have now been solved and it is hoped that the implementation of the diode array can continue without further delays. With the present time table, it should be possible to scan limited areas of plates on the OPTRONICS this fall.

The usage of the Grant measuring machine has been less than 50 hours over the past year. We regard this to be a result of the very few coudé plates taken during the last years and thus a continuing trend. It is therefore under consideration to discontinue the operation of the GRANT machine if the usage does not increase significantly. People who would like to use it for measurements of coudé and image tube spectra are kindly asked to do so.

## New CCD Control Camera and First Test of a TEK 512 CCD at La Silla

At the beginning of February 1987 a new CCD control camera has been successfully installed at the 3.6-m telescope by R. Reiß and P. Sinclair. It will be used with all of the CCD-based instruments like CASPEC, EFOSC and the

B & C spectrograph. The camera is a so-called generation V system from Princeton Scientific Instrument. It has been interfaced to the standard ESO computer in Garching in such a way that the observers will not detect any differ-

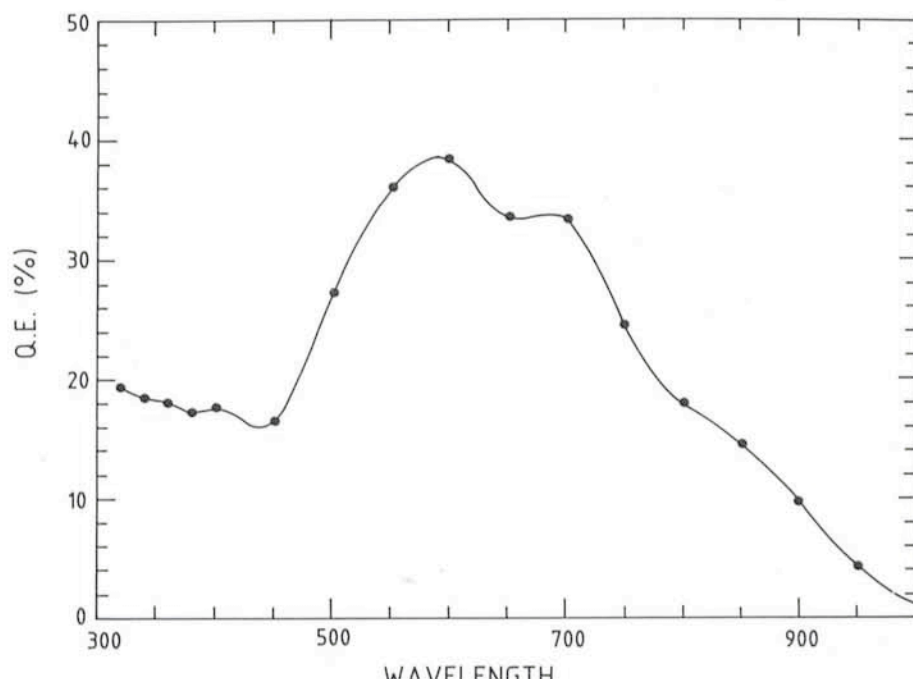


Figure 1: The quantum efficiency curve of the thick TEK 512M-11 device measured in the ESO detector lab after coating.

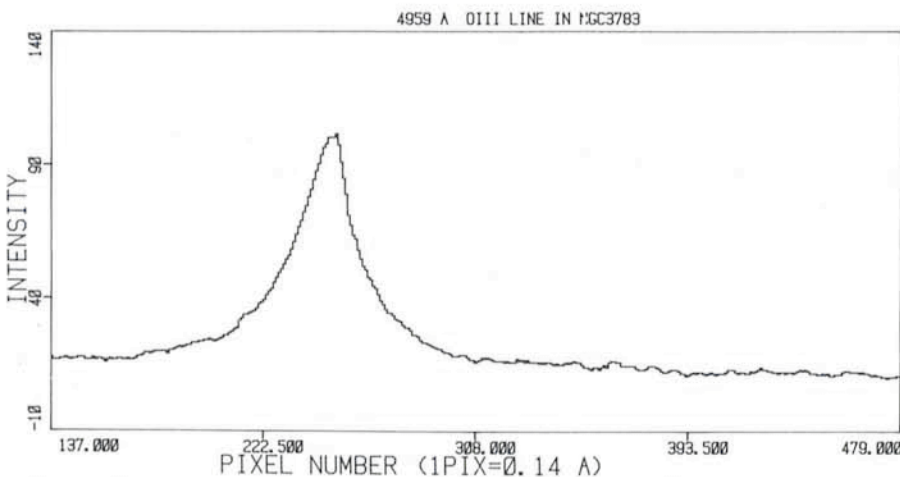
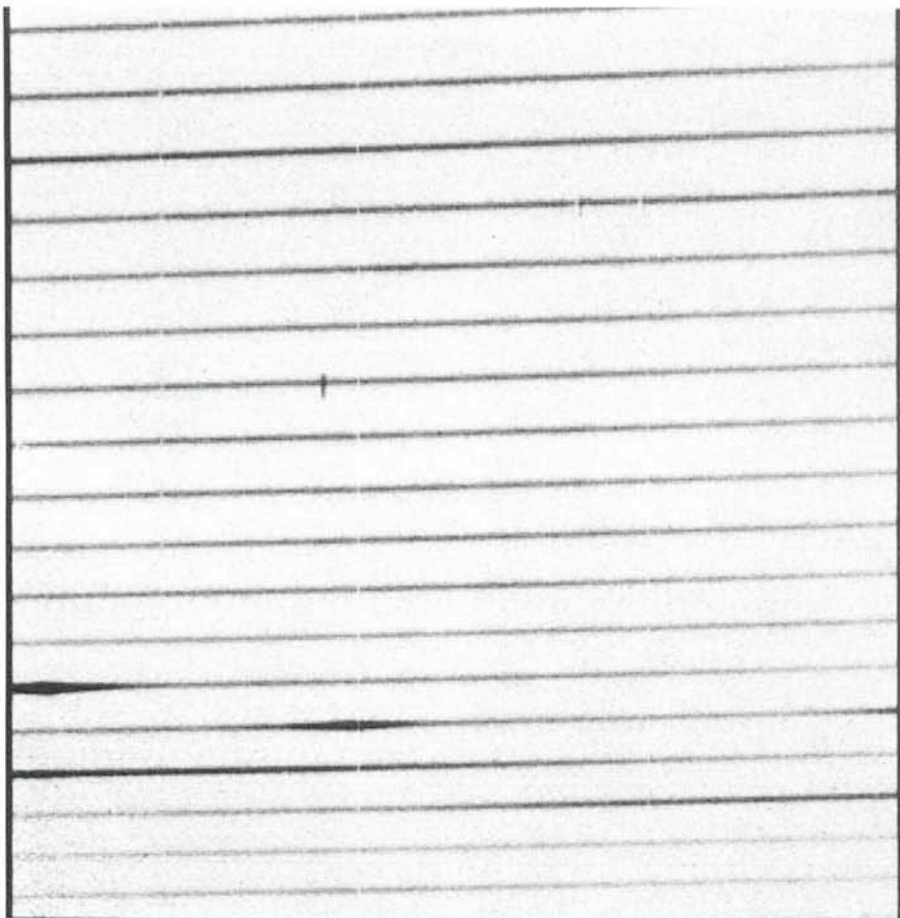


Figure 2: (a) An echelle spectrum of the Seyfert galaxy NGC 3783 centred at  $\lambda 5500 \text{ \AA}$ , obtained with CASPEC and the front illuminated TEK 512 CCD. The orders in the lower part of the frame show the broad  $H\beta$  and the [OIII] emission lines. The Galactic absorption lines of Na I are seen close to the corresponding emission from the night sky in the fourth order from the top. Average of two 1-hour exposures cleaned of the radiation events.

(b) The profile of the  $\lambda 4959 \text{ \AA}$  emission line of [OIII] from one order of the echelle spectrum of the galaxy. X coordinates are the CCD pixels, corresponding to  $0.14 \text{ \AA}$ . The resolution is  $0.25 \text{ \AA}$ .

ence in the control programme of the instruments. Notable advantages with respect to the previous system come from the use of electronic components of improved quality, such as the on-chip amplifiers and high speed 16-bit converters, shorter read-out time and a simplified procedure in the set-up of different CCD types.

The new system operated without problems from the first night of installation. When used with the ESO CCD #3 on CASPEC, it resulted in an improvement of the read-out noise of about 20 % (present value:  $35 \text{ e}^-$ ), a not negligible advantage in the observations of faint objects. The implementation of this new system has freed a CCD control

camera that most likely will be installed at the ESO 1.52-m spectrograph by the middle of this year.

In the same test period, we have also used a front-illuminated TEK 512 M-11 CCD on CASPEC. It has  $512 \times 512$  square pixels  $27 \mu\text{m}$  in size or the largest collecting areas ever as it goes for CCDs at La Silla. The chip had been coated in the detector laboratory at ESO Garching to enhance the UV-blue sensitivity. The quantum efficiency measured after the coating is shown in Figure 1. In this CCD the low noise on-chip amplifier was damaged and we had to switch to the C-amplifier and the C-output shift register. This is probably the cause of a read-out noise of  $30 \text{ e}^-/\text{pix}$ , a value definitely higher than one would expect. Given this value and the relatively low quantum efficiency, this particular device is not better than the CCDs now in operation at La Silla and for the time being is not offered to visitors. Cosmetic and charge transfer efficiency however are quite good (see Fig. 2) and would make this device quite useful on some ESO instruments if operating with a r.o.n. of the order of  $10 \text{ e}^-$ . The radiation event frequency is 1.4 events/minute,  $\text{cm}^2$  or a factor of four lower than in RCA CCDs.

S. D'Odorico

## STAFF MOVEMENTS

### Arrivals

#### Europe:

FRANÇOIS, Patrick (F), Fellow  
MEURS, Evert (NL), Fellow  
RICHICHI, Andrea (I), Student

#### Chile:

BOOTH, Roy (GB), Associate

### Departures

#### Europe:

SCHARRER, Rebekka (D), Laboratory  
Technician (Photography)

## New Staff Association Committee in Garching

Elections for the renewal of the Staff Association Committee were held in Garching in January. As a result Fons Maaswinkel, Lothar Noethe and Gianni Raffi were elected.

Many thanks to Anton van Dijsseldonk and Claus Madsen, who terminated their duty, while L. Noethe is the chairman of the newly appointed Committee.

The present Staff Association Committee in La Silla is composed of Gaetano Andreoni, John van den Brenk (chairman) and Michel Maugis.

# Observation of the Cluster A 370

J.P. DUPIN, B. FORT, Y. MELLIER, J.P. PICAT, G. SOUCAIL, Observatoire de Toulouse, France  
 H. DEKKER, S. D'ODORICO, ESO

## 1. Introduction

Since the first experiment with Multi-object Object Spectroscopy (MOS – see *The Messenger* 41, September 1985) made on EFOSC, the announced new facility called PUMA 2 has been implemented. This is a small, computer-controlled punching machine with which the observer (on the site and during his own run) can make the aperture masks he or she needs.

The PUMA 2 system was developed by the Toulouse Observatory from a prototype PUMA first used at CFHT in Hawaii (Fort et al. 1986). PUMA 2 was implemented for the first time on the 3.6-m ESO telescope in February 1986 during a technical run in order to check the machine operation on-site and to develop and test the software facilities. Since then several astronomers have used the system. Two of us (B.F. and G.S.) took part in a run in November 1986 to measure velocities in clusters of galaxies. We believe it would be interesting for future users to comment on the way MOS has been used, and to present the performance which can be achieved with EFOSC. This paper should be considered as a run report and will give first results from the data reduction made in Toulouse on the observations of galaxies in the cluster Abell 370, using partially automated software. Results of MOS observations are also presented by D'Odorico and Dekker (1986).

## 2. Equipment and Procedures

### 2.1 EFOSC

For a detailed description of EFOSC we refer to the ESO Operating Manual. The detector in use during the November run was the ESO CCD #8, which is a high resolution ( $15 \mu\text{m}$  pixel) RCA CCD that we used in  $2 \times 2$  binned mode. The quantum efficiency is about 80 % and the read-out noise 35 electrons rms.

### 2.2 PUMA 2

The PUMA 2 system is a microprocessor-controlled machine with which holes and slits can be punched in thin (0.15 mm thick) copper sheets called masks or starplates. Two different punch heads (0.3 and 0.5 mm corre-

sponding to 2.1 and 3.6 arcseconds) allow the choice between two hole sizes. It is also possible to punch slits with these widths by punching a series of adjacent, partly overlapping holes. The relative positioning accuracy of the holes is  $10 \mu\text{m}$ , given by stepper motors of the Microcontrole XY tables. The PUMA 2 is linked to the HP 1000 instrument control computer and the file with positions to be punched may be sent directly to the PUMA 2 microprocessor or temporarily stored on disk or cassette.

### 2.3 Preparing the masks

To prepare a mask one needs an EFOSC image of the field of interest. An inexperienced user should obtain it on a previous night, so he/she can go at ease through the interactive object selection process and the preparation of the mask the day before the observing night. This implies the use of MOS on the second night of an observing run, except when the preceding observer agrees to take the short exposures which are required. In our case Dr. A. Pickles kindly agreed to take an image of A 370 during his run, thus allowing us to make the spectrographic observations during our first night. It was a real chance as it turned out to be the best night of the whole run.

### 2.3.1 Taking direct pictures of the field

Images of the field are usually taken in white light. 1-minute exposures are sufficient to detect all objects suitable for spectroscopy.

It is important to note that, depending on the grism used and on the desired spectral range, the field image may have to be decentred in order to put the spectra of interesting objects in a suitable place of the CCD. As an example, with the B 300 grism, and if the spectral range 4500–6500 Å is desired, the objects must be chosen between the lines 100 and 300 on the CCD frame (decentring of the field about 30" south).

### 2.3.2 Selecting the objects

The selection of the objects is done interactively on an image of the field at the 2-D display in the 3.6-m control room. The batch programme used for this purpose runs within the IHAP data reduction system and requires pointing with the cursors at the targets and at the positions of free sky to be used for comparison. Mistakes in the entering of the cursor positions can be corrected and the programme gives a warning if the spectra overlap. The procedure takes less than half an hour if the number of objects is less than about 10.

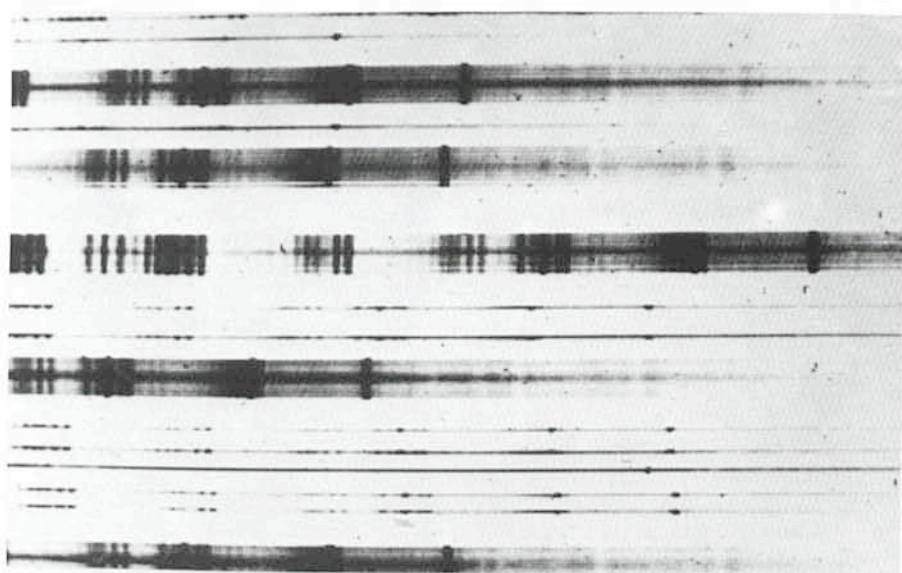


Figure 1: CCD frame obtained with MOS using the B 300 grism. The mask has 5 slits and 11 holes and contains 12 object spectra. Note the number of radiation events in this 1h 30-minute exposure.

For survey-type observing programmes which require an optimization of the distribution of objects and sky apertures to optimally fill the CCD, a semi-automatic programme like the one used by the Toulouse group at the CFHT (Fort et al. 1986) is more effective. The objects are automatically detected in the field image, using for example criteria like magnitude, colour or size. The batch procedure then optimizes the selection, given boundary conditions like length of the spectrum, minimum separation between the objects, need of sky reference. ESO is investigating the possibility to implement such a procedure as well but interfacing an existing Fortran programme into IHAP is not straightforward.

### 2.3.3 Punching the masks

This is a very efficient procedure as 6 masks with a given hole size can be prepared at a time. The size of the holes or slits can be chosen at this step. Holes and slits can be easily mixed on the same mask by punching the same mask twice before dismounting it from the PUMA 2 table. The hole shapes and sizes are very accurate, better than 10 µm. Repeating the punching on the same starplate may remove the burrs that sometimes remain and then give holes a slightly irregular shape.

The machine usually runs quite smoothly except for an occasional punch break. Replacing the punch takes a few minutes and is taken care of by the ESO maintenance staff.

### 2.3.4 Mounting and aligning the masks

The masks are put in place on EFOSC by the night assistant or by the astronomer after a short instruction. This operation is easy and the masks are maintained in a very accurate and repetitive position.

The observer is assisted in the alignment of the mask on the field by using an IHAP batch procedure that compares an image of the mounted mask (illuminated with a calibration lamp) with an image of the field. Provided the guide probe and telescope coordinates have been carefully noted when taking the direct picture, it takes at most two iterations and about 10 minutes to align the mask on the field with an accuracy as good as 0.25 arcsec rms.

The operation of the instrument rotator has been improved a few months ago. It now sets to an accuracy of 0°.1. This is sufficient for accurate alignment and makes the rotation of the EFOSC wheel (which is more complex since it also involves a translation of the mask) unnecessary.

### 2.3.5 Taking the spectra

The procedure is described in the EFOSC Operating Manual and from the experience we obtained during our run we would like only to mention some precautions to be taken to secure accurate results after reduction.

The so-called blue halogen lamp covers very well the range 3500–7500 Å and is normally used for flat-fielding.

It is necessary to take calibration lamp spectra through each mask as the dispersion is not exactly linear and changes with the position in the field, along the columns.

It is useful to keep a short direct image of the mask (with the halogen lamp or the dome lighting) for future automated reduction. It gives also information about the transmission of the different apertures.

All of these calibration exposures can be taken during daytime. However, we preferred to take them directly before or after the science exposure since almost no telescope time is lost and one makes sure that no important calibrations are

forgotten. Also, when using this method, data and related calibrations are stored consecutively on the same tape, reducing the chance of errors during data reduction.

As the exposure times are long, we always chose to work at hour angles smaller than 1.5 hour and zenith distance less than 30° in order to minimize the effects of atmospheric refraction.

Figure 1 is an example of a CCD frame obtained in MOS with a mask punched with both slits and holes.

## 3. An Example of MOS Observations: Galaxies in the Cluster A 370

### 3.1 The astrophysical programme

Very little is known about the dynamic evolution of clusters of galaxies and the evolution of the galaxies in clusters. Multi-object spectroscopy is an ideal tool to investigate these problems. For example, the normal evolution models for galaxies (Bruzual 1981, Guiderdoni 1986) do not explain the excess of blue



Figure 2: Image of A 370 cluster of galaxies taken with a B filter on EFOSC (20-minute exposure). The elongation of the images is due to the reproduction process from the TV screen.

Table 1: Spectra obtained during the observing run at the 3.6-m with EFOSC in MOS mode (1–4 November 1986)

Cluster	Number of apertures	Number of objects	exposure time
A 2444	28 holes	14 objects	1h
A 551	26 holes	13 objects	40 mn + 45 mn
A 370	25 holes	13 objects	1h 30 mn + 1h 30 mn
	11 holes + 5 slits	12 objects	1h 30 mn
	16 holes + 4 slits	13 objects	1h 30 mn
	21 holes + 3 slits	14 objects	1h 30 mn

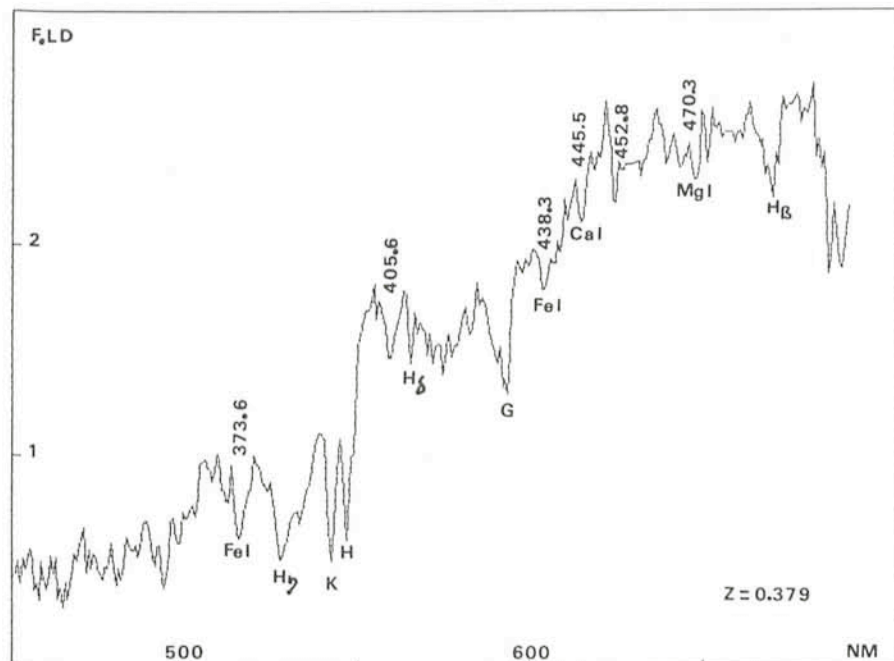


Figure 3: Spectrum of the brightest galaxy of the cluster A 370 (No. 20, cD type) with a redshift of  $z = 0.379$ .

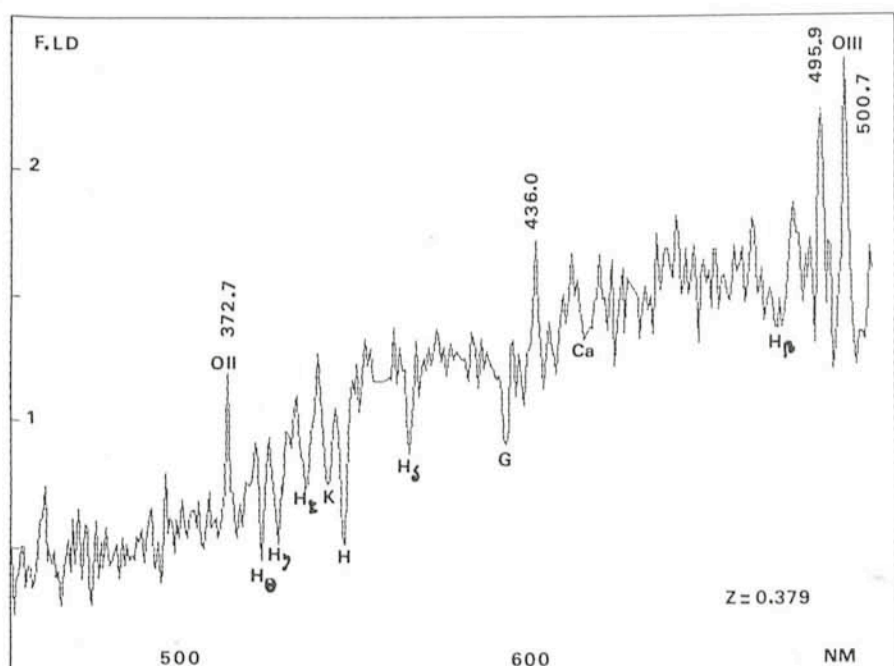


Figure 4: Spectrum of a blue galaxy of the cluster identified as an irregular type (No. 41,  $z = 0.379$ ). Note the emission lines typical of H II regions and the strong Balmer absorption lines.

objects found in clusters with  $z \geq 0.2$  (Butcher-Oemler effect, hereafter referred to as B.O.). This effect raises a lot of questions on the physical processes involved, the time scales, the initial conditions and their role in evolution. It is clear that it is necessary to accumulate spectrographic observations on clusters of varying richness, shape and redshift.

For the ESO run, we chose A 370, a very rich cluster at  $z = 0.374$  (Fig. 2), as the first priority target. Some preliminary low dispersion observations at CFHT (Mellier et al., 1987) have shown a very unexpected high content of spirals which had to be confirmed at higher resolution.

### 3.2 Observational results

Of the 3 nights given for our run only 2 nights were useable for the MOS mode because of bad weather conditions. 79 spectra were obtained with a mean of 13 per mask. Two other clusters were studied besides A 370 and the observations are summarized in Table 1.

No problems arose during the observations but we feel that if it is to be efficiently exploited, this type of observation demands two observers, especially if most of the programme is devoted to MOS spectroscopy and they are not familiar with MOS or EFOSC.

### 3.3 Data reduction

All the spectra were reduced in 6 full weeks, using the software developed in Toulouse for the PUMA 1 system on the CFHT (see Soucail et al., 1987 for a full description). Changes needed for the ESO images were minimal and no particular problem arose in the reduction process. The only remark concerns a rather large number of radiation events on the CCD (ESO #8 has a frequency of 5.2 events/minute/cm<sup>2</sup>). Twin exposures on the same field are useful to identify and correct them. The reduction software has been developed on a VAX computer in Toulouse, and it could be integrated in MIDAS, the ESO reduction package which runs on the same computer. It includes some interesting features related to the special format of the data, like the different positions of the apertures on the CCD and the faintness of the objects.

## 4. The Results

### 4.1 Performance

Despite the poor weather conditions, the limiting magnitudes are quite good: in one hour's exposure, with the B 300 grism, we obtained spectra of  $B = 22$ ,  $V = 21.2$ ,  $R = 20.7$  galaxies at a signal-

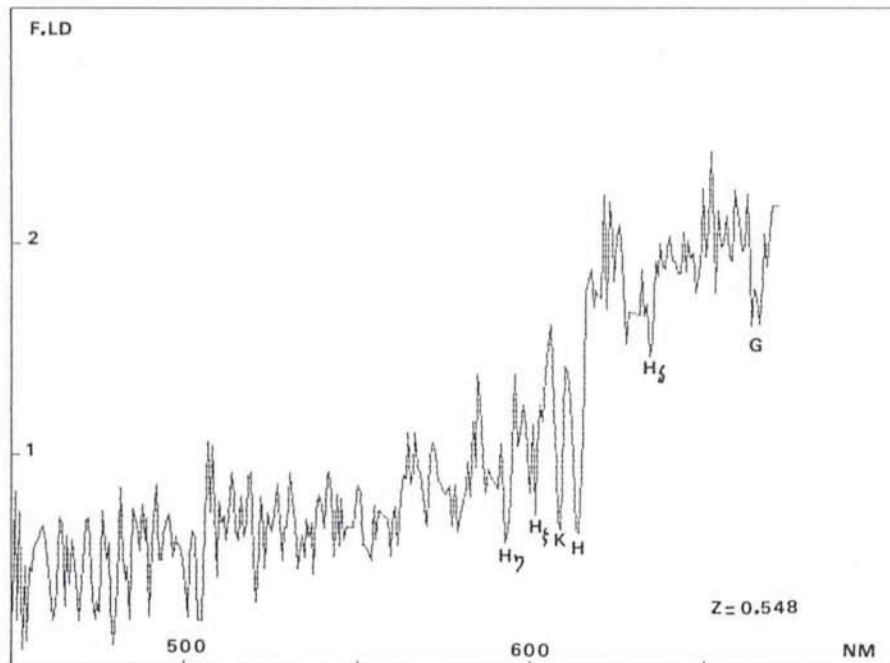


Figure 5: Spectrum of a background galaxy found in the field of the cluster (No. 14,  $z = 0.548$ ).

to-noise ratio on the continuum of 10. These performances are about 0.7 magnitude fainter than the ones obtained at CFHT with a focal reducer that has not been specially designed for this kind of experiment. It is possible to go even fainter by co-adding several exposures which has the additional advantage of better removal of radiation events. Examples of spectra of galaxies in the field of A 370 are given in Figures 3 to 5.

#### 4.2 Astrophysical results

From a run at CFHT in 1985 and the last run at ESO, we have 90 spectra in the field of A 370, which represents an unusually large number for such a redshift ( $z = 0.374$ , see Fig. 6). About 55 spectra are from cluster members and they give a velocity dispersion of 1300 ( $\pm 230, -150$ ) km/sec and a M/L ratio of 130 (with the virial approximation), very similar to those measured on closer clusters. A complete study of A 370 will be given in a forthcoming paper (Mellier et al., 1987) but we summarize here the most significant results.

A 370 is a very rich cluster (richness similar to Coma), X-ray emitting, and shows a large population of blue B.O. objects. The proportion of 21 % given by the photometry (Butcher and Oemler, 1983) has been reduced to about 11 % from our spectrographic measurements, because of a better evaluation of the contamination by foreground objects but the B.O. effect is now well confirmed by the spectroscopic measurements.

The B.O. objects are more precisely spirals or Magellanic galaxies but no

active nuclei are present. By comparing these observational results with star population synthesis models with the same resolution (Guiderdoni and Rocca-Volmerange, 1987) one obtains a good galaxy type distribution. The result is an unexpectedly high rate of spiral

galaxies (50 % as compared with 5 % in Coma) at a time  $2/3 \text{ H}_0^{-1}$ .

Both more observations and theoretical investigations have to be made to explain why at about the same redshift, clusters showing about the same overall properties seem to have so different galaxy contents. Could the pressure effect of the dense intergalactic gas in the centre of rich clusters be a possible answer?

#### 5. Conclusion and Future Developments

As a conclusion we shall say that now the MOS mode on EFOSC in its present status is certainly one of the most efficient systems used on 4-metre class telescopes. It is clear from our experience that the performance in terms of limiting magnitude is quite good.

Further improvements could be made soon in the object selection procedure by allowing a mixed (manual and automatic) procedure for selecting the targets. With a more flexible and user-friendly procedure, the possibility of mask preparation and observation in the same night could be implemented.

An important question is the choice between holes and slits. The trade-off is the number of objects per mask compared to the sky subtraction accuracy which depends on the crowdedness of

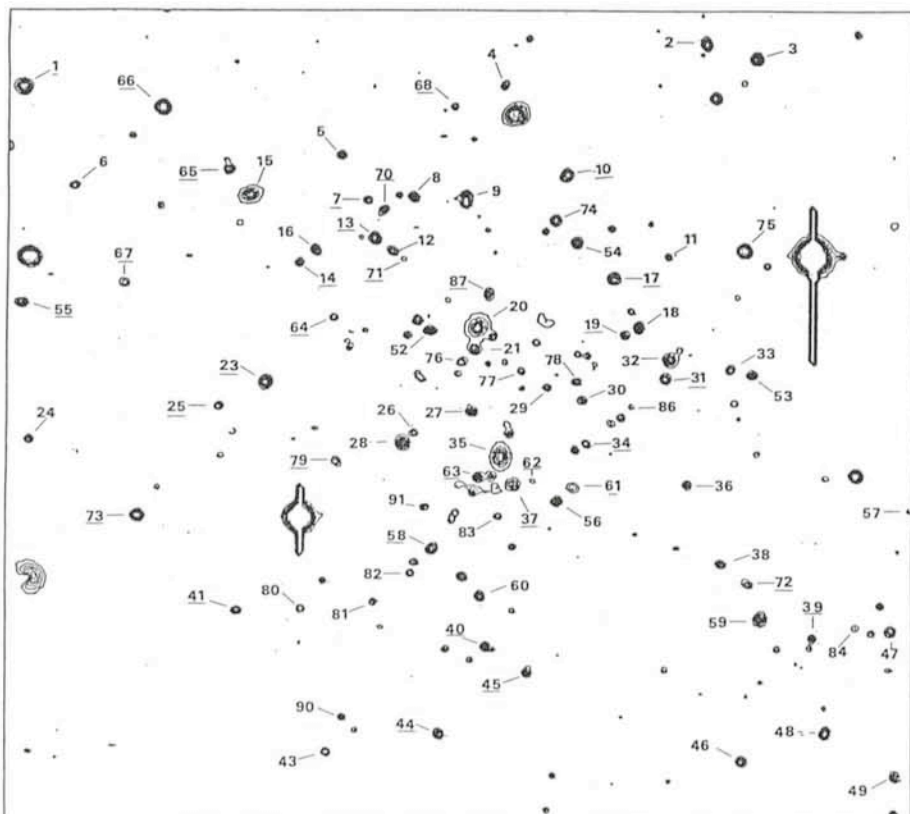


Figure 6: Field of the A 370 cluster with the identification of all the objects from which a spectrum has been obtained at ESO or at CFHT with the PUMA system. The underlined numbers correspond to objects of which the spectra were obtained at ESO in November 1986.

As an example, slits do not seem very well fitted for programmes where a lot of spectra in a rather crowded field are needed. The advantage of slits is certainly a better sky subtraction in the case of very faint objects. In the case of bad seeing, slits are also more efficient. More accurate extraction algorithms such as e.g. the one proposed by Hornes (1986) could also be used on slit spectra. These might yield a considerable improvement in the S/N ratios and in the limiting magnitudes. An efficient future EFOSC/MOS facility should allow both round holed and rectangular slits to be used in a flexible way, depending on the astrophysical project. It should be possible to interactively adapt the aperture sizes to the prevailing seeing.

Work is now being carried out at ESO and Toulouse Observatory to investigate other mechanisms for the making of the mask, such as laser cutting and

the punching of precise rectangular slits.

On the data reduction side, further work is necessary to develop optimized software in order to cope with the large amount of data generated by this powerful observing technique.

## References

- Bruzual, A.G., 1981, PhD Thesis.  
Butcher, H., Oemler, A. and Wells, D.C., 1983, *Ap. J. Suppl.* **52**, 183.  
D'Odorico, S., Dekker, H., 1986, Proceedings of the ESO-OHP Workshop on the Optimi-

- zation of the Use of CCD Detectors in Astronomy, J.P. Baluteau and S. D'Odorico eds., published by ESO, 315.  
Fort, B., Mellier, Y., Picat, J.P., Rio, Y. and Lelièvre, G., 1986, Proc. SPIE Instrumentation in Astronomy VI, Vol. 627, 321.  
Guiderdoni, B., 1986, PhD Thesis.  
Guiderdoni, B., and Rocca-Volmerange, B., 1987, in preparation.  
Hornes, K., 1986, *Publ. Astr. Soc. Pac.*, **98**, 609.  
Mellier, Y., Fort, B., Mathez, G., and Soucail, G., 1987, in preparation.  
Soucail, G., Mellier, Y., Fort, B., Picat, J.P. and Cailloux, M., 1987, submitted to *Astron. Astrophys.*

## NOTE ADDED IN PROOF

In a recent note in *NATURE* (Vol. 325, 572), B. Paczynski discusses the "discovery" of a giant luminous arc in the core of the cluster A370, as announced in January 1987 at the 169th Meeting of the AAS. It should be pointed out that this object was

already identified in a poster paper which was presented at IAU Symposium No. 124 in Peking in August 1986. A further discussion may be found in a recent paper by Soucail et al. (*Astronomy & Astrophysics*, 172, L14; January 1987). More observations of this interesting structure were obtained in October 1986 with EFOSC.

## Nuevos meteoritos encontrados en Imilac

H. PEDERSEN, ESO, and F. GARCIA, c/o ESO

(Traducido del inglés por C. EULER, ESO)

Desde tiempos prehistóricos han sido coleccionadas piedras que caen del cielo. Hasta hace poco eran la única fuente para hacer estudios de laboratorio de la materia extragaláctica, e incluso en nuestra era espacial, siguen siendo una valiosa fuente de investigación de la temprana historia del sistema solar.

Se estima que como término medio cada kilómetro cuadrado de la superficie terrestre es golpeada cada millón de años por un meteorito con un peso superior a 500 gramos. La mayoría se pierden en los océanos o caen en regiones con escasa población. Como resultado, los museos en el mundo reciben anualmente tan sólo alrededor de 6 meteoritos cuya caída fuera atestiguada. Otros llegan por hallazgos casuales que en la mayoría de los casos son meteoritos que han caído en tiempos prehistóricos.

Desde el punto de vista mineralógico pueden ser divididos en tres clases: piedras, hierros y hierros pétreos. Los meteoritos que caen son en su gran parte pétreos, mientras que aquellos que se encuentran tienen un alto porcentaje de hierro. Esto se debe a que los meteoritos pétreos tienen una erosión más rápida y son menos visibles. Geográficamente las caídas de meteoritos están muy relacionadas con la densidad de la población, la mayor parte descubiertos en Europa y Norteamérica.

La mayoría de los meteoritos se encuentran por casualidad. La búsqueda activa en general requiere demasiado tiempo para ser de interés. Sin embargo, los glaciares de la Antártica han demostrado ser un "buen terreno de caza".

### Meteoritos de Imilac

Otras áreas donde se han hecho muchos hallazgos son algunas de las regiones desér-

ticas del mundo, como el lado occidental de Australia, las estepas de Norteamérica, y el Desierto de Atacama en Chile. En este último las precipitaciones anuales son menores que en cualquier otra parte del mundo, menos de 5 mm, lo que obviamente ayuda a la preservación de los meteoritos. Como resultado, uno de los meteoritos atacameños, encontrado en el Tamarugal, tiene una edad terrestre de 2.700.000 años, conocida como la más antigua.

Muchos meteoritos chilenos pertenecen al tipo "Pallásito" y provienen muy probablemente de una sola caída. Llevan el nombre de las localidades esparcidas geográficamente en un área de 100 por 100 km. En muy pocos casos, sin embargo, se pudo indicar con precisión el lugar del hallazgo y hasta muy reciente se creyó que los meteoritos habían sido encontrados dentro de un área de 100 por 500 m cerca del pequeño Salar de Imilac, que se encuentra aproximadamente a 170 km de Antofagasta. En este lugar existe una excavación similar a un cráter con un diámetro de 8 metros. Este puede haber sido cavado por indios en busca de la imaginada veta de hierro. Varias excavaciones en colinas adyacentes muestran lugares donde en

el pasado se han coleccionado meteoritos. Aun la parte superior del suelo contiene muchos pequeños fragmentos de hierro que pesan típicamente 1 gramo.

Los meteoritos de Imilac han llegado a muchos museos y colecciones particulares en todo el mundo. El ejemplar más grande conocido, de 198 kg, se encuentra en el Museo Británico. Otro fragmento, originalmente de 95 kg, está en Copiapo. El monto total del material encontrado, plausiblemente de origen de Imilac, se calcula en 500 kg.

### Los principales hallazgos

Después de varias expediciones se pensó que todos los grandes meteoritos habían sido coleccionados. Sin embargo, podemos informar sobre el reciente descubrimiento de tres meteoritos más, totalizando 59 kg. El hallazgo fue hecho por uno de los autores (F.G.), geólogo. (Nota del editor: F.G. es el esposo de una de las secretarias de la ESO en Santiago, Mariam G., a través de quien los científicos de La Silla fueron informados del descubrimiento). Mientras buscaba agua para una empresa minera supo de la caída en Imilac. Un poblador de la zona le informó de que algunos meteoritos habían sido encontrados algunos kilómetros al sur-oeste del "cráter". Dedicándose a la búsqueda pudo encontrar otros tres con un peso de 5, 19 y 35 kg, respectivamente.

La Universidad del Norte en Antofagasta examinó los fragmentos de 5 y 35 kg y los clasificó como "Pallásitos". Por razones de peso específico creemos que también el hierro de 19 kg pertenece a ese grupo. Ya que en todo el mundo se han descrito tan solo 33 hallazgos "Pallásitos" (y dos caídos), es un fuerte indicio que los nuevos ejemplares son parte de la conocida caída de Imilac.

\* Los meteoritos se pueden dividir en tres clases: piedras, hierros y hierros pétreos. Un sub-grupo de este último es bastante especial: una mezcla de hierro y níquel forma una estructura de tipo esponjoso. Cristales olivinos, con un diámetro de 1 a 10 mm llenan los orificios, lo que da una relación de volumen metal/olivina de aproximadamente 1 : 1. El primer meteorito de esta índole fue encontrado en 1771/72 por el explorador alemán Peter Simon Pallas en sus viajes a través de Rusia oriental. Meteoritos del tipo "Pallásito" son muy escasos: tan solo menos que un porcentaje de todas las caídas y 3.5 porcientos de todos los hallazgos pertenecen a este grupo.

ESO, the European Southern Observatory, was created in 1962 to ... establish and operate an astronomical observatory in the southern hemisphere, equipped with powerful instruments, with the aim of furthering and organizing collaboration in astronomy ... It is supported by eight countries: Belgium, Denmark, France, the Federal Republic of Germany, Italy, the Netherlands, Sweden and Switzerland. It operates the La Silla observatory in the Atacama desert, 600 km north of Santiago de Chile, at 2,400 m altitude, where thirteen telescopes with apertures up to 3.6 m are presently in operation. A 3.5-m New Technology Telescope (NTT) is being constructed and also a 15-m radio telescope (SEST). A giant telescope (VLT=Very Large Telescope), consisting of four 8-m telescopes (equivalent aperture = 16 m) is being planned for the 1990's. Six hundred scientists make proposals each year for the use of the telescopes at La Silla. The ESO Headquarters are located in Garching, near Munich, FRG. It is the scientific-technical and administrative centre of ESO, where technical development programmes are carried out to provide the La Silla observatory with the newest instruments. There are also extensive facilities which enable the scientists to analyze their data. In Europe ESO employs about 150 international Staff members, Fellows and Associates; at La Silla about 40 and, in addition, 150 local Staff members.

The ESO MESSENGER is published four times a year: normally in March, June, September and December. ESO also publishes Conference Proceedings, Preprints, Technical Notes and other material connected to its activities. Press Releases inform the media about particular events. For further information, contact the ESO Information and Photographic Service at the following address:

**EUROPEAN  
SOUTHERN OBSERVATORY**  
Karl-Schwarzschild-Str. 2  
D-8046 Garching bei München  
Fed. Rep. of Germany  
Tel. (089) 32006-0  
Telex 5-28282-0 eo d  
Telefax: (089) 3202362

**The ESO Messenger:**  
Editor: Richard M. West  
Technical editor: Kurt Kjær

Printed by Universitätsdruckerei  
Dr. C. Wolf & Sohn  
Heidemannstraße 166  
8000 München 45  
Fed. Rep. of Germany

ISSN 0722-6691

También se visitó el lugar de la vieja excavación tipo "cráter". En el "área de las astillas" se coleccionaron aproximadamente 1 kg de fragmentos menores (0,1 hasta aproximadamente 250 gramos). Algunas partículas fueron encontradas hasta 1000 m al noreste del "cráter". Estimamos que en este área aun se encuentran aproximadamente 1000 kg de hierro meteórico.

La existencia del "área de las astillas" indica que un gran trozo del meteorito sufrió una quebradura violenta. Esto tiene que haber sucedido en un punto tardío durante la trayectoria a través de la atmósfera.

Meteoritos "Pallásitos" forman un grupo bastante homogéneo, claramente distinto de otros tipos de hierros pétreos, los "mesosiderites". Podrían dar indicios sobre el origen de la consistencia del sistema solar. Por eso su creación es muy discutida entre los versados en cosmogonía. Una teoría dice que se formaron en asteroides.

El origen asteroide podría, en principio,

investigarse por el cálculo orbital de la caída de meteoritos. Esto se ha efectuado en tres oportunidades, pero ninguno de los meteoritos en cuestión eran "Pallásitos". Sin embargo, observaciones terrestres podrían ayudar a resolver la pregunta. Con ayuda de la espectrografía infrarroja se descubrieron tres candidatos de origen asteroide: 246 Asporina, 289 Nenetta, 446 Aeternitas. Su espectro muestra una banda de absorción en 1.06 μm, como es el caso con olivina en su forma meteórica. También la tendencia general del espectro concuerda con la presencia de una fase metálica.

Es extraño que un asteroide pueda ser asociado con un tipo particular de mineral. En general, estudios detallados de asteroides y cometas necesitarán de naves espaciales para que colecten muestras. En efecto, se están considerando. Pero quizás sería superfluo incluir Asporina, Nenetta o Aeternitas en el itinerario: el material podría ya encontrarse en nuestras manos ...

## Contents

H. Pedersen and F. Garcia: New Meteorite Finds at Imilac . . . . .	1
Tentative Time-table of Council Sessions and Committee Meetings for First Half of 1987 . . . . .	3
J. Melnick: Giant HII Regions and the Quest for the Hubble Constant . . . . .	4
Visiting Astronomers (April 1–October 1, 1987) . . . . .	7
Italian Delegation Visits ESO . . . . .	9
List of ESO Preprints (December 1986–February 1987) . . . . .	9
First Announcement of an ESO/NOAO Conference on "High-Resolution Imaging by Interferometry" . . . . .	9
B. Wolf, C. Sterken, O. Stahl and J. Manfroid: Long-term Photometric Campaign at ESO and the New Eclipsing P Cygni Star R 81 in the LMC . . . . .	10
J. Sommer-Larsen and P. R. Christensen: Blue Horizontal Branch Field Stars in the Outer Galactic Halo . . . . .	13
And then there were Three . . . . .	14
R. Kroll: Where Peculiars Turn Normal – Infrared Observations of CP Stars . . . . .	15
ESO Press Releases . . . . .	17
P. Magain: BD +03°740: a New Extreme Metal-poor Dwarf . . . . .	18
H. Barwig and R. Schoembs: BD Pavonis, a New Double Lined Eclipsing Cataclysmic Binary . . . . .	19
Announcement of a Summer School on "Observing with Large Telescopes" . . . . .	23
F. Murtagh, A. Heck and V. Di Gesù: Strengthening Research Links Between Astronomy/Astrophysics and Computing/Statistics . . . . .	23
Announcement of a ST-ECF Conference on "Astronomy from Large Databases: Scientific Objectives and Methodological Approaches" . . . . .	24
K. J. Mighell: Crowded Field Photometry Using EFOSC and ROMAFOT . . . . .	24
Storm Petersen and Astronomy . . . . .	25
The Supernova in the LMC . . . . .	26
U. Heber and K. Hunger: CASPEC Observations of sdO Stars: Are Some sdOs Lazy Remnants from the AGB? . . . . .	36
A. Dollfus and J.-L. Suchail: P/Halley: Characterization of the Coma Dust by Polarimetry . . . . .	39
Messenger Index . . . . .	41
A. Mazure, D. Proust, L. Sodré, H. Capelato and G. Lund: Multiple Object Redshift Determinations in Clusters of Galaxies Using OPTOPUS . . . . .	41
F. Paresce and C. Burrows: Coronography at La Silla: High Resolution Imaging of Faint Features Near Bright Objects . . . . .	43
L. Hansen, H. U. Nørgaard-Nielsen and H. E. Jorgensen: Search for Supernovae in Distant Clusters of Galaxies . . . . .	46
NEWS ON ESO INSTRUMENTATION:	
S. D'Odorico and S. Deiries: On the Rates of Radiation Events in ESO CCDs . . . . .	49
M. Tarenghi: New Technology Telescope Taking Shape . . . . .	50
G. Raffi: NTT Control/Acquisition Software . . . . .	51
ESO Image Processing Group: MIDAS Memo . . . . .	53
S. D'Odorico: New CCD Control Camera and First Test of a TEK 512 CCD at La Silla . . . . .	53
Staff Movements . . . . .	54
New Staff Association Committee in Garching . . . . .	54
J. P. Dupin, B. Fort, Y. Mellier, J. P. Picat, G. Soucail, H. Dekker and S. D'Odorico: Multiple Spectroscopy with EFOSC: Observation of the Cluster A 370 . . . . .	55
Spanish Summary (Nuevos meteoritos encontrados en Imilac) . . . . .	59